



The
University
Of
Sheffield.

Glycosaminoglycan-based scaffolds for bone repair

A thesis submitted in partial fulfilment of the
requirements for the degree of Doctor of Philosophy

Beatriz de Jesus da Cruz Monteiro

School of Clinical Dentistry
The University of Sheffield

March 2021

Contents

Table of Figures	8
Abstract	18
Acknowledgements	20
Outputs	22
Glossary	24
Introduction	28
Chapter 1 Literature review	30
1.1 Bone Tissue	30
1.1.2 Bone development	31
1.1.2.1 Intramembranous Ossification	31
1.1.2.2 Endochondral Ossification	32
1.1.3 Fracture Healing	32
1.1.4 Bone Remodelling	33
1.1.5 Osteoclasts and Lining cells	35
1.1.6 Osteoblasts and Osteocytes	35
1.1.7 The role of TGF- β /BMP-2 signalling in bone	38
1.1.8 WNT Pathway	39
1.1.9 Bone Mineralization	40
1.1.10 <i>In Vitro</i> Osteogenesis	41
1.1.11 Cell Lines	42
1.2 Stem Cells	42
1.2.1 Mesenchymal Stem Cell	43
1.2.2 Stem Cell Niche	45
1.2.3 Extracellular Matrix	47
1.3 Cell-Surface and Cell-Cell Interactions	48
1.4 Glycomics	50
1.4.1 Glycosaminoglycans (GAGs)	51
1.4.2 Heparan sulphate/Heparin	53
1.4.3 HS Biosynthesis	56
1.4.5 GAG-protein Interactions	59
1.4.7 GAGs Processing	62
1.4.8 High-Performance Liquid Chromatography (HPLC)	64

1.4.9 Modified Heparins	68
1.4.10 Glycans as a therapeutic solution	69
1.5 GAG-based biomaterials	70
1.5.1 Scaffolds manufacture	71
1.5.2 Electrospinning	73
1.5.3 Polycaprolactone	75
1.5.4 Scaffolds Functionalisation	76
1.5.4.1 Physical absorption.....	76
1.5.4.2 Covalent bonding.....	76
1.5.5 Bottle-brush Polymers	77
1.5.6 Ring opening metathesis polymerization (ROMP)	78
1.5.7 Biomaterials characterisation	79
1.5.8 Commercially available bone repair substrates	80
Chapter 2 Aims and Objectives	82
Chapter 3 Adding complexity to electrospinning scaffolds.....	84
3.1 Introduction	84
3.2 Chapter objectives	85
3.3 Materials and methods	86
3.3.1 Polymer solutions	86
3.3.2 Electrospinning parameters and collectors	86
3.3.3 Stainless-steel collectors.....	86
3.3.4 Scaffolds characterisation.....	87
3.3.5 Micropattern heparin coating.....	87
3.3.6 Scaffolds sterilisation	88
3.3.7 Detecting the presence of fluorescent heparin on scaffolds	88
3.3.8 Rat Mesenchymal stem cell culture	88
3.3.9 Cells Freezing and Thaw	89
3.3.10 MSCs passage.....	89
3.3.11 MSCs seeding onto scaffolds	89
3.3.12 Cell proliferation assay	90
3.3.13 MSCs staining.....	90
3.3.14 Polymeric solutions and electrospinning	90
3.3.15 Heparin incorporation into flat electrospinning scaffolds	91
3.3.16 Heparin detection.....	91
3.3.17 Dimethylmethylen blue dye (DMB) assay for heparin quantification	92

3.3.18 Mechanical testing	92
3.3.19 X-ray spectroscopy (XPS)	93
3.3.20 Statistics	93
3.4 Results and discussion	93
3.4.1 Micropatterned Scaffolds	93
3.4.1.1 Fibres alignment and diameter	94
3.4.1.2 Micropattern size diameters	98
3.5.1.3 Heparin detection on coated micropatterns	98
3.5.2 Biocompatibility assays	100
3.5.2.1 Micropatterned scaffolds vs plain scaffolds	100
3.5.2.2 Heparin coated vs non-coated micropatterned scaffolds	102
3.5.3 Heparin incorporation into PCL scaffolds	103
Chapter 4 Heparin processing and characterisation	Error! Bookmark not defined.
4.1 Introduction	Error! Bookmark not defined.
4.2 Chapter objectives	Error! Bookmark not defined.
4.3 Materials and methods	Error! Bookmark not defined.
4.3.1 Depolymerisation methods	Error! Bookmark not defined.
4.3.2 Size exclusion chromatography (SEC)	Error! Bookmark not defined.
4.3.3 Strong anion exchange (SAX)-HPLC	Error! Bookmark not defined.
4.3.4 PAGE	Error! Bookmark not defined.
4.3.5 Anticoagulation assay	Error! Bookmark not defined.
4.3.6 C2C12 culture	Error! Bookmark not defined.
4.3.7 Cells Thawing	Error! Bookmark not defined.
4.3.8 Cells Freezing	Error! Bookmark not defined.
4.3.9 ALP assay	Error! Bookmark not defined.
4.3.10 Osteogenic gene expression via quantitative real-time PCR (qPCR)....	Error! Bookmark not defined.
4.3.11 Osteogenic differentiation and mineralization	Error! Bookmark not defined.
4.3.12 Smad 1/5/8 phosphorylation assay	Error! Bookmark not defined.
4.3.13 Statistics	Error! Bookmark not defined.
4.4 Results and discussion	Error! Bookmark not defined.
4.4.1 Heparin depolymerisation	Error! Bookmark not defined.
4.4.2 Heparin oligosaccharides isolation (Biogel P10 column)	Error! Bookmark not defined.
4.4.4 Oligosaccharide anticoagulation activity	Error! Bookmark not defined.

4.4.5 Oligosaccharide effect on BMP-2 induced osteogenic gene expression by qPCR	Error! Bookmark not defined.
4.4.7 Oligosaccharide effect on BMP-2-induced mineralisation	Error! Bookmark not defined.
4.4.6 Oligosaccharide effect on BMP-2-induced Smad 1/5/9 phosphorylation	Error! Bookmark not defined.
Chapter 5 Synthesis of bioactive copolymers and scaffold manufacture	Error! Bookmark not defined.
5.1 Introduction	Error! Bookmark not defined.
5.2 Chapter objectives	Error! Bookmark not defined.
5.3 Materials and methods	Error! Bookmark not defined.
5.3.1 Thin layer chromatography (TLC)	Error! Bookmark not defined.
5.3.2 Fourier-transform infrared spectroscopy (FTIR)	Error! Bookmark not defined.
5.3.3 Nuclear magnetic resonance (NMR)	Error! Bookmark not defined.
5.3.4 Synthesis of norbornene initiators	Error! Bookmark not defined.
5.3.5 Synthesis of oligosaccharide macromonomer via coupling reaction	Error! Bookmark not defined.
5.3.6 Synthesis of PCL based norbornene macromonomer via ROPE	Error! Bookmark not defined.
5.3.7 Synthesis of bioactive polymers	Error! Bookmark not defined.
5.3.8 Synthesis of norbornene-mPEG5000-PCL polymer	Error! Bookmark not defined.
5.3.9 Polymeric solutions	Error! Bookmark not defined.
5.3.10 Electrospinning	Error! Bookmark not defined.
5.3.11 Scaffolds mechanical characterisation.....	Error! Bookmark not defined.
5.3.11.1 Contact angle	Error! Bookmark not defined.
5.3.11.2 Stiffness	Error! Bookmark not defined.
5.3.12 Oligosaccharides distribution on electrospinning scaffolds	Error! Bookmark not defined.
5.3.13 PCL/copolymer scaffold bioactivity.....	Error! Bookmark not defined.
5.3.14 Statistics.....	Error! Bookmark not defined.
5.4 Results and discussion.....	Error! Bookmark not defined.
5.4.1 Oligosaccharide structural analysis	Error! Bookmark not defined.
5.4.2 Synthesis of norbornyl initiators.....	Error! Bookmark not defined.
5.4.3 Synthesis of oligosaccharide macromonomer	Error! Bookmark not defined.
5.4.4 Synthesis of PCL homopolymer – macromonomer B...	Error! Bookmark not defined.
5.4.5 Synthesis of bioactive polymers	Error! Bookmark not defined.

5.4.6 Scaffolds mechanical characterisation.....	Error! Bookmark not defined.
5.4.7 Heparin distribution within bioactive scaffolds.....	Error! Bookmark not defined.
5.4.8 Scaffold bioactivity.....	Error! Bookmark not defined.
Chapter 6 Semi-synthetic heparan sulphate	Error! Bookmark not defined.
6.1 Introduction	Error! Bookmark not defined.
6.2 Chapter objectives	Error! Bookmark not defined.
6.3 Materials and methods	Error! Bookmark not defined.
6.3.1 Semi synthetic heparan sulphate manufacture	Error! Bookmark not defined.
6.3.2 Surface plasmon resonance (SPR) BMP-2 competitive binding assay ...	Error! Bookmark not defined.
6.3.3 Surface plasmon resonance (SPR) BMP-2 and VEGF ₁₆₅ affinity binding assay	Error! Bookmark not defined.
6.3.4 Alkaline phosphatase assay and osteogenic gene expression via quantitative real-time PCR (qPCR)	Error! Bookmark not defined.
6.4 Results and discussion.....	Error! Bookmark not defined.
6.4.1 Binding affinity of HS/heparin variants for BMP2.....	Error! Bookmark not defined.
6.4.1.1 Surface plasmon resonance (SPR) BMP-2 competition binding assay	Error! Bookmark not defined.
6.4.1.2 Surface plasmon resonance (SPR) BMP-2 and VEGF ₁₆₅ affinity binding assay	Error! Bookmark not defined.
6.4.2 Ability of HS/heparin variants to enhance BMP2-mediated osteogenic gene response by quantitative real-time PCR (qPCR)	Error! Bookmark not defined.
6.4.3 Alkaline phosphatase assay (ALP)	Error! Bookmark not defined.
Chapter 7 Summary and future work.....	Error! Bookmark not defined.
7.1 Adding complexity within electrospinning membranes.....	Error! Bookmark not defined.
7.2 Heparin Oligosaccharides	Error! Bookmark not defined.
7.3 ROMP-based bioactive copolymers.....	Error! Bookmark not defined.
7.4 Future work	Error! Bookmark not defined.
7.5 Final conclusion	110
Covid-19 Impact on the PhD project	110
References.....	112
Supplementary data A.....	Error! Bookmark not defined.

Table of Figures

Figure 1.1 The chemical composition and multiscale structure of natural bone tissue. Cancellous bone (Image adapted from (Gao et al., 2017)30

Figure 1.2 Phases of bone healing and key growth factors during catabolic and anabolic processes. Bone regeneration is divided into four phases that overlap each other. (A) inflammatory phase, (B) soft callus formation, (C) mineralization and resorption of the soft callus, and (D) bone remodelling. BMP = bone morphogenetic protein, FGF = fibroblast growth factor, GDF-5 = growth/differentiation factor 5, IGF-1 = insulin-like growth factor 1, M-CSF = macrophage colony-stimulating factor, OPG = osteoprotegerin, PDGF = platelet-derived growth factor, PIGF = placenta growth factor, PTH = parathyroid hormone, RANKL = receptor activator of nuclear factor κ B ligand, SDF-1 = stromal cell-derived factor 1, TGF- β = transforming growth factor β , TNF- α = tumour necrosis factor α , VEGF = vascular endothelial growth factor. Adapted from (Martino et al., 2015)34

Figure 1.3 Cell surface markers expressed during osteogenesis differentiation. Osteogenic mesenchymal progenitor cells express Stro1, CD105, CD73, CD90 and Col I before their differentiation. An important step for differentiation is the expression of RUNX2 and Osterix transcription factors by MSCs. Osteoblasts, while producing bone matrix, express several factors such as Runx2, Osterix, ALP, Col I, casein kinase II and in a later stage osteocalcin. Once trapped inside the osteoid matrix, osteoblasts start to extend, connect to other cells in the surrounding environment and differentiate into an early stage osteocyte (expression of PHEX, MEPE, E11/GP38, destrin, MT1-MMP, DMP1, CapG). A mature osteocyte has a dendritic morphology and a higher expression of FGF23, ORP150 and sclerostin which is a marker of mature osteocytes. Image adapted from (Miron and Zhang, 2012).37

Figure 1.4. BMP-2 signalling pathway in skeletal bone development. Noggin, Grem1, Chordin, Chordin-like proteins (CHL) and follistatin are BMP-2 antagonists. When BMPs bind to homomeric type II receptors Smad-dependent and non-dependent signalling pathways are activated. In Smad-dependent pathways, phosphorylation of R-Smad (Smad1,5, 8) with Smad4 complexes translocate into the nuclei that along with co-factors recruitment regulates osteogenic gene expression of Runx2, Dlx5 and Oxs. The Smad non-dependent pathway phosphorylated TAK1 that recruits TAB1 to initiate MKK-p38 MAPK or MKK-Erk1/2 signalling pathways. MKK-p38 MAPK promotes Runx2 transcription while Smad7 acts as an antagonist for preventing R-Smads phosphorylation. Schematic adapted from (Wu et al., 2016). 38

Figure 1.5. The canonical Wnt signalling pathway. Wnt protein are found are normally found associated to cell membranes and the ECM. This pathway is activated by the binding of specific Wnt ligand to Fz receptors and low-density lipoprotein receptor-related 5 or 6 (LPR5\6) co-receptors. In the absence of Wnt, β -catenin is continuously degraded but once the Wnt-receptor binding is established, destruction complex is degraded while cytoplasmatic β -catenin is accumulated and translocated to the nuclei. While non-canonical Wnt antagonists, nuclear β -catenin activates gene transcription Runx2/Osterix. Image adapted from (Houschyar et al., 2019)..... 40

Figure 1.6 Effect of surface stiffness on stem cells. A) In vivo tissue elasticity (kPa) from soft tissue to hard tissues. B) Cells cultured in vitro on soft and hard surfaces. On stiffer substrates focal adhesions, stress fibers number and spreading is higher than on soft surfaces. Cells signaling pathways are influenced by growth factor and surface anchoring. These mechanisms also stimulate Rho-GTPase activity and subsequently fibers stress. Rac and Rho have important roles in stem cell motility, contractility and anchoring. (Discher et al., 2009) 49

Figure 1.7 Main biological roles of glycans. A) Energy source, B) Structural elements and C) recognition elements in cell-cell and cell-pathogen interactions. For having such wide possible biologic interactions, glycans equally have great interest for clinical applications. Adapted from (Valverde et al., 2019)..... 51

Figure 1.8 Glycosaminoglycans structure according to main disaccharide composition. GAG are composed of combined uronic acids [β -d-glucuronic acid (GlcA) or α -l-iduronic acid (IdoA)] and amino sugars [α -d- or β -d-glucosamine (GlcN), N-acetylglucosamine (GlcNAc) or N-acetyl-galactosamine GalNAc)].Image adapted from (Neves et al., 2020) 52

Figure 1.9. HS chain biosynthesis. This schematic represents the consecutive enzymatic actions during chain initiation, chain polymerization and chain modification. The main enzymes involved in HS biosynthesis are: xylosyltransferase-1-2; galactosyltransferase-1-2; GlcA/GlcNAc transferases; N-deacetylase/N-sulfotransferase-1, -2, -3, -4 (NDST); D-glucuronyl C5-epimerase; 2- 3- 6- O-sulfotransferase (-2 -3 -5-OST). Sulphate donor 3'-phosphoadenosine-5'-phosphosulfate (PAPS). Sulphate groups are represented (2, NS, 6S) d. Image adapted from (Esko and Lindahl, 2001)..... 57

Figure 1.10 Heparinases cleavage specificity. Adapted from (Wang and Boons, 2011).62

Figure 1.11. SEC fundamentals. A) Schematic of a simple experimental set up for SEC that shows a buffer and samples flasks, a supported packed column while elution occurs with the aid of gravity. b) Sample separation within a packed bed after sample injection. The sample is separated into different populations based on their molecular size (Hagel, 2011). 66

Figure 1.12 Schematic representation of scaffolding methods (Choong et al., 2004).. 73

Figure 1.13 Classical electrospinning set up. The image also represents a charged "Taylor cone" and a SEM image of a nanofibrous type of scaffold as example. (Li and Xia, 2004) 73

Figure 1.14 Synthetic strategies of graft copolymers. a) Graft-to, side chains are coupled to initiators side on the backbone polymer b) Graft-from: individual polymerization of backbone and side chains c) Graft-through: macromonomers copolymerization normally occurring by ROMP. Adapted from (Uchida, 2013)..... 78

Figure 1.15 ROMP catalysts (Choinopoulos, 2019)..... 79

Figure 3.1 Schematic representation of micropatterns sizes on stainless steel collectors (2750 μm (N1), 1000 μm (N2), 500 μm (N3) and 100 μm (N4)). After the electrospinning of 10 wt.%PCL solutions into these collectors, a PCL membrane can be created and peeled off. The produced membrane will acquire the inverse patterned from the collector and later used as an scaffold with topographical cues.	87
Figure 3.2 Patterned collectors and patterned PCL scaffolds. A) A patterned stainless steel collector manufactured by SLM (3cmx7cm) was used to obtain B) micropatterned electrospinning 10 wt.% PCL scaffolds.	94
Figure 3.3 SEM images of micropatterned PCL scaffolds. A) Micropatterns B) Fibres located at bottom of the micropattern C) Fibres located at micropattern walls D) Fibres located outside the micropattern	95
Figure 3.4 Schematic representation of an electrospinning micropattern. Scaffolds fibres were measured in different locations of the micropattern. Measurements were taken from the areas highlighted in red. SEM	95
Figure 3.5 Histogram of fibres angle distribution (%) in PCL electrospinning scaffolds. Results are displayed between 80° and -80° and separated per micropattern location (n=40). Data was normalized by mean subtraction.	96
Figure 3.6 Electrospinning PCL fibres average diameters (n=10). Results are displayed as mean \pm SD, *p < 0.05; **p < 0.01; ***p < 0.001; ****p < 0.0001; ns – not significant (p > 0.05).	96
Figure 3.7 Heparin detection on micropatterned electrospinning PCL scaffolds coated with heparin-FITC. Confocal microscopy images were obtained during 15 days from samples incubated in PBS at 37°C . Scale bar = 500 μm	99
Figure 3.8 Rat MSCs proliferation on electrospinning PCL scaffold with and without micropatterns during 4 days of culture. Results are displayed as mean \pm SD (standard deviation). (n=1).....	101
Figure 3.9 Rat MSCs (P5) nuclei (DAPI) and actin filaments (FITC) staining after 7 days of culture on scaffold with and without micropatterns. (n=1).....	101
Figure 3.10 Rat MSCs (P4) cultured on micropatterned PCL electrospinning scaffolds coated with heparin sodium salt (1mg/mL and 0,1mg/mL), heparin-FITC (1mg/mL and 0,1mg/mL) versus no coated scaffolds. Cells proliferation was measured every 3 rd , 7 th and 10 th days by PrestoBlue assay. Results displayed as mean \pm SD	103
Figure 3.11 SEM images of 3 different types of electrospinning scaffolds. A) PCL only, B) PCL/heparin emulsion and C) PCL scaffold after heparin covalent binding. Scale bar represents 50 μm . The fibre diameter for PCL, PCL/heparin emulsion and PCL/Heparin covalent binding scaffolds was determined by ImageJ. Values are represented as Mean \pm SD. (n=3)	104
Figure 3.12 Heparin staining with toluidine blue dye solution. Heparin incorporation into PCL flat films (n=1) and electrospinning PCL scaffolds by simple adsorption, heparin emulsion and covalent binding (n=2). Purple dye identifies GAGs. PCL/heparin emulsion showed more consistency between replicate scaffolds.....	105
Figure 3.13 ^1H -NMR spectra of heparin, PCL/heparin emulsion electrospinning scaffolds extract and PCL electrospinning scaffolds extract (water peak suppression at 4.7 ppm). NMR, nuclear magnetic resonance.	106

Figure 3.14 XPS elemental quantification of C (carbon 1s), O (oxygen 1s), N (nitrogen 1s) and Sulphur (S 2p) on heparin functionalised scaffolds. C and O are the main elements from PCL scaffolds with residual detection of N and S present on heparin. (n=1)..... 107

Figure 3.15 XPS surface mapping (sulphur) of heparin functionalised electrospinning scaffolds versus non-functionalised PCL electrospinning scaffold. Sample 2 (simple coating) contains the most N and S followed by sample 3 (PCL/heparin emulsion). PCL control only contains C and O. 108

Figure 3.16 Shown data compares stiffness of polycaprolactone (PCL) versus PCL/Heparin emulsion electrospinning scaffolds, obtained using a unidirectional tensiometer (EnduraTEC elf3200 BOSE) Results are shown as mean \pm SD. Data from 2 independent experiments including five technical repeats per condition. Statistical analysis shows no significant differences between groups ($p > 0.05$). 109

Figure 4.1 PAGE gel. Heparin JX04 (5 μ g) digested during A) 1h versus 4 h, B) 8 h versus 12 h, C) 14 h versus 16 h and D) 24 h at different natural heparinase I concentrations (0.25, 0.5, 1, 1.5 and 2 mIU) versus native heparin and respective heparin standards dp12 dp14 and dp16 (2 μ g).**Error! Bookmark not defined.**

Figure 4.2 PAGE gel. Heparin JX04 (5 μ g) digested during 1-24 h at different recombinant heparinase I concentrations (100 and 200 mIU) versus native heparin and respective oligosaccharides standards dp10, dp12, dp14 and dp16 (2 μ g).**Error! Bookmark not defined.**

Figure 4.3 PAGE gel. Heparin (5 μ g) treated with nitrous acid at different time points (5-120min), and respective heparin standards dp10 - dp18 (2 μ g). This image is representative of 2 independent experiments.**Error! Bookmark not defined.**

Figure 4.4 Total percentage of N-sulphated disaccharides determined via SAX-HPLC N-sulphated relative composition was determined by the sum of Δ UA-GlcNS, Δ UA-GlcNS6S, Δ UA(2S)-GlcNS and Δ UA2S-GlcNS6S disaccharide compositions for each nitrous acid depolymerisation time point (5-120 min). Data normalised to the total amount of digested material per run. (n=1)**Error! Bookmark not defined.**

Figure 4.5 Total percentage of N-sulphated disaccharides determined via SAX-HPLC N-sulphated relative composition was determined by the sum of Δ UA-GlcNS, Δ UA-GlcNS6S, Δ UA(2S)-GlcNS and Δ UA2S-GlcNS6S disaccharide compositions for each nitrous acid depolymerisation time point (5-120 min). Data normalised to the total amount of digested material per run. Results are shown as Mean \pm S.D. Statistical analysis showed no significant difference between groups ($p > 0.05$). (n=3)**Error! Bookmark not defined.**

Figure 4.6 Size exclusion chromatography (SEC) fractionation chromatogram of heparin JX04 depolymerised by nitrous acid during A) 5 minutes and B) 10 minutes (200 mg/mL (200 mg total), 2 ml injection loop, 8 fractions). Elution (mL) of samples was monitored via absorbance at 232 nm (heparin). A Biogel P10 column (16 x 2000 mm, BioRad) was equilibrated using a ÄKTA Pure 25M with 200mM ammonium bicarbonate running buffer at a flow rate of 0.27 ml/min. Fractions (F1-F8) were pooled and separated by PAGE.**Error! Bookmark not defined.**

Figure 4.7 Size exclusion chromatography (SEC) fractionation chromatogram of heparin JX04 depolymerised by nitrous acid during 15 minutes (200 mg/mL (200 mg total), 2 ml injection loop, 8 fractions). Elution (mL) of samples was monitored via absorbance at 232 nm (heparin). A Biogel P10 column (16 x 2000 mm, BioRad) was equilibrated using a ÄKTA Pure 25M with

200mM ammonium bicarbonate running buffer at a flow rate of 0.27 mL/min. Fractions (F1-F8) were pooled and separated by PAGE.**Error! Bookmark not defined.**

Figure 4.8 PAGE gel. Heparin USP digested for A) 10 min and B) 15 min in nitrous acid was fractionated by SEC (Biogel P10 column, 16 x 2000 mm, BioRad) and obtained fractions (F2-F8) before polish (2µg) were separated in PAGE gel versus heparin standards (dp10 - dp16, 2 µg). Fraction F2 was completely degraded and cannot be detected after 15 min digestion with nitrous acid. Presence of small oligosaccharides can be detected for all fractions before polishing.**Error! Bookmark not defined.**

Figure 4.9 PAGE gel. Polished (Superdex peptide column) nitrous acid digested heparin fractions F6, F7 and F8 (2 µg) were run in PAGE versus heparin standards (dp12 - dp14, 2 µg). Presence of small oligosaccharides can be detected for all fractions.**Error! Bookmark not defined.**

Figure 4.10 Size exclusion chromatography (SEC) fractionation chromatogram of heparin SPL digested by nitrous acid during 15 minutes (300mg, 1 ml injection loop, 8 fractions). Elution (mL) of samples was monitored via absorbance at 232 nm. A Superdex PG 30 (2x2000 mm, Mw ≤10000, GE Healthcare) was equilibrated using a AKTA Pure 25M with 200mM ammonium bicarbonate running buffer at a flow rate of 0.66 ml/min. Peaks (F1-F8) were pooled and sizing determined by PAGE. This chromatograph is representative of several runs.**Error! Bookmark not defined.**

Figure 4.11 PAGE gel. Heparin SPL depolymerised for 15 min in nitrous acid was fractionated by SEC (Superdex™ PG 30 (2x2000 mm, Mw ≤10000, GE Healthcare) and eluted fractions (F2- F8) pre-polishing (2µg) were run in PAGE gel versus heparin standards dp12 - dp16 and native heparin (2 µg). Presence of small oligosaccharides can be detected for all fractions.**Error! Bookmark not defined.**

Figure 4.12 Size exclusion chromatography (SEC) fractionation chromatogram of pre-polish fractions (F6, F7, F8; 0.5 mg). Elution (mL) of samples was monitored via absorbance at 232 nm. A Superdex peptide 10/300 GL column (Mw=100-7000; GE Healthcare) was equilibrated using a GE ÄKTA Pure 25M with 200mM ammonium bicarbonate running buffer at a flow rate of 0.5 ml/min.**Error! Bookmark not defined.**

Figure 4.13 Size exclusion chromatography (SEC) fractionation chromatogram of after polish fractions (F6, F7, F8; 0.5 mg). Elution (mL) of samples was monitored via absorbance at 232 nm. A Superdex peptide 10/300 GL column (Mw=100-7000; GE Healthcare) was equilibrated using a ÄKTA pure 25M with 200mM ammonium bicarbonate running buffer at a flow rate of 0.5 ml/min.**Error! Bookmark not defined.**

Figure 4.14 Nitrous acid depolymerised (15 min) heparin SPL pooled SEC fractions (F2-F8, 2 µg) after polishing versus respective heparin standards dp10 dp16 and native heparin (2 µg). These results indicate that polished samples contain oligosaccharides of homogenous sizing (low polydispersity with no to low presence of smaller oligosaccharide).**Error! Bookmark not defined.**

Figure 4.15 Anticoagulation activity of heparin oligosaccharides obtained by nitrous acid digestion versus native heparin. Comparing with full-length heparin (anti-factor Xa= 187 IU/mg), oligosaccharides F6 (dp10), F7 (dp12) and F8 (dp14) anti-Xa activity (IU/mg) decreased to 46.7 (IU/mg), 65.8 (IU/mg) and 65.8 (IU/mg) respectively. Results are shown as Mean ± S.D. * p < 0.05, ns – p > 0.05. Data obtained from two independent experiments (n=2).**Error! Bookmark not defined.**

Figure 4.16 Anti-factor Xa properties of nitrous acid generated oligosaccharides F6 (dp10), F7 (dp12) and F8 (dp14). Human antithrombin was incubated with factor Xa in the presence heparin oligosaccharides at different GAG concentrations (0.05-10 µg/mL) and unbound factor Xa activity was measured using a chromogenic substrate with detection at 405 nm. Data representative of two independent experiments. (n=2) ... **Error! Bookmark not defined.**

Figure 4.17 BMP2-mediated expression of osteogenic mRNA transcripts assessed by qPCR. C2C12 cells were stimulated with BMP-2 (100 ng/mL) in combination with native heparin or nitrous acid generated oligosaccharides F6, F7 and F8 (5 µg/mL) for 3 days after which A) *alpl*, B) *runx2*, and C) *sp7* mRNA transcript levels was determined. Results were normalised to BMP-2 and are shown as Mean ± S.D. **Error! Bookmark not defined.**

Figure 4.18 BMP2-mediated expression of osteogenic mRNA transcripts assessed by qPCR. C2C12 cells were stimulated with BMP-2 (100 ng/mL) in combination with native heparin (10 µg/mL) or nitrous acid generated oligosaccharide F6 (10, 20 and 40 µg/mL) for 3 days after which a) *alpl*, b) *runx2* and c) *sp7* mRNA transcript levels was determined. Results were normalised to BMP-2 and are shown as Mean ± S.D. *p < 0.05; **p < 0.01; ***p < 0.001; ****p < 0.0001; ns – not significant (p > 0.05). Data obtained from two independent experiments (n=2). ***** BMP-2 alone **Error! Bookmark not defined.**

Figure 4.19 BMP2-mediated expression of osteogenic mRNA transcripts assessed by qPCR. C2C12 cells were stimulated with BMP-2 (100 ng/mL) in combination with heparin or heparin oligosaccharide F7 (10, 20 and 40 µg/mL) for 3 days after which a) *alpl*, b) *runx2* and c) *sp7* mRNA transcript levels was determined. Results were normalised to BMP-2 and are shown as Mean ± S.D. *p < 0.05; **p < 0.01; ***p < 0.001; ****p < 0.0001; ns – not significant (p > 0.05). Data obtained from two independent experiments (n=2). ***** BMP-2 alone **Error! Bookmark not defined.**

Figure 4.20 BMP2-mediated expression of osteogenic mRNA transcripts assessed by qPCR. C2C12 cells were stimulated with BMP-2 (100 ng/mL) in combination with heparin or nitrous acid heparin oligosaccharides F8 (10, 20 and 40 µg/mL) for 3 days after which A) *alpl*, B) *runx2* and C) *sp7* mRNA transcript levels was determined. Results were normalised to BMP-2 and are shown as Mean ± S.D. *p < 0.05; **p < 0.01; ***p < 0.001; ****p < 0.0001; ns – not significant (p > 0.05). Data obtained from two independent experiments (n=2). ***** BMP-2 alone **Error! Bookmark not defined.**

Figure 4.21 BMP-2-mediated ALP activity. C2C12 cells were stimulated with BMP-2 (50 ng/mL) in combination with **A)** heparin standard (dp10) versus nitrous acid generated oligosaccharide F6 (2.5-40 µg/mL) or **B)** heparin standard (dp14) versus nitrous acid generated oligosaccharide F8 (2.5-40 µg/mL) for 3 days. Results were normalised to BMP-2 and are shown as Mean ± S.D. *p < 0.05; **p < 0.01; ***p < 0.001; ****p < 0.0001; ns – not significant (p > 0.05). Data obtained from three independent experiments (n=2), replicate 1 (●) and 2 (●). ***** BMP-2 alone **Error! Bookmark not defined.**

Figure 4.22 BMP-2-mediated ALP activity. C2C12 cells stimulated with BMP-2 (100 ng/mL) in combination with A) heparin standard (dp10) or nitrous acid generated oligosaccharides F6 (2.5-40 µg/mL) or B) heparin standard (dp12) or nitrous acid generated oligosaccharides F7 (2.5-40 µg/mL) for 3 days. Results were normalised to BMP-2 and are shown as Mean ± S.D. *p < 0.05; **p < 0.01; ***p < 0.001; ****p < 0.0001; ns – not significant (p > 0.05) Data obtained from two independent experiments (n=3), replicate 1 (●), 2 (●) and 3 (●). ***** BMP-2 alone **Error! Bookmark not defined.**

Figure 4.23 BMP-2-mediated ALP activity. C2C12 cells stimulated with BMP-2 (100 ng/mL) in combination with heparin standard (dp14) or nitrous acid generated oligosaccharides F8

(2.5-40 µg/mL) for 3 days. Results were normalised to BMP-2 and are shown as Mean ± S.D. *p < 0.05; **p < 0.01; ***p < 0.001; ****p < 0.0001; ns – not significant (p > 0.05). Data obtained from three independent experiments (n=3), replicate 1 (●), 2 (●) and 3 (●). **Error! Bookmark not defined.**

Figure 4.24 BMP-2-mediated ALP activity. C2C12 cells stimulated with **A)** BMP-2 (50 ng/mL) **B)** BMP-2 (100 ng/mL) in combination with native heparin or nitrous acid generated oligosaccharides F6, F7 and F8 (5 µg/mL) for 3 days after which ALP activity was determined. Results were normalised to BMP-2 and are shown as Mean ± S.D. *p < 0.05; **p < 0.01; ***p < 0.001; ****p < 0.0001; ns – not significant (p > 0.05) Data obtained from three independent experiments (n=3), replicate 1 (●), 2 (●) and 3 (●). **Error! Bookmark not defined.**

Figure 4.25 Osteogenic differentiation, BMP-2 dosing assay. C2C12 cells stimulated with or without BMP-2 (50, 100, 200 and 400 ng/mL) for 10 days after which calcium deposition was stain with Alizarin Red. Data represents one independent experiment, and two technical repeats. (n=1) **Error! Bookmark not defined.**

Figure 4.26 Osteogenic differentiation ,BMP-2 dosing assay. C2C12 cells stimulated with or without at BMP-2 at a concentration of A) 50 ng/mL or B) 100 ng/mL in combination with heparin or F6 oligosaccharides (10 - 40 µg/mL) for 10 days after which calcium deposition was stain with Alizarin Red. Data represents one independent experiment, and two technical repeats. (n=1) **Error! Bookmark not defined.**

Figure 4.27 Osteogenic differentiation BMP-2 dosing assay. C2C12 cells stimulated with or without BMP-2 (50 or 100 ng/mL) in combination with heparin or F8 oligosaccharides (10 - 40 µg/mL) for 10 days after which calcium deposition was stain with Alizarin Red. Data represents one independent experiment, and two technical repeats. (n=1) **Error! Bookmark not defined.**

Figure 4.28 Osteogenic differentiation BMP-2 dosing assay. C2C12 cells stimulated with or without BMP-2 at a concentration of A) 50 ng/mL or B) 100 ng/mL in combination with heparin or F7 oligosaccharides (10 - 40 µg/mL) for 10 days after which calcium deposition was stain with Alizarin Red. Data represents one independent experiment, and two technical repeats. (n=1) **Error! Bookmark not defined.**

Figure 4.29 BMP-2-induced Smad 1/5/9 phosphorylation detection by Western Blot. C2C12 cells stimulated without (control) or with BMP-2 (25 ng/mL) in combination with native heparin or nitrous acid generated oligosaccharides F6 (dp10), F7 (dp12) or F8 (dp14) at a concentration of 5 µg/mL for 24 or 48 hours after which Smad 1/5/9 phosphorylation, total Smad 1/5/8 and actin was detected via Western blot. Smad 1/5/9 = 52 kDa, Smad 1/5/8 = 52 Kda; actin = 42 kDa. Data obtained from two independent experiments (n=2). **Error! Bookmark not defined.**

Figure 4.30 Quantification of BMP-2-induced Smad 1/5/9 phosphorylation normalised to total Smad 1/5/8. C2C12 cells stimulated with or without BMP-2 (25 ng/mL) in combination with native heparin or F6(DP10), F7 or F8 oligosaccharides (5 µg/mL) for 24 or 48hours after which Smad 1/5/9 phosphorylation was detected via Western blot. Data obtained from two independent experiments (n=2). **Error! Bookmark not defined.**

Figure 5.1 Norbornyl random bottlebrush copolymers by ROMP. Purified heparin fragments obtained from nitrous acid digests were used to develop BMP-2 binding scaffolds for bone repair. Monomer A and B were individually synthesised, optimised and used to create a ROMP-derived NB backbone bioactive copolymer. **Error! Bookmark not defined.**

Figure 5.2 Condensation reaction for the synthesis of NB-PEG initiator (initiator A).**Error! Bookmark not defined.**

Figure 5.3 Condensation reaction for the synthesis of NB-aminopropanol initiator (initiator B).
.....**Error! Bookmark not defined.**

Figure 5.4 Optimised heparin synthesis via chemical coupling. Three types of macromonomers were synthesised using heparin oligosaccharides generated by nitrous acid digestion of heparin F6 (dp10), F7 (dp12) and F8 (dp14) coupled with initiator B (NB-PEG1000 amine). One control macromonomer was synthesised using commercially available heparin dp12 (Iduron) and NB-PEG3400 amine or NB-PEG1000 amine.**Error! Bookmark not defined.**

Figure 5.5 Optimised PCL macromonomer B synthesis by ROP.**Error! Bookmark not defined.**

Figure 5.6 ROMP of bioactive copolymers containing heparin oligosaccharides and PCL. Three types copolymers were synthesised using heparin fragments obtained by nitrous acid: heparin F6 (dp10), F7 (dp12) and F8 (dp14) containing PEG1000. One control was synthesised using commercially available heparin dp12 (Iduron) containing NB-PEG3400 linker. n,m,p,q,r = repeating units per monomers**Error! Bookmark not defined.**

Figure 5.7 Samples setup for mechanical testing. A) Electrospinning sample was assembled on a paper for support and cut on the indicated red areas prior analysis B) Sample during testing on extensometer.....**Error! Bookmark not defined.**

Figure 5.8 ¹H NMR spectra of heparin dp12 standard (Iduron). Characteristic heparin residues peaks can be noticed between 5-3ppm and ~2 ppm.**Error! Bookmark not defined.**

Figure 5.9 ¹H NMR spectra of heparin F6 (dp10) lab generated by nitrous acid. Characteristic heparin residues peaks can be noticed between 5-3ppm and ~2 ppm.**Error! Bookmark not defined.**

Figure 5.10 ¹H NMR spectra of heparin F7 (dp12) lab generated by nitrous acid. Characteristic heparin residues peaks can be noticed between 5-3ppm ~2 ppm.**Error! Bookmark not defined.**

Figure 5.11 ¹H NMR spectra of heparin F8 (dp14) lab generated by nitrous acid. Characteristic heparin residues peaks can be noticed between 5-3ppm ~2 ppm.**Error! Bookmark not defined.**

Figure 5.12 Thin Layer chromatography (TLC) and bromocresol staining of carboxylic acid of heparin s. A) Commercial oligosaccharides standards from Iduron® (dp6, dp10 and dp12) and B) lab made generated oligosaccharides F6 (dp10), F7 (dp12) and F8 (dp14) by nitrous acid digestion. Carboxylic acid was detected in all samples (yellow dots and slow migration).
.....**Error! Bookmark not defined.**

Figure 5.13 FTIR spectra of commercially available heparin dp12 standard (Iduron) where carboxylic acid presence can be detected at the 3000-3500 cm⁻¹ O - H stretch. Control sample.
.....**Error! Bookmark not defined.**

Figure 5.14 FTIR spectra of nitrous acid generated heparin s F6 (dp10), F7 (dp12) and F8 (dp14). All tested oligosaccharides presented a similar FTIR profile and carboxylic acid presence at the 3000-3500 cm⁻¹ O - H stretch similarly to heparin standard dp12 (control).
.....**Error! Bookmark not defined.**

Figure 5.15 ^1H NMR spectra of NB-aminopropanol and respective peak assignments. **Error! Bookmark not defined.**

Figure 5.16 ^1H NMR spectra of NB-PEG3400 and respective peak assignments. **Error! Bookmark not defined.**

Figure 5.17 ^1H NMR spectra of NB-PEG1000 and respective peak assignments. **Error! Bookmark not defined.**

Figure 5.18 ^1H NMR spectra of NB-PEG1000-dp12 (Iduron) macromonomer B and respective peak assignments. Water peak detected at ~ 4.6 ppm.... **Error! Bookmark not defined.**

Figure 5.19 ^1H NMR spectra of NB-PEG1000-F6 (dp10) macromonomer B and respective peak assignments. Water peak detected at ~ 4.6 ppm.... **Error! Bookmark not defined.**

Figure 5.20 ^1H NMR spectra of NB-PEG1000-F7 (dp12) macromonomer B and respective peak assignments. Water peak detected at ~ 4.6 ppm.... **Error! Bookmark not defined.**

Figure 5.21 ^1H NMR spectra of NHP-PCL ($M_n = 4574$) macromonomer B and respective peak assignments..... **Error! Bookmark not defined.**

Figure 5.22 ^1H NMR spectra of bioactive copolymer PCL-NB-PEG1000-dp12 (Iduron®) respective peak assignments. A small broad NB peak is observed when conversion is not complete. This copolymer is used as a reference..... **Error! Bookmark not defined.**

Figure 5.23 ^1H NMR spectra of bioactive copolymer PCL-NB-PEG1000-F6 (dp10) respective peak assignments. A small broad NB peak is observed when conversion is not complete. **Error! Bookmark not defined.**

Figure 5.24 ^1H NMR spectra of bioactive copolymer PCL-NB-PEG1000-F7 (dp12) respective peak assignments. A small broad NB peak is observed when conversion is not complete. **Error! Bookmark not defined.**

Figure 5.25 ^1H NMR spectra of bioactive copolymer PCL-NB-PEG1000-F8 (dp14) respective peak assignments. A small broad NB peak is observed when conversion is not complete. **Error! Bookmark not defined.**

Figure 5.26 Scanning electron microscopy (SEM) images of PCL electrospinning scaffolds. Controls versus samples containing ROMP derived polymer with nitrous acid generated oligosaccharides F6 (dp10), F7 (dp12) and F8(dp14). Scale bar: 10 μm . ($n=3$)..... **Error! Bookmark not defined.**

Figure 5.27 Heparin detection on electrospinning scaffolds by toluidine blue staining. The positive control is PCL/heparin (emulsion) (2 mg heparin/mL, flat scaffold), negative control is a PCL alone electrospinning scaffold versus electrospinning bioactive scaffold ([PCL]:[PCL-PEG1000-dp12]). **Error! Bookmark not defined.**

Figure 5.28. BMP-2 stimulated ALP activity. C2C12 cells were cultured onto electrospinning scaffolds pre-incubated with BMP-2 (100 ng/mL) for 3 days. Results are shown as Mean \pm S.D and were normalised to electrospinning PCL scaffolds pre-incubated with BMP-2. Non-treated PCL and PCL-dp12 scaffolds were used as a control. No significant difference was found between BMP-2 pre incubated scaffolds. Data obtained from three independent experiments ($n=3$). **Error! Bookmark not defined.**

Figure 6.1 SPR sensograms. BMP2 (25 nM) binding (response unit. R.U.) to a heparin-immobilized sensor chip in competition with increasing solution concentrations of SSHS dp12

or heparin dp12. HS/heparin GAG concentrations: A) 2.5 µg/mL B) 5 µg/mL C) 10 µg/mL D) 20 µg/mL. BMP-2 alone is represented as initial and final cycle (black curve). (n=1).**Error! Bookmark not defined.**

Figure 6.2 Quantification of SPR-based competitive binding assay in Figure 1.1. BMP-2% in solution when complexed to increasing concentrations of HS/heparin dp12. GAG concentrations in solution: a) 2.5 µg/mL b) 5 µg/mL c) 10 µg/mL d) 20 µg/mL. (n=1)**Error! Bookmark not defined.**

Figure 6.3 SPR sensorgram for binding affinity of BMP-2 and VEGF₁₆₅ for SSHS dp12. SPR-based dosing assay using a range of concentrations (1.56, 3.125, 6.25, 12.5, 25, 50, 100, 200, 400, 800 nM) of A) BMP-2 and B) VEGF₁₆₅ on an SSHS dp12-coated sensor chip was used to determine binding affinity constant (K_d). (n=1)**Error! Bookmark not defined.**

Figure 6.4 BMP2-mediated expression of osteogenic mRNA transcripts assessed by qPCR. C2C12 cells were stimulated with BMP2 (50 ng/mL) in combination with heparin dp12 (20 µg/mL) or SSHS dp12 (20 and 40 µg/mL) for 3 days after which a) alpl, b) runx2 and b) sp7 mRNA transcript levels was determined. Results were normalised to BMP-2 and results are shown as Mean ± S.D. "***** BMP-2 alone, (n=1).....**Error! Bookmark not defined.**

Figure 6.5 BMP2-mediated expression of osteogenic mRNA transcripts assessed by qPCR. C2C12 cells were stimulated with BMP2 (100 ng/mL) in combination with heparin dp12 (20 µg/mL) or SSHS dp12 (20 and 40 µg/mL) for 3 days after which a) alpl, b) runx2 and b) sp7 mRNA transcript levels was determined. Results were normalised to BMP-2 and results are shown as Mean ± S.D. (n=1).....**Error! Bookmark not defined.**

Figure 6.6 BMP-2-mediated ALP activity. C2C12 cells stimulated for 3 days with A) C) 50 ng/mL or B) D) 100 ng/mL BMP2 in combination with SSHS dp12 or heparin dp12 at A) B) low GAG concentrations (2.5 - 20 µg/mL). and C) D) higher GAG concentration (40-80 µg/mL) for 3 days after which ALP activity was determined. Results were normalized to BMP-2 and shown as Mean ± S.D. "***** BMP-2 alone, (n=1).....**Error! Bookmark not defined.**

Abstract

Adding complexity to biomaterials by mimicking extracellular matrix-like components as well as biomechanical cues is a powerful strategy for enhancing the performance of implantable materials for orthopaedic purposes. In recent years, bone morphogenetic protein 2 (BMP-2), a potent osteoinductive factor has gained popularity within the orthopaedic community to stimulate bone regeneration. Despite showing strong osteoestimulatory effects, the short half-life of BMP-2 requires supraphysiological doses to achieve efficacious clinical outcomes which has been repeatedly associated with life-threatening side effects. Glycosaminoglycans (GAGs) of the heparin/heparan sulphate (HS) are key components of the extracellular matrix that bind, stabilise and protect factors such BMP-2 from degradation. Despite being available at a clinical grade, the anticoagulant property of heparin coupled with its ability to bind non-selectively to a wide range of stimulatory and inhibitory osteogenic factors is driving strategies to generate heparin structures that overcome these limitations. The actions of heparin/HS GAGs are dependent on their sulphation pattern and overall chain length. Recent findings from our group suggest that heparin fragments of 12 saccharides in length (dp12) optimally bind and stabilise BMP-2 to enhance its osteogenic effects. This suggests a path to increasing the selectivity of heparin for BMP-2 through a sizing strategy to reduce off-target effects.

Therefore, this thesis aims to develop heparin-functionalised scaffolds for bone repair. Initially, we have explored adding micropatterns into electrospinning scaffolds or biomaterial biofunctionalisation (i.e., heparin) for increased scaffolds complexity. In search for a more sophisticated and reliable functionalisation method, bioactive copolymers containing nitrous acid generated heparin oligosaccharides were synthesised by ring opening metathesis polymerisation (ROMP) to sustain BMP-2 signals over a prolonged period and manufactured into electrospinning scaffolds. Bioactive oligosaccharides F6 (dp10), F7 (dp12) and F8 (dp14) were successfully isolated from nitrous acid digested mixtures by size exclusion chromatography (SEC). Data obtained from BMP-2 response C2C12 cells suggested that heparin oligosaccharides have the ability to enhance BMP-2-mediated osteogenic responses determined by quantitative polymerase chain reaction (qPCR) of osteogenic genes, alkaline phosphatase (ALP) assay, mineralisation assays and Smad 1/5/9 phosphorylation assays. Nitrous acid generated oligosaccharides presented low anti-Factor Xa in comparison with native heparin and retained a dose and chain length dependent bioactive properties as a cheap alternative to enzymatic depolymerisation. Bioactive oligosaccharides were then used to synthesise bioactive copolymers for bone repair. ROMP-derived bioactive copolymers were synthesised using polycaprolactone (PCL) macromonomers and oligosaccharide macromonomers with high conversion. The final copolymers presented a ~3-3.5 wt.% incorporation of oligosaccharide macromonomer into the final copolymer. The structural variability of bioactive electrospinning scaffolds was characterised in terms of fibre diameter, hydrophobicity, stiffness and thickness. In conclusion, the presented bioactive copolymers are a relevant platform for the design of advanced bone repair scaffolds able to tackle interdisciplinary tissue engineering challenges.

Acknowledgements

In no particular order, I would like to thank my supervisors Ildia Ortega, Paul Hatton, Simon Cool and Peili Teo for the opportunity to do my PhD and join their research groups. I would like to thank all the students, postdocs, mentees and researchers I have met along my PhD that contributed to my work and personal growth. A huge thank you to Tom Paterson who enthusiastically mentored me at the beginning of my PhD, thank you all the support, great advice and sarcastic humour. A big thank you to Alex Smith who introduced me to the vast world of GAGs. For being extra helpful, the immense knowledge, all the mentoring and definitely for being patient enough to answer the same question 3 times. To Tuan Chun, Selene and Arya for being a positive energy in the lab, the ability to sort out any problems and still find time to train me on new protocols. To Eun Jun, Jiayi, Yew Chin, Asyraf and Teck Huat for all the help in the chemistry Lab and lunch breaks. To Seeta and Nathan for their advice on my work, long talks and longer laughter. To Katya for all the support, motivational messages and simply for being an amazing soul. To my fellow PhD colleagues and friends back in Sheffield, Danilo, Maha and Alex. We walked this PhD journey together and I couldn't ask for better mates to go through this emotional roller-coaster. To my friends from the postgraduate society, Sheen, Roja, Anas, Belle and Laura for joining me for so many activities, board game nights, dinner parties and zoom gatherings. To my good friends Nidia and Tomas who had a terrible PhD journey and then advised me to not do a PhD but now here I am writing

this acknowledgement. To my childhood friends Joana and Sara for always being there no matter what and my friends Flor and Rita for always checking up on me. Thank you to all the awesome people I have met in Singapore but especially to my flatmates Shan and Jessi. Thank you for being a family far away from home and listening to all my complains in loop, buy me snacks and make me addicted to prata and muah chee. To the kindest person and the best travel planner, Bowy. Thank you for all the motivation, support and ability to put things into perspective, you have the biggest faith in the future and for that so have I. To my Family. To my Mom, Dad and baby brother Alberto, for your unconditional care since the first day I stepped into this world and your trust that whatever the outcome I will always succeed. To my Grandma, the most strongminded yet stubborn women that I will ever meet and whom I believe is also cheering for me today. Obrigada!

“Wisdom is like a baobab tree; no one individual can embrace it.”

Akan and Ewe (Benin, Ghana and Togo) Proverb

Outputs

Presentations

B.J.C. Monteiro, T. Paterson, P. Hatton, S. Cool, I. Ortega, "Bioinspired topographically-tailored electrospinning substrates for studying mesenchymal stromal cell behaviour" at 29th Annual Meeting of the European Society for Biomaterials, Maastricht, The Netherlands, September 2018

B.J.C. Monteiro, T. Paterson, P. Hatton, S. Cool, I. Ortega, "Biomimetic scaffolds for bone repair" A*STAR International Conference, Sheffield, UK, 2017. Talk and Poster

Posters

"Biomimetic scaffolds for bone repair" 18th Biomaterials & Tissue Engineering Group (BiTEG), Durham University, UK 2017.

"Synthetic Stem cell niches for applications in regenerative medicine" International Polymer Process Engineering (PPE)(in collaboration with UK-China Advanced Materials Research Institute), Bradford, UK, 2017.

“Synthetic Stem cell niches for bone repair” MeDe Innovation Fourth Annual Conference, Bradford University, UK, 2017.

Paper

Abdelmoneim, D.; Alhamdani, G.M.; Paterson, T.E.; Santocildes Romero, M.E.; Monteiro, B.J.C.; Hatton, P.V.; Ortega Asencio, I. Bioactive and Topographically-Modified Electrospinning Membranes for the Creation of New Bone Regeneration Models. *Processes* 2020, 8, 1341

Glossary

ALIF - lumbar interbody fusion

ALP - alkaline phosphatase

ATIII - antithrombin III

BCA – protein assay kit

BMP – bone morphogenetic

DCM – dichloromethane

DMF - dimethylformamide

DIPEA, iPr₂EtN - N,N-Diisopropylethylamine

DMEM - Dulbecco's Modified Eagle Medium

DMF - dimethylformamide

DP - degree of polymerisation

DTAB - dodecyltrimethylammonium bromide

ECM - extracellular matrix

ELISA – enzyme linked immunosorbent assay

FDA - food and drug administration

FTIR - Fourier-transform infrared spectroscopy

GAG - glycosaminoglycan

GlcA - Glucuronic acid
GlcA - β -d-glucuronic acid
GlcNac - N-acetylglucosamine
GlcNS - N-sulphoglucosamine
GPC - gel permeation chromatography
HBTU - carbodiimine
HOBt - N-hydroxybenzotriazole
HPLC - high-performance liquid chromatography
HS – heparan sulphate
HSC - hematopoietic stem cells
IdoA - iduronic acid
IGF - insulin-like growth factor
IHC - immunohistochemistry
IL– interleukin
MAPK - mitogen-activated protein kinases
MeOH – methanol
MSC - mesenchymal stem cell
NB - norbornene
NDST - N-deacetylase/ N-sulfotransferase enzymes
SDF - stromal cell-derived factor
NMR – nuclear magnetic resonance
OST – O-sulphotransferase
PBS - phosphate-buffered saline
PCL - polycaprolactone
PDI - polydispersity
PEG - poly(ethylene glycol)
PEG - polyethylene glycol
PPi - pyrophosphate
RGD - arginine-glycine-aspartic acid

RIPA - aadioimmunoprecipitation assay

ROMP - ring opening metathesis polymerisation

ROP - ring opening polymerisation

RT-PCR - reverse transcription polymerase chain reaction

SEC- size exclusion chromatography

SEM - scanning electron microscopy

TGF - transforming growth factor

THF - Tetrahydrofuran

EDC/NHS - 1-Ethyl-3-(3-dimethylaminopropyl)carbodiimide/ N-hydroxysuccinimide

TLC - thin layer chromatography

UV - ultraviolet

VEGF - vascular endothelial growth factor

WCA - water contact angle

GF - growth factor

SOX - sex determining region Y-box 2

Introduction

According to the World Health Organization (WHO), musculoskeletal disorders can affect joints, muscle, the spine, connective tissues and bones. In 2017, the Global Burden of Disease study showed that musculoskeletal disorders have a high impact on worldwide populations contributing to the increase of global disability that has continued to rise since 1990 (GBD 2017 Disease and Injury Incidence and Prevalence Collaborators, 2018; Kjaer, 2004). Musculoskeletal disorders can translate to an annual burden of 3% of gross national product related to direct and indirect costs (WHO, 2003) (Odén et al., 2015). In particular, bone fracture is the most common orthopaedic problem in developed countries where the growth of the ageing population is expected to increase continuously (Gibon et al., 2016) and 12 million bone fractures are predicted to occur per year by 2050 in Europe (Vukicevic et al., 2014). Osteoporosis - often observed in elderly populations – can weaken bones strength and increase the risk of fracture. Although old age might be an important risk factor, nutrition, congenital diseases and falls are also determinant factors in bone fracture frequency (Aspray and Hill, 2019).

While small bone fractures have the ability to heal naturally, this does not occur if the extension of bone fracture is too large which might require an invasive intervention as treatment (J Hill et al., 2019). Autologous bone graft is the gold standard method for treating complex bone defects but this is associated with postsurgical morbidity, surgical complications

and high surgical costs. To overcome the limitations associated to traditional methods, different cell-based and tissue engineering approaches have been proposed in order to enhance the stimulation of bone repair.

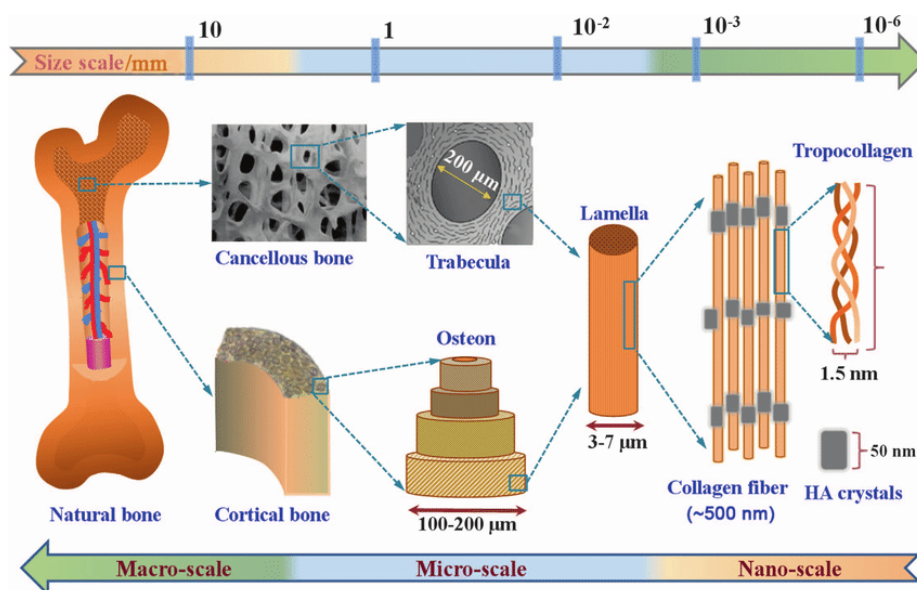
In bone biology, bone morphogenetic-2 (BMP-2) is the most revolutionary protein for its osteogenic potential when implanted in the extracellular soft tissue. After Food and Drug Administration (FDA) approval for single-level anterior lumbar interbody fusion (ALIF) in the United States of America (USA), BMP-2 clinical use increased from 0.7% to 24.9% of all spine fusion procedures performed between 2002 to 2006 (James et al., 2016). In 2007, BMP-2 use was higher than 50% for all primary ALIF and in many occasions its use has been endorsed as a promising alternative for autografts. Initially, industry-sponsored publications have not indicated the existence of adverse events associated with the use of BMP-2 but preliminary human trials suggested the contrary. The independent assessment of the previous data revealed complications associated with the use of BMP-2 in 20% to 70% of the cases (James et al., 2016). Therapeutic BMP-2 is normally administered at supra-physiological BMP-2 dosage as an attempt to overcome its faster degradation due to BMP-2 short half-life (7-16 min as determined by pharmacokinetic animal studies) (Poynton and Lane, 2002). With the use of carriers such as GAGs (i.e. heparin) one can stabilise, protect and extend growth factors (GF) half-life and eventually decrease the need of BMP-2 high dosages which is associated with life threatening side effects (i.e. cancer, ectopic bone formation). The current strategies applied for bone repair can improve patient's health condition but not significantly. Therefore, there is a demand for the development of innovative bone tissue engineering strategies to ultimately provide a cost-effective solution that allows not only osteoinduction and osteoconduction but also vascularization and engraftment as observed on healthy bone tissue; this will only be possible if new strategies result from interdisciplinary solutions combining chemical and physical cues on the guidance of stem cells and the presence of key extra cellular matrix (ECM) components to enhance biomaterials' performance.

Chapter 1 Literature review

1.1 Bone Tissue

Bone tissue is composed of cells, matrix molecules, crystallized minerals (hydroxyapatite), vessels and water. Bone's composition, structure and shape may vary according to bone function, age, genetic inheritance and living conditions (Smeltzer et al., 2010a). Bone plays an important role in the human body with three main functions a) calcium homeostasis and phosphate, magnesium, potassium and bicarbonate storage; b) mechanical support to soft tissues and c) haematopoiesis. In order to maintain functions, bone is continuously remodelling - cycling between bone formation and breakdown (Rodan, 1992). Structurally, bone tissue compromises a nanocomposite combination of a compact layer (i.e cortical bone) for mechanical support and a porous/spongy core (i.e. trabecular/cancellous bone) with higher metabolic activity (**Figure 1.1**). Dense cortical bone is composed of circular osteon repeat units (100-200 μ m) composed by bone cells, the osteocytes. Osteons are concentric collagens

Figure 1.1 The chemical composition and multiscale structure of natural bone tissue. Cancellous bone (Image adapted from (Gao et al., 2017))



layers (lamellae) surrounding blood vessels and nerves. Cancellous bone is composed of a framework of trabeculae filled with contain bone marrow. Although cancellous bone only counts to 20% of bone tissue, its porosity reaches to 50%-90% with a surface area almost 20 times higher than cortical bone. Cancellous bone – the organic phase - is mainly made of 90% of collagen type I and is responsible for high tensile strength while cortical bone - the inorganic phase - is composed by hydroxyapatite (HA) crystals and is a resistor of compression. Both trabeculae and osteon units are made of collagen fibres (diameter: ~500nm) containing triple helical tropocollagen fibrils (diameter: 1.5nm) with embedded calcium phosphate nanocrystals (HA) between collagen gaps increasing structure rigidity (Cheng et al., 2014; Gong et al., 2015a; Hadjidakis and Androulakis, 2006; Smeltzer et al., 2010b). Based on osteoid collagen formation and organization, two types of bone tissue can be distinguished: woven bone and lamellar bone. Woven bone occurs during fast collagen formation by the osteoblasts leading to a disorganized collagen fibril disposition only present in foetal tissues or fracture healing. The woven bone is always replaced by the high mechanically strong lamellar bone constituted by parallel collagen fibrils that is mainly found in the healthy adult skeleton (Kini and Nandeesh, 2012).

1.1.2 Bone development

Bone formation is a complex process which includes ECM synthesis (osteoid formation) by osteoblasts, matrix mineralization and tissue remodelling. Widely known as osteogenesis or ossification, osteoblasts can form bone via two different pathways: Intramembranous and endochondral ossification. These processes, however, are still not completely understood. (Kini and Nandeesh, 2012; Percival and Richtsmeier, 2013). While endochondral ossification is defined by the gradual substitution of cartilage by bone and marrow, intramembranous ossification is characterised by MSCs condensations that mature and directly differentiate towards the osteogenic lineage (Walmsley et al., 2016).

1.1.2.1 Intramembranous Ossification

This process is observed when primitive mesenchymal tissue condensations give rise to the formation of flat and long bones or during the healing process of fractures treated by open reduction or stabilization with metal. The main steps of this process are ossification centre formation, matrix mineralization, trabeculae development and periosteum development (Kini and Nandeesh, 2012).

1.1.2.2 Endochondral Ossification

This process occurs when cartilage tissue gives rise to the formation of long bones or during fracture healing treating by cast immobilization. Endochondral ossification occurs in several steps: cartilage development, cartilage growth, primary ossification centre formation during foetal development, secondary ossification centre development (after birth), articular cartilage and medullar cavity development and blood vessel formation. The first ossification initiates at the middle of bone diaphysis while the second ossification centre is localized in both epiphysis (long bone ends) (Kini and Nandeesh, 2012). The most widely accepted model for endochondral ossification suggests that hypertrophic chondrocytes undergo apoptosis in order to enable cartilage remodelling and cavity formation. As vasculature invasion transports progenitor cells into the cartilage tissue stimulating the subsequent replacement of cartilage for bone tissue. This idea has been challenged by recent studies which proposed a different view. In a study utilizing mice by *Hu et. al.*, it was observed that hypertrophic chondrocytes inside the trabecular bone can adopt a stem cell-like state expressing pluripotent markers such as sex determining region Y-box 2 (SOX2) before transdifferentiate into osteoblasts. Still, vascular invasion is essential for cartilage to bone transformation which is triggered by hypoxia and chondrocytes and endothelial cells expression of VEGF which regulates chondrocytes differentiation into osteoblast and lining cells. Regardless of these findings, origin and identity of signals for chondrocytes trans differentiation are unknown (Hu et al., 2017; Kini and Nandeesh, 2012).

1.1.3 Fracture Healing

Bone regenerates at a higher rate than other tissues. The spontaneous healing process must be done at a fast pace in order to restore tissue functions, however, if the tissue damage is too extensive, self-repair is substituted by the formation of non-union and scar tissue (Walmsley et al., 2016). The fracture healing process starts with an acute inflammatory response followed by MSCS recruitment from adjacent tissues due to BMP-2 release (Marsell and Einhorn, 2011). Bone fracture often heals through endochondral ossification (Hu et al., 2017). The healing process is divided by an initial anabolic phase and a long catabolic phase (**Figure 1.2**). During anabolic phase, tissue volume increases via the recruitment and differentiation of stem cells next to the fracture area leading to cartilaginous callus formation. Recruited cells are responsible for the start of the angiogenesis process, development of new vessels and higher blood flow in order to supply the new tissue with nutrients, minerals, GFs and others. After this stage, chondrocytes differentiation is stimulated by ECM mineralization and chondrocyte apoptosis indicates the end of anabolic phase. During catabolic phase, the previously formed cartilaginous callus decreases and specific anabolic activities remain. Subsequently, cartilage resorption is followed by secondary bone formation and primary angiogenesis continues. Bone and vascular remodelling also take place while tissue slowly regenerates and stabilizes functions to values observed pre-injury (Einhorn and Gerstenfeld, 2015).

1.1.4 Bone Remodelling

Bone remodelling combines a wide range of cell types for the continuous substitution of old or damaged tissue to newly synthesized bone while maintaining the balance between bone absorption and formation. Triggered by mechanical loading and biochemical cues, this process is regulated by several hormones, GFs, proteins, cytokines and others. A general overview about regulator molecules in bone formation or absorption is summarized on **Table 2.1**. This coordinated process regulated by osteoblasts and osteoclasts, is a lifelong

mechanism essential for maintaining the homeostasis of bone minerals and bone strength.

(Hadjidakis and Androulakis, 2006; Kini and Nandeesh, 2012)

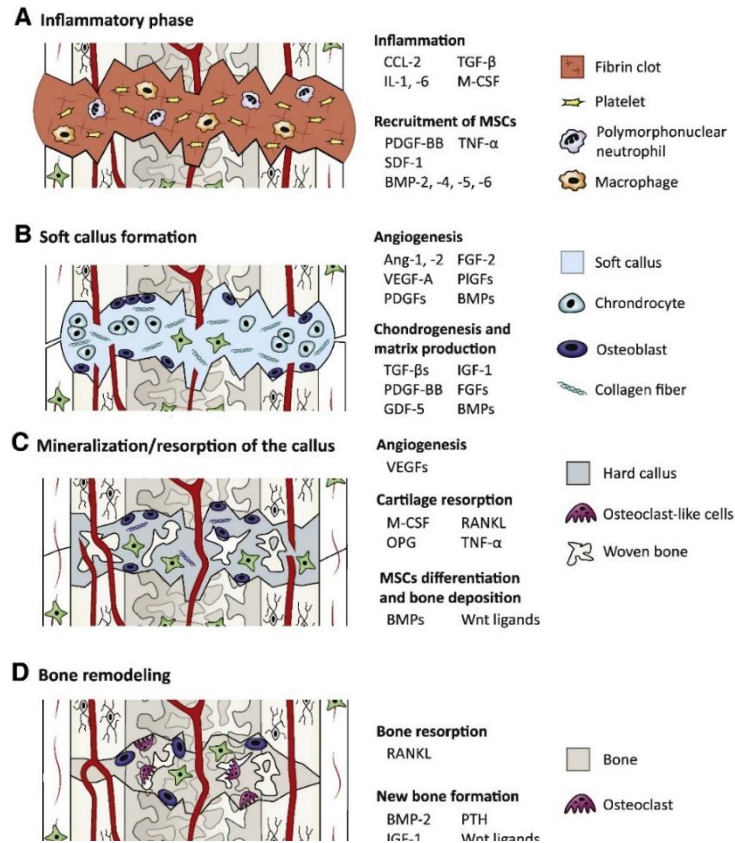


Figure 1.2 Phases of bone healing and key growth factors during catabolic and anabolic processes. Bone regeneration is divided into four phases that overlap each other. (A) inflammatory phase, (B) soft callus formation, (C) mineralization and resorption of the soft callus, and (D) bone remodelling. BMP = bone morphogenetic protein, FGF = fibroblast growth factor, GDF-5 = growth/differentiation factor 5, IGF-1 = insulin-like growth factor 1, M-CSF = macrophage colony-stimulating factor, OPG = osteoprotegerin, PDGF = platelet-derived growth factor, PlGF = placenta growth factor, PTH = parathyroid hormone, RANKL = receptor activator of nuclear factor κ B ligand, SDF-1 = stromal cell-derived factor 1, TGF- β = transforming growth factor β , TNF- α = tumour necrosis factor α , VEGF = vascular endothelial growth factor. Adapted from (Martino et al., 2015)

Table 1.1 Molecules responsible for stimulating bone formation and absorption. Specific cell markers are expressed during these processes. Adapted from Kini and Nandeesh, 2012.

	Bone formation	Bone absorption
Hormones	Growth hormone, Vitamin D metabolites, androgens, insulin, Low-dose PTH/PTHrP, progestogens	PTH/PTHrP, glucocorticoids, thyroid hormones, high dose of vitamin D
Growth Factors	BMP-2, BMP-4, BMP-6, BMP-7, IGF1, IGF2, TGF- β , FGF, PDGF	TNF, EGF, PDGF, FGF, M-CSF, GM-CSF
Cytokines	IL-4, IL-13, IFN, OPG	IL-1, IL-6, IL-8, IL-11, PGE ₂ , PGE1, PGG2, PGI2, PGH2
Cell Markers	Alkaline Phosphatase, osteocalcin, procollagen peptides	Hydroxylysine glycosides, acid phosphatase

1.1.5 Osteoclasts and Lining cells

Osteoclasts are multinucleated cells mainly derived from mononuclear bone marrow monocyte-macrophage precursor cells. These cells are the only ones identified to be capable of bone resorbing and play an essential role in bone remodelling. Cell receptor activator of nuclear factor Kappa-B (RANK; TNF superfamily) is present on osteoclasts precursors and its activation by ligand RANKL in combination with colony factor 1(C-FMS) signalling pathway, allows their differentiation into fully mature osteoclasts. Parathyroid hormone (PTH) receptor is highly expressed by osteoblasts and once activated, bone reabsorption increases. RANKL, macrophage CSF and osteoprotegerin (differentiation inhibitor) are secreted by osteoblasts and are essential for osteoclasts regulation (Atkins et al., 2006; Crockett et al., 2011; Kini and Nandeesh, 2012). Lining cells are early osteoblastic flat cells that protect bone surfaces from bone resorption or formation by preventing osteoblasts and osteoclasts from interacting with the surface. These quiescent cells might have a role in osteoclast differentiation however further studies are needed (Florencio-Silva et al., 2015).

1.1.6 Osteoblasts and Osteocytes

Mesenchymal stem cells have the ability to differentiate into mononucleated osteoblasts by triggering the canonical Wnt/ β -catenin pathway and associated proteins. During their differentiation process, osteoblasts morphology changes depending on their activity and maturation stage (**Figure 1.3**). Once differentiated, osteoblasts are responsible for

extracellular matrix synthesis and mineralization, osteoclasts function regulation and haematopoiesis regulation. (Kini and Nandeesh, 2012). Located along the bone surface, osteoblasts secrete 90% of bone matrix forming the osteoid. At the same time as this structure starts to mineralize, some of the osteoblasts get trapped inside. Slowly losing they capacity to synthetize ECM, mineralized osteoblasts differentiate into dendritic osteocytes – bone forming units.

Bone formation is controlled by bone morphogenic proteins (BMPs) by recruiting and activating Smad proteins that regulate the expression of an essential transcription factor for osteoblast differentiation, Runx2. An osteoblast progenitor population expressing Runx2 and CollA1 are defined to be in a proliferative state and their differentiation into preosteoblasts can be identified by alkaline phosphatase (ALP) activity. Preosteoblasts maturation to osteoblast can be identified by the expression of bone matrix proteins such as osteocalcin (OCN), bone sialoprotein (BSP) I/II, and collagen type I (Col I) as well as the expression of osterix (Osx) factor (**Figure 1.3**) (Crockett et al., 2011; Florencio-Silva et al., 2015; Kini and Nandeesh, 2012).

At the last stage of bone formation, osteocytes downregulate the expression of osteoblast markers (ALP and Col I) but upregulate the expression of dentine matrix protein 1 (DMP1) and sclerostin. Overall, ALP, Col I and osteocalcin are widely used as differentiation markers for osteoblasts while sclerostin and DMP1 are used as differentiation markers for mature osteocytes. (Crockett et al., 2011; Florencio-Silva et al., 2015) By sensing their surrounding environment, mature osteocytes act as mechanosensors that regulate tissue homeostasis, adaptation and remodelling according with daily external and internal forces. Osteocytes are connected metabolically and electrically by gap junctions with the disadvantage that with ageing gap junctions can develop malfunctions, stimulating osteocytes apoptosis (Florencio-Silva et al., 2015; Kini and Nandeesh, 2012). To determine which physical or chemical cues have a higher impact on the expression of specific osteogenic genes quantification by Real-Time Polymerase Chain Reaction (RT-PCR) is of great use.

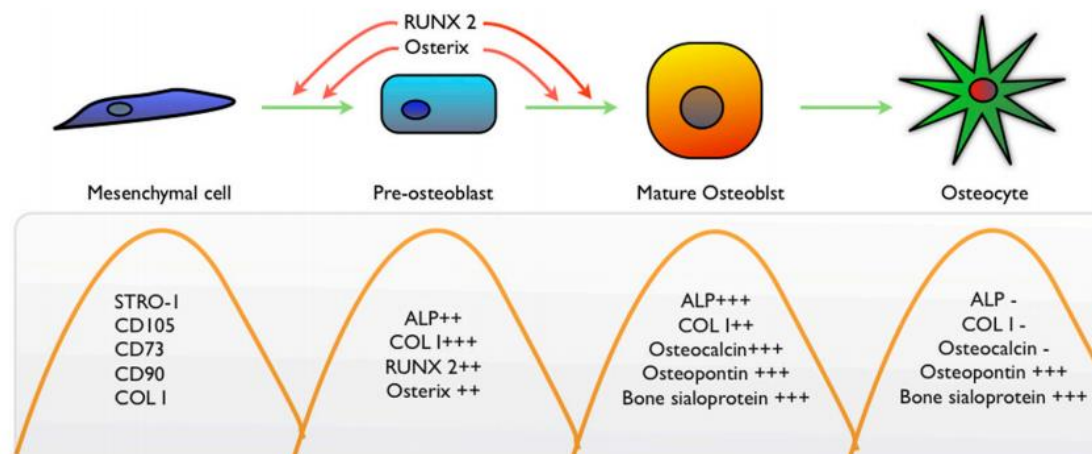


Figure 1.3 Cell surface markers expressed during osteogenesis differentiation. Osteogenic mesenchymal progenitor cells express Stro1, CD105, CD73, CD90 and Col I before their differentiation. An important step for differentiation is the expression of RUNX2 and Osterix transcription factors by MSCs. Osteoblasts, while producing bone matrix, express several factors such as Runx2, Osterix, ALP, Col I, casein kinase II and in a later stage osteocalcin. Once trapped inside the osteoid matrix, osteoblasts start to extend, connect to other cells in the surrounding environment and differentiate into an early stage osteocyte (expression of PHEX, MEPE, E11/GP38, destrin, MT1-MMP, DMP1, CapG). A mature osteocyte has a dendritic morphology and a higher expression of FGF23, ORP150 and sclerostin which is a marker of mature osteocytes. Image adapted from (Miron and Zhang, 2012).

1.1.7 The role of TGF- β /BMP-2 signalling in bone

In 1965, Marshall Urist identified a presence of a substance in the ECM with the ability to induce osteogenesis - BMP-2 from the TGF- β superfamily. Since this discovery, BMP-2 has leaped from basic biology to clinical applications where several human clinical trials have effectively shown positive effects on fracture healing induced by BMP-2 treatments. (Majidinia et al., 2018). Among the existent 14 BMPs, BMP-2, 4, 5, 6, 7 and 9 have demonstrated high osteogenic activity (Wu et al., 2016). TGF- β /BMP bind to specific type 1 and type 2 serine/threonine kinase receptors (**Figure 1.4**) triggering both canonical Smad-dependent pathway (TGF- β /BMP ligands, receptors and Smads) and non-canonical Smad-independent signalling pathway (e.g. p38 mitogen-activated protein kinase pathway, mitogen-activated protein kinases (MAPK)). In different ways, Smad and MAPKs upregulate osteoblastic

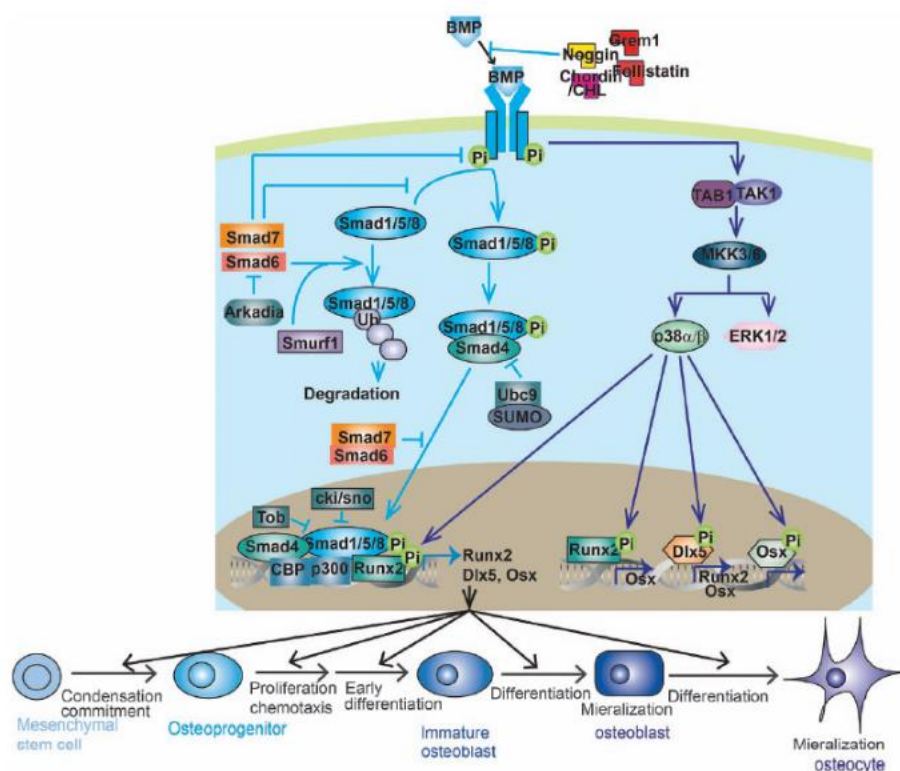


Figure 1.4. BMP-2 signalling pathway in skeletal bone development. Noggin, Gremlin, Chordin, Chordin-like proteins (CHL) and follistatin are BMP-2 antagonists. When BMPs bind to homodimeric type II receptors Smad-dependent and non-dependent signalling pathways are activated. In Smad-dependent pathways, phosphorylation of R-Smad (Smad1, 5, 8) with Smad4 complexes translocate into the nuclei that along with co-factors recruitment regulates osteogenic gene expression of Runx2, Dlx5 and Osx. The Smad non-dependent pathway phosphorylates TAK1 that recruits TAB1 to initiate MKK-p38 MAPK or MKK-Erk1/2 signalling pathways. MKK-p38 MAPK promotes Runx2 transcription while Smad7 acts as an antagonist for preventing R-Smads phosphorylation. Schematic adapted from (Wu et al., 2016).

differentiation genes and bone formation (Chen et al., 2012; Majidinia et al., 2018). These signalling pathways are important during bone development and postnatal skeleton homeostasis. GFs are easily susceptible of degradation but by manipulating their bioavailability (e.g., ECM), stability and respective signalling pathways, new treatments can be developed for bone disorders.

1.1.8 WNT Pathway

The signalling pathway Wnt is essential for osteoblast differentiation alongside the sympathetic nervous system (Crockett et al., 2011; Florencio-Silva et al., 2015). Wnts are secreted glycoproteins that regulate a wide range of cellular activities (e.g proliferation, survival, differentiation, polarity and gene expression). The regulation of these processes varies at different stages of osteogenesis and when impaired activities of Wnt pathway are observed, osteoporosis can occur (Kini and Nandeesh, 2012). The canonical Wnt signalling cascade depends on β -catenin (**Figure 1.5**). In the absence of Wnt binding to Frizzles (Fz) receptors β -catenin is sequestered, phosphorylated and degraded by the proteasome. In contrast, if Wnt binds to Fz this leads to β -catenin accumulation within the cytoplasm which is translocated into the nuclei targeting a specific gene expression and protein synthesis.

As previously reported, β -catenin can promote osteoblasts differentiation and maturation while suppressing chondrogenesis and adipogenesis. BMPs and Wnt signalling pathway are interconnected and share common targets but other signalling pathways are also involved. The full picture of Wnt pathway interactions is still not fully characterised (Houschyar et al., 2019).

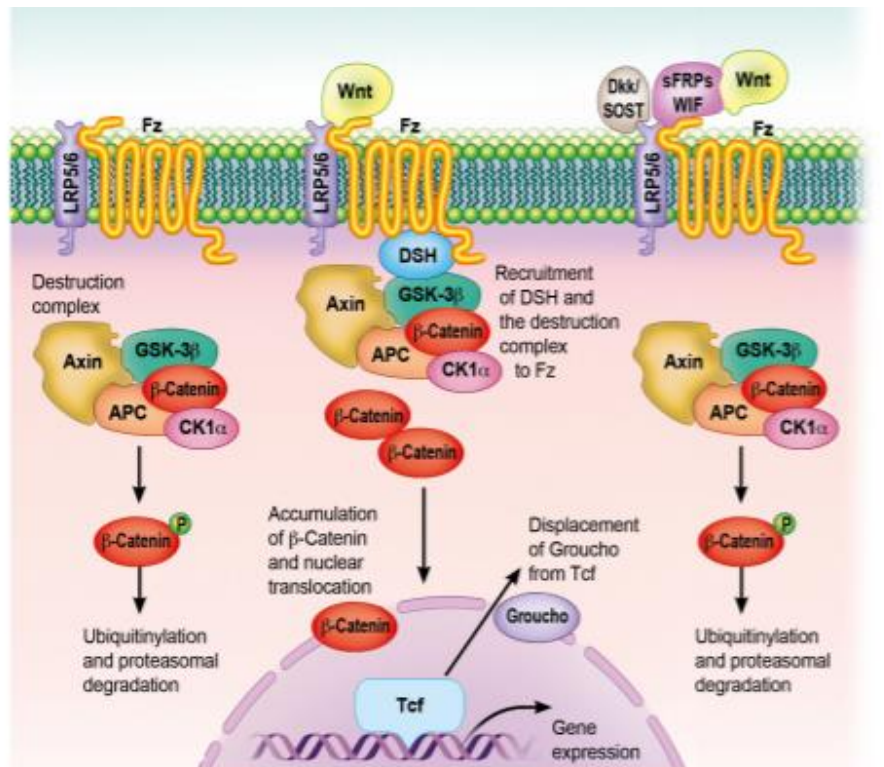


Figure 1.5. The canonical Wnt signalling pathway. Wnt protein are found are normally found associated to cell membranes and the ECM. This pathway is activated by the binding of specific Wnt ligand to Fz receptors and low-density lipoprotein receptor-related 5 or 6 (LPR5\6) co-receptors. In the absence of Wnt, β -catenin is continuously degraded but once the Wnt-receptor binding is established, destruction complex is degraded while cytoplasmatic β -catenin is accumulated and translocated to the nuclei. While non-canonical Wnt antagonists, nuclear β -catenin activates gene transcription Runx2/Osterix. Image adapted from (Houschyar et al., 2019)

1.1.9 Bone Mineralization

Biomineralization is a dynamic process that occurs not only in bones but also in other tissues (i.e. dentin, enamel, cementum) and is characterised by mineral crystals deposition around and within ECM and cells. Matrix mineralization starts at the osteoid in the presence of calcium and phosphorus, the main components of hydroxyapatite (HA) crystals formed inside collagen fibril gaps. Vitamin D stimulates the mineralization of the osteoid as well as the upregulation of osteocalcin, collagen type I and alkaline phosphatase (Abou Neel et al., 2016; Ye et al., 2016).

Numerous theories are still under debate regarding if calcium and phosphorous precipitation acts as a precursor step in hydroxyapatite crystals formation. Regardless of controversy, it is believed that non-collagenous proteins present in bone ECM have an important role on apatite

nucleation and assembly. For example, osteocalcin, the most abundant non-collagenous ECM protein present in the bone has shown in different studies the potential to increase bone formation by improving osteoblast-like cells attachment to mineralized matrix. In contrast with these evidences, it was also previously reported in a mouse study where absence of osteocalcin did not affect bone adsorption but increases bone formation. These contradictory findings open a question mark about the true function of osteocalcin as a bone mineralization regulator. Bone mineral deposits contain, besides HA, other minerals previously identified by Raman spectroscopy, such as, amorphous calcium phosphate (ACP), octacalcium phosphate (OCP), β -tricalcium phosphate (β -TCP), and dicalcium phosphate dehydrate (DCPD) (Tsao et al., 2017). On non-mineralized tissues, the mineralization process is inhibited by the presence of inorganic pyrophosphate (PPi). Osteoblasts and osteoclasts have the ability to control the level of extracellular PPi through the production of nucleotide pyrophosphatase phosphodiesterase 1, ankylosis protein (ANK) and tissue-nonspecific alkaline phosphatase (TNAP) (Tsao et al., 2017).

1.1.10 *In Vitro* Osteogenesis

Standard osteogenic differentiation media are commonly used during experimental assays. For an optimal effect, osteogenic media is routinely supplemented with dexamethasone (10-100 nM), ascorbic acid (50 μ M) and β -glycerophosphate (≥ 2 mM), although other components, such as BMP-2 or FGF2, might be added to stimulate differentiation. Dexamethasone is a corticosteroid that induces Runx2 expression through TAZ and MKP1 activation. Ascorbic acid promotes collagen type 1 secretion which is essential for osteoblast differentiation while β -glycerophosphate promotes mineralization as a phosphate source (Ghali et al., 2015; Langenbach and Handschel, 2013). Despite this standard guidelines, media formulations are optimized according to each lab and cell line.

1.1.11 Cell Lines

In regenerative medicine is essential to understand how specific cues control cellular differentiation. To achieve this purpose, the use of immortalized cell lines such as the C2C12 murine myoblast line are very useful. C2C12s, firstly isolated from mouse muscle, is a cell line with the ability to undergo steps in differentiation from muscle precursor to myoblast. Step-by-step differentiation allows a more detailed characterisation of which regulates C2C12s transdifferentiation. This cell line is not only restricted to muscle differentiation but also has the ability to differentiate into different lineages and thus can be used for bone lineage commitment studies. C2C12 cell lines treated with BMP-2 recapitulate osteoblastic-like differentiation from precursor cell to osteoblasts, expressing stage-specific markers such as RUNX2, OSX and ALP as well as cellular matrix deposition (Montano M., 2014). Although MSCs have great potential for bone repair studies, by staging osteoblast differentiation C2C12 cells are commonly used due to their well establish protocols, easy maintenance and less time consuming experiments.

1.2 Stem Cells

Stem cells are essential for tissue regeneration. These cells can be defined as totipotent, pluripotent or multipotent depending on their differentiation ability. A totipotent stem cell - harvested from a fertilized egg - has the potential to differentiate into any kind of cell including extraembryonic tissues. During development, the fertilized egg matures into a 4- to 8- cell embryo and loses its totipotent potential. As maturation continues, a blastocyst is formed and cells harvested from its inner layer have now pluripotent potential which allows the differentiation into all 3 embryonic germ layers (ectoderm, mesoderm and endoderm). On subsequent divisions, stem cells continue to lose their differentiation potential until a multipotent adult stem cell is formed with the ability to differentiate – however with a limited potential – into multiple lineages (Brignier and Gewirtz, 2010; Hwang et al., 2009). In 2006 a huge scientific breakthrough was achieved by Yamanaka's group by reporting the conception of a new type of stem cell, the induced pluripotent stem cell (iPS). According with their findings,

differentiated cells under embryonic stem cell culture conditions can be reprogrammed into an embryonic-like state by introducing 4 nuclear factors (Oct3/4, Sox2, cMyc, Klf4). (Takahashi and Yamanaka, 2006). In bone regeneration research, osteoblasts and multipotent cells can be used as cell sources. Multipotent stem cells have been localized in different locations: bone marrow, periosteum, skeletal muscle and umbilical cord blood. Nevertheless, multipotent mesenchymal stem cells (MSCs) from bone marrow appear to be the most promising choice for bone regeneration due to its easy isolation, high proliferation rate and differentiation potential which confers them a high therapeutic capacity when compared with other sources. (Walmsley et al., 2016)

1.2.1 Mesenchymal Stem Cell

In musculoskeletal tissue regeneration strategies, mesenchymal stem cells (MSCs) appear as the most promising choice due to their high therapeutic potential. MSCs were for the first time identified and isolated from guinea pig bone marrow by Friedenstein in 1976 and since then these cells have been extensively used, studied and characterised (Chen et al., 2008). MSCs are adult multipotent stem cells with high proliferation rate, immunomodulatory capacity, trophic ability and capable to differentiate into mesenchymal tissues (e.g. bone, cartilage, adipose, muscle, tendon, ligament and marrow stroma). These spindle-shaped cells can be harvested from several tissues such as adipose tissue, synovium, dental pulp, cord blood and umbilical cord, being bone marrow considered the “classical” reservoir of MSCs since it is the most used and convenient source. Minimal criteria for MSCs was proposed by the International Society for Cellular Therapy and states that in order for a cell to be classified as a human MSCs it must be plastic adherent, express CD105, CD73 and CD90, lack hematopoietic markers (e.g. CD45 – classic hematopoietic marker, CD34, CD14) and differentiate into osteoblasts, adipocytes and chondroblasts *in vitro* (Brignier and Gewirtz, 2010; Dominici et al., 2006; Marot et al., 2010; Viganò et al., 2016).

In addition to the expression of this wide range of markers, MSCs can also express markers not exclusive of this population. For example, Stro-1 is a well-studied MSCs positive marker

that is not present in rat cells but is expressed in human MSCs with colony-forming unit (CFU-F) capacity. It is known that this marker can be identified in early passages but it is lost during extensive cell expansion which may be linked with its role in cell stemness maintenance. CD106, also expressed in MSCs, has a role in signal transduction and cell adhesion and when expressed in Stro-1 positive cells it increases the frequency of CFU-Fs. MSCs also express embryonic gene markers - *oct-4*, *sox-2* and *rex-1*. This expression may only probably occur during a cellular quiescent state which can be altered once a differentiation pathway is activated (Kolf et al., 2007). The immunophenotype characterisation of rat bone marrow MSCs by International Society for Stem Cell Research (ISTC) have shown similarities with human MSCs. 90% of rat MSCs population is positive for CD29, CD49e, CD73, CD90, CD105, Stro-1 and negative for CD11b, CD45. This phenotype is more homogenous between passage 3 to 8 where a higher degree of enrichment can be achieved using techniques such as MACS and FACS can be applied (Harting et al., 2008).

Besides their self-renew and differentiation capacity, generally, MSCs can be stimulated to migrate and populate inflamed/tumorigenic areas and assist in wound repair. GFs such as platelet derived growth factor (PDGF), insulin like growth factor 1 (IGF-1) and chemokines (CCR2, CCR3, CCR4 or CCL5) proved to regulate MSCs migration and homing in *in vitro* studies (Farini et al., 2014). MSCs homing capacity is essential in the cellular therapy field. During bone fracture, the stromal cell-derived factor-1 (SDF-1)/CXCR4 signalling pathway is mainly responsible for the recruitment of MSC while monocyte chemoattractant proteins (MCPs) are regulators for MSCs migration to fracture sites and subsequent healing (Lin et al., 2017). In fact, MSCs can trigger other cells differentiation and proliferation or even decrease inflammation and immune reactions by secreting soluble factors. For example, the soluble factors hepatocyte growth factor-1 (HGF), interleukin-1 (IL-1), IL-1 β , IL-3, IL-6, IL-7, IL-11, stem cell factor (SCF) and FMS-like tyrosine kinase 3 ligand stimulate angiogenesis process and mitosis. MSCs immunomodulatory properties allows them to suppress inflammation by inhibiting memory T cells proliferation and function by decreasing pro-inflammatory cytokine

release and increasing anti-inflammatory cytokines (e.g. IL-4 and IL-10) (Ben-Ami et al., 2011; Chen et al., 2008).

1.2.2 Stem Cell Niche

The stem cell niche is a concept primarily described by Schofield in 1978 in hematopoietic stem cells (HSC) in bone marrow (Schofield, 1978). In vivo, stem cells are surrounded by a microenvironment - the niche - that regulates their survival, self-renewal and differentiation by establishing growth factor-cell, cell-cell and cell-ECM interactions. Inside the niche, MSCs stemness and self-renewal is vital. The stemness stage is regulated by Wnt signalling pathway and factors such as leukaemia inhibitor factor (LIF) and fibroblast growth factors (FGFs). As it was previously observed in *in vitro* studies, stem cell niches are naturally hypoxic environments to maintain stem cells under their undifferentiated state and only increasing stem cells proliferative potential when required (Tsai et al., 2011). Hypoxia can be observed on bone tissue niches, as low as 10mmHg, stimulating bone formation and angiogenesis mediated by hypoxia inducible factor 1 α (HIF-1 α) (Kolf et al., 2007; Stiers et al., 2016). Within the stem cell niche, the homeostatic balance between self-renewal and differentiation is maintained by the asymmetric and symmetric stem cell division. This balance is crucial to avoid stem cell population reduction or tumorigenesis. Bone marrow is a widely studied niche where two different types of stem cell niche coexist, the osteoblastic niche localized on the endosteal bone surface (MSCs) and the vascular niche localized on the sinusoidal vessel. These two niches have different and important roles during HSC regulation (Yin and Li, 2006). Normally localized near trabecular bone, bone marrow niches, have been mimicked by scientists but with few successes since HSCs are not able to expand efficiently *in vitro*. The exact location and size of MSCs niches are still not fully defined, however, examples of spatially and structurally characterised niches exist, such as, the hair follicle (Wang et al., 2015) cornea and crypts of intestinal villus (Ortega et al., 2013a). For example, the bulge area in the hair follicle is the skin stem cell niche where dermal fibroblasts, melanocyte stem cells and adipocytes act as supportive cells (Rompolas and Greco, 2014; Wang et al., 2015) while limbal stem cells in

the eye cornea are located in 120-150 μm size crypts named palisades of Vogt (Ortega et al., 2013a; Schermer et al., 1986). In the intestine, stem cell niches are localized in the villi bases crypts known as Paneth area with an approximate area of 51.1 μm^2 in healthy humans (Elmes et al., 1983). In this structure stem cells proliferate and migrate upwards the crypts while differentiating into epithelial cells. Other niches can also be identified in muscles (satellite cells), brain (hippocampus) and bone marrow (sinusoidal surface) (Turner and Dalby, 2014). The characteristics of some musculoskeletal tissues stem cell niches are summarized in **Table 2.1**.

Within these niches, a comprehensive understanding on which interactions and components are responsible for tissue regeneration was not possible. The current overall knowledge about stem cell niches composition and function is increasing however the exact evidence related to the identity of all its components is still unknown. More than a defined area, a niche may probably be a development process that adapts to tissue needs and can be found spread in different parts of the tissue instead of one single cluster. Through all the existent literature, it is possible to notice that niche size and frequency of appearance varies according with tissue type and is often measured by the number of progenitor cells. For example, a study showed that osteoblasts are activated by the PTH/PTHrP receptor (PPR) to produce hematopoietic growth factors which influences positively the HSC niche size by upregulating Notch signalling molecules (Bianco, 2015; Calvi et al., 2003). Low sulphated GAGs can be found in stem cell niches protecting cell from overexposure of chemical stimuli (i.e. GFs). As cells lose their pluripotency, ECM GAGs composition increase in sulphation content allowing protein binding and cells stimulation towards a differentiation pathway (Soares da Costa et al., 2017). Regardless of present findings stem cell niches size still remains a subject of debate and study.

Table 1.2. Musculoskeletal tissues: stem cell niche location, composition and stiffness. This table summarizes the main information about human bone, articular cartilage, skeletal muscle and tendon. *This value was obtained from a rat experiment.

	Niche Location	ECM Composition	Stiffness	Reference
Bone	Trabecular bone endosteal surface	Organic phase (20-40%) collagen type I, proteoglycans and non-collagenous proteins. Lipids (3%) Hydroxyapatite (50-70%) Water (5-10%) Osteoid: 95% Col I	Dense Bone: 10^6 kPa Osteoid: 27 ± 10 kPa Osteogenesis occurs between 25 - 40kPa.	(Clarke, 2008; Coulson-Thomas et al., 2015; Engler et al., 2006; Guerrouahen et al., 2011; Hu et al., 2017)
Articular Cartilage	Cartilage surface, perichondrium (groove of Ranvier), synovium and fat pad	Water (80%) Collagen type II Proteoglycans (10-15%) Non-collagenous proteins	100 - 2000 kPa	(Candela et al., 2014; Sophia Fox et al., 2009; Zhang et al., 2009)
Skeletal Muscle	Beneath basal lamina and the outside the myofiber plasma membrane	Up to 7 types of collagen: mainly type I, III and IV (1-10%) Glycoproteins Proteoglycans Non-collagenous proteins	8 – 17 kPa	(Engler et al., 2006; Kjaer, 2004; Yin et al., 2013)
Tendon	Vasculature capillaries walls, small blood vessels, arteries adventitia, peritenon	Collagen (60 – 85%) mainly type I, proteoglycans Non-collagenous proteins Water (55 – 70%)	310 kPa*	(Kjaer, 2004; Levental et al., 2007)

1.2.3 Extracellular Matrix

Secreted by cells, ECM is a non-cellular component responsible for the structural support that acts as a water and growth factor reservoir. By presenting biochemical and biomechanical cues to cells the ECM regulates tissue morphogenesis, homeostasis and differentiation. This dynamic structure is mainly composed by water, fibrous proteins (e.g. collagen, elastin), adhesive glycoproteins (e.g. fibronectin, laminin), proteoglycans, polysaccharides and ECM receptors (e.g. integrins) that mediate cells attachment. Fibrous proteins provide ECM tensile strength and elasticity. Collagen is a fibrous protein that constitutes 30 wt.% of all proteins and 90 wt.% of all ECM which provides tensile strength, cell migration support, cell adhesion

regulation and directs tissue development (Discher et al., 2009; Frantz et al., 2010). In bone, several GFs can be identified such as TGF- β), insulin-like growth factor-1 (IGF-1), bone morphogenetic proteins (BMPs), platelet-derived growth factor (PDGFs) and cytokines interleukin-1 (IL-1) (Cheng et al., 2014). ECM content and characteristics vary according to tissue type. In bone tissue, ECM is mainly composed of collagen Type I, also contains collagen Type III but in lower percentage (Walmsley et al., 2016).

1.3 Cell-Surface and Cell-Cell Interactions

Mechanobiology is a recently emerging research field focused in the importance of biological mechanical properties. The ability of cells to sense their surrounding environment using the actin skeleton, integrins and other proteins is vital. This ability allows the formation of cell-cell and cell-ECM focal adhesion regions leading to a subsequent cellular chemical response. (Levental et al., 2007) Focal adhesion regions are an assembly of transmembrane adhesion receptors which stability is dependent on ECM stiffness. Higher ECM stiffness stimulates cells to a higher degree of cytoskeleton organization and anchoring as a result of substrate stiffness in comparison with soft ECM (**Figure 1.6**) (Discher et al., 2009; Engler et al., 2006; Wells, 2008). Cytoskeleton tension is an important transducer of physical stimuli to cells. The tractional force, high on focal complexes and lower on focal adhesions, influences cytoskeleton tension (Turner and Dalby, 2014). Cells sensing is reduced to short distances thus cells that grow on a stiff ECM will have a different response to the ones that grow on top of other cells. The influence that a substrate has on cells can be detected by their expressed phenotype. (Wells, 2008). When changing surface topography, cells shape, adhesion, size and polarity vary (Newman et al., 2016) as cells can respond to objects as small as 5nm (Beachley and Wen, 2010). For example, surface roughness can increase protein adsorption by increasing the available surface area which affects cells shape and/or adherence. On flat surfaces cells tend to have higher spreading area when compared with the rounder shapes observed on nanofibers scaffolds. These changes can also be observed on fibres with higher diameter (higher spreading) in contrast with lower diameter (rounded morphology). These

observations come from the fact that cells might sense a surface with thinner fibres closer to a flat surface (Beachley and Wen, 2010). Surface topography seems to guide cells towards specific differentiation pathways by activating specific mechanotransduction pathways but these mechanisms still remain poorly understood. In contrast with previous studies, Newman et al. found that aligned surfaces do not stimulate osteogenesis, instead, myogenesis is stimulated (Newman et al., 2016). For example, surface effect on cells shape and differentiation were analysed by Kim et al. 2014 on PLGA nanogrooved, nanopillar and nanopit arrays. Elongated nanogrooved arrays aligned cells spreading along the grooves in comparison with random oriented shapes on flat surfaces. Osteogenesis potential decreased on micropattern substrates in comparison with nanopattern substrates. These findings suggest that nanoscale topography have an important role between cell-substrate interaction and directing cells function. In this study it was observed that nanopost density and spacing might have influence on cells cytoskeleton by regulating cell spreading while nanopits order and symmetry showed potential to increase significantly osteopontin and osteocalcin expression. In completely ordered or completely random nanopits human MSCs (hMSC) cultures the upregulation of osteogenic proteins was not observed, only when cultured on

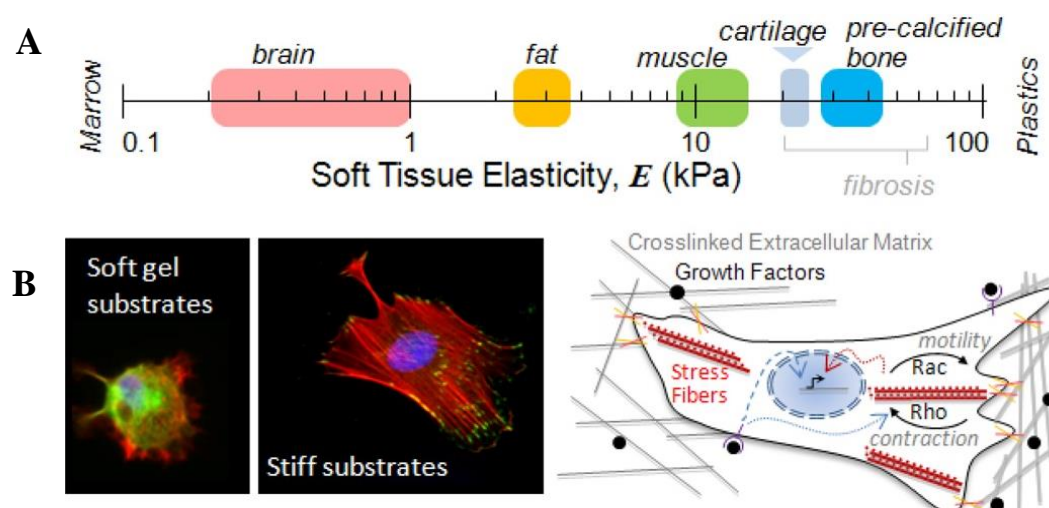


Figure 1.6 Effect of surface stiffness on stem cells. A) In vivo tissue elasticity (kPa) from soft tissue to hard tissues. B) Cells cultured in vitro on soft and hard surfaces. On stiffer substrates focal adhesions, stress fibers number and spreading is higher than on soft surfaces. Cells signaling pathways are influenced by growth factor and surface anchoring. These mechanisms also stimulate Rho-GTPase activity and subsequently fibers stress. Rac and Rho have important roles in stem cell motility, contractility and anchoring. (Discher et al., 2009)

slightly irregular surfaces (Gong et al., 2015a; Kim et al., 2014). In another study, Sun et al. observed that microgrooved arrays with a width of 1-2 μm enhanced MG-63 sarcoma cells osteogenesis (Sun et al., 2016). Overall, numerous studies suggest that scaffolds nano-topography enhances bone formation and implant integration (Amini et al., 2012). GAGs are an important part of ECM which characteristics and potential are described in the next section.

1.4 Glycomics

Nucleic acids, proteins, lipids and glycans are the four major cellular macromolecules essential to life. Addition of glycans to protein and lipids is the most diverse and abundant post-translational modification in nature. The possible structural arrangements are immense and its diversity increases by adding chemical modifications such as, phosphorylation, sulfation and acetylation (Hart and Copeland, 2010). The challenge that researchers face in glycomics is like no other. Glycomics, is a new emerging field that aims to decipher glycans physiological role, structure and biosynthesis by studying the entire glycan collection of an organism, tissue, cell or protein. Involved in almost all physiological processes, these natural biopolymers are present in all cellular surfaces (**Figure 1.7**) (Lanctot, 2007; Valverde et al., 2019). In the 1970s, Dietrich et al. studied for the first time glycan distribution in all classes of invertebrates but then the analytical techniques available at the time were not sufficient to determine glycans composition (Bertozzi and Sasisekharan, 2009). For example, while databased methods are commonly used for protein analysis, glycans analysis is far behind. Despite progress and existence of more effective analytical methods, the fact that glycans biosynthesis is not template-driven but rather depends on a combination of enzymatic reactions, the ability to predict glycans structure based on genomic or transcriptomic information is not entirely possible (Duan and Amster, 2018; Wang and Boons, 2011). Partial sequence analysis of shorter HS and heparin derivatives analysis has been performed by different methods such as exoenzymes, radioactive end-labelling, mass spectroscopy and more recently labelling with biorthogonal reaction pair (“click-chemistry”) (van Kuppevelt et al., 2017). Overall, having

different hierarchical levels of structural complexity, the glycome is far more complex and dynamic than any genome or proteome and this translates in higher difficulty of analysis. Slowly catching up, glycomics continues to lag behind genomics and proteomics as its future depends on improved automated, accurate and high-throughput analytical methods (Bertozzi and Sasisekharan, 2009; Duan and Amster, 2018).

1.4.1 Glycosaminoglycans (GAGs)

Proteoglycans are macromolecules composed by a protein core attached covalently to one or more chains of unbranched glycosaminoglycans (GAGs), except hyaluronan. GAGs are composed of repeating disaccharide units usually composed of an amino sugar with a uronic sugar (Figure 4). By being the most common component in ECM interstitial space, GAGs have important roles in cellular processes and growth factor interaction. These highly hydrophilic molecules have the capacity to acquire a hydrogel structure to support compressive forces acting as modulators of tissue biomechanical properties (Esko et al., 2009; Frantz et al., 2010; Lanza et al., 2020). Some studies have proposed that GAG function adjusts and adapts according to the type of tissue. For example, GAG molecules extracted from the cellular

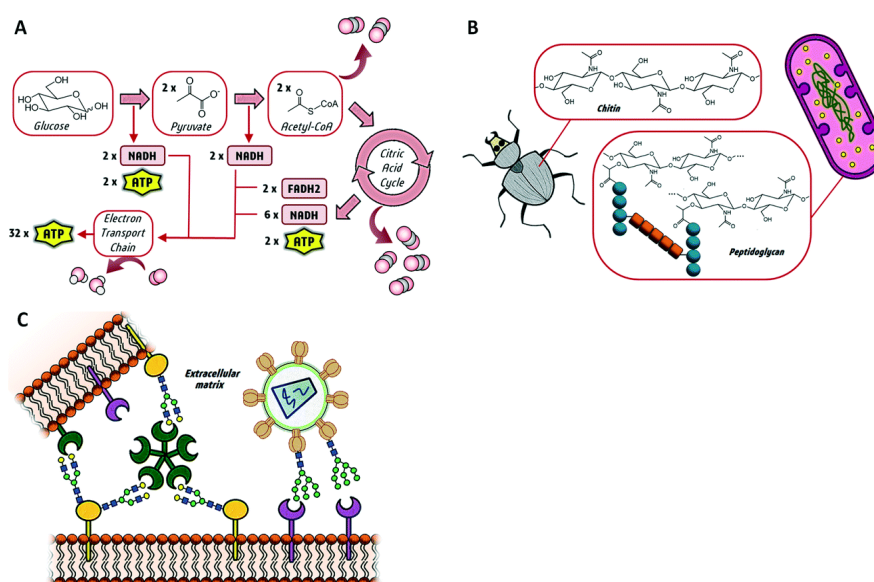


Figure 1.7 Main biological roles of glycans. A) Energy source, B) Structural elements and C) recognition elements in cell-cell and cell-pathogen interactions. For having such wide possible biologic interactions, glycans equally have great interest for clinical applications. Adapted from (Valverde et al., 2019).

surface of osteoblasts have proved to have special affinity to RANKL growth factor inhibiting the osteoclastogenesis (Ling et al., 2010a). These molecules have a vital importance on cell-cell, cell-ECM and growth factor interactions which makes them very interesting molecules for tissue engineering research. For example, in bone tissue, a special proteoglycan family named small leucine-rich proteoglycans (SLRPs) is known for its participation in bone formation, remodelling, mineralization and cell proliferation. Two previously described bone SLRPs molecules are biglycan (expressed during cell growth) and decorin (expressed in the early stages of ECM deposition) (Coulson-Thomas et al., 2015). GAGs are divided by groups: Hyaluronan (HA), heparan sulfate/heparin (HS), chondroitin sulphate (CS)/dermatan sulphate (DS) and keratan sulphate (**Figure 1.8**). GAG molecules containing negatively charged sulphate groups bind with positively charged amino acids of several proteins and GFs increasing their availability in the local area (Coulson-Thomas et al., 2015). A study by Mathews et al., described that hMSCs cultures on GAG treated plates stimulated the osteogenic differentiation by upregulating the expression of osteogenic genes (Mathews et al., 2014) probably by protecting cellular GFs from degradation.

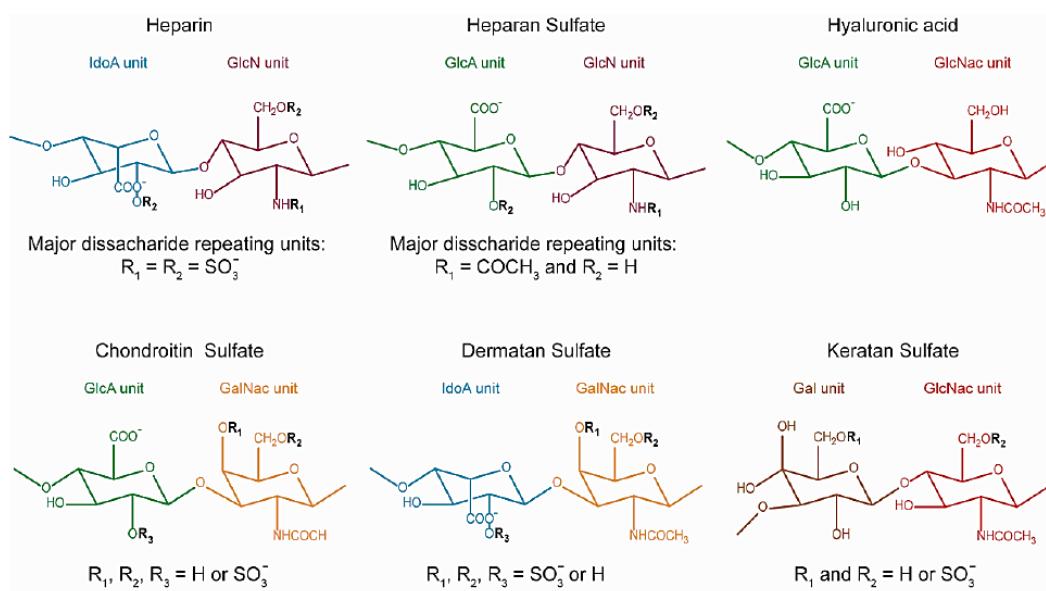


Figure 1.8 Glycosaminoglycans structure according to main disaccharide composition. GAG are composed of combined uronic acids [β -d-glucuronic acid (GlcA) or α -l-iduronic acid (IdoA)] and amino sugars [α -d- or β -d-glucosamine (GlcN), N-acetylglucosamine (GlcNAc) or N-acetyl-galactosamine (GalNAc)]. Image adapted from (Neves et al., 2020)

1.4.2 Heparan sulphate/Heparin

Heparin is a highly sulphated analogue of heparan sulphate (HS) found in granules within mast cell of lungs, liver and kidney (Murali et al., 2013). HS/heparin have an important role in a wide array of biological regulatory functions. This multifunctionality depended on their structural microheterogeneity that is controlled by various tissue/cell-specific enzymes during biosynthesis (**Table 1.3**) (Shriver et al., 2012). HS/Heparin molecules have been linked to neurodegenerative diseases, viral and bacterial infection mediation and GAG composition in tumours was shown to differ from healthy tissue (Weiss et al., 2017). The only intracellular GAG – heparin – is a natural anticoagulant that activates antithrombin, an inhibitor of coagulation signalling cascade. Normally obtained from porcine tissues, heparin highly charged heterogeneous structure confers this molecule the ability to interact with a wide range of proteins where some interactions not yet fully understood can lead to unexpected biological activities (Taylor et al., 2019; Valverde et al., 2019).

Table 1.2. Structural differences between heparan sulphate and heparin. Adapted from (Xu and Esko, 2014)(Baik et al., 2012)(Baik et al., 2012)(Baik et al., 2012)(Baik et al., 2012)(Baik et al., 2012)

Characteristic	Heparan sulphate	Heparin
Size	20-100kDa	7-20kDa
Cell membrane attached?	Yes	No
Site of synthesis	Virtually all cells	Mast Cells
Core Protein	Many (~17)	Serglycin
Sulphate groups per disaccharide	0.6-1.8	1.8-2.6
N-sulfate	30-60%	>80%
2-O-Sulfate	10-40%	>80%
6-O-Sulfate	10-40%	>80%
Iduronic Acid (IdoA)	20-50%	>70%
Binding to antithrombin (ATII)	0-0.3%	~30%
Commercially available	Miligrams	Kilograms

The possibility of side-effects alongside with its anticoagulant potential makes heparin less desirable for tissue engineering applications than HS. Heparin is a large polysaccharide with an average molecular weight of 12000 Da and polydispersity of 1.2-1.4. Being a hydrophilic molecule, heparin has the ability to retain 2-10% water even after extensive drying process and can maintain its charge inalterable in a wide range of pH values. The high content of reactive functional groups gives heparin the advantage prone to attach surfaces when using specific chemistry methods (Murugesan et al., 2008). This characteristic is of great use in the development of biofunctional scaffolds for tissue repair. Biologically, heparin enhances FGF-2 activity increasing osteoblast differentiation and proliferation (Ling et al., 2010). Bone formation is also potentiated by heparin which regulates BMP-2 release and enhances its osteogenic activity. (Bhakta et al., 2012) Besides osteogenic stimulation - and due to its

complex interaction with several proteins - heparin can also stimulate bone resorption when interacts with osteoprotegerin (OPG) (Ling et al., 2016). Aside structural similarities, heparin makes a useful model for HS protein-binding sites and its biological functions since it is already used therapeutically and its optimized production allows it to be readily available (Mulloy and Forster, 2000). Besides, heparin has a more homogeneous composition than HS that combined with a well-optimised process of isolation produces molecules that display lower batch-to-batch variability (Shriver et al., 2012). Heparan sulphate (HS) is a linear sulphated heterogeneous polysaccharide found in virtually all animal tissues, ECM and cell membranes. Like heparin, HS can interact with different GFs (i.e, BMP-2, FGF-2) increasing their stability, bioavailability, bioactivity and half-life leading to the enhancement of bone healing (Murali et al., 2013). Interactions between Wnt signalling and HS/heparin have been previously studied and it was recognized these interactions activate not only the canonical β -catenin signalling but, in cooperation with Wnt3a, it also stimulates non-canonical PI3K/Akt/RUNX2 signalling pathway activity and subsequent osteoblastic differentiation. In particular, heparin N-sulfation have shown to be essential for the binding and cooperation with Wnt3a (Ling et al., 2010). Despite complexity of HS interactome, with the characterisation of phenotypes of knockout mice it was possible to single out processes that are particularly affected by alterations in HS biosynthesis. Some of these processes include cartilage and bone formation, as well as lung, kidney, eye, brain, lacrimal gland, and mammary gland development (Kreuger and Kjellén, 2012). The raw potential of GAGs is extraordinary but by affecting too many cellular processes it requires refinement. Based on this potential, is crucial to develop low molecular weight GAGs with the ability to bind GFs that regulate certain signalling pathways to develop tissue repair therapies. Continuous efforts are being made to develop synthetic GAGs along with effective ways to obtain monodisperse oligosaccharides in large scale. This approach is vital to bring target-specific oligosaccharides closer to be available as a promising therapy (Valverde et al., 2019).

1.4.3 HS Biosynthesis

Heparan sulphate structural composition varies in length, degree/pattern of sulfation, conformation and flexibility depending on tissue and cell type. HS biosynthesis (**Figure 1.9**) begins in the reticulum endoplasmic (ER) and proceeds in the Golgi, after which HS is either secreted as a component of the ECM, expressed at the cell surface or stored in granules (Wang and Boons, 2011). HS synthesis is initiated by xylosyltransferase at Ser-Gly regions. In this region the assembly of a tetrasaccharide occurs linked to a serine residue of a protein core. When assembly is completed, two galactosyl transferases and a glucuronyltransferase add galactose and glucuronic acid (GlcA) to the chain, respectively. Chain elongation is characterised by the initial addition of one GlcNAc catalysed by N-acetylglucosaminyltransferase and the polymerization of GlcA and GlcNAc at the non-reducing end of the growing chain catalysed by glucuronyltransferases II (GlcAT II) and N-acetylglucosaminyltransferase (GlcNAcT II) which are more commonly known as exostosin 1 and 2 (EXT1 and 2) (Esko and Lindahl, 2001; Wang and Boons, 2011). These enzymes are key elements for HS synthesis where the chain elongation phase will result in the addition of more 50-150 disaccharides (Wang and Boons, 2011).

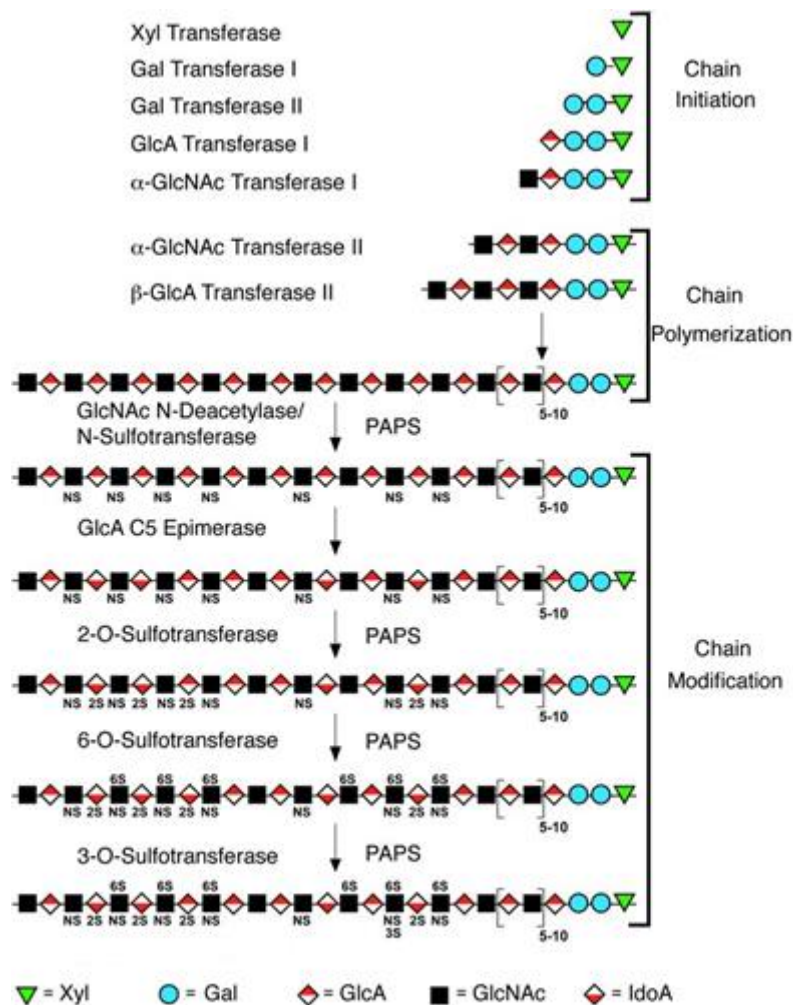


Figure 1.9. HS chain biosynthesis. This schematic represents the consecutive enzymatic actions during chain initiation, chain polymerization and chain modification. The main enzymes involved in HS biosynthesis are: xylosyltransferase-1-2; galactosyltransferase-1-2; GlcA/GlcNAc transferases; N-deacetylase/N-sulfotransferase-1, -2, -3, -4 (NDST); D-glucuronyl C5-epimerase; 2- 3- 6- O-sulfotransferase (-2 -3 -5-OST). Sulphate donor 3'-phosphoadenosine-5'-phosphosulfate (PAPS). Sulphate groups are represented (2, NS, 6S) d. Image adapted from (Esko and Lindahl, 2001).

2.3.4 GAG Structural modifications

After polymerization the HS chain is firstly modified within the Golgi by N-deacetylase/N-sulfotransferase-1, -2, -3, -4 (NDST1-4), N-deacetylase/N-sulfotransferase-1, -2, -3, -4, C5 epimerase, -2-3-6-O-sulfotranferases (2OST, 6OST1-3, 3OST1-7).

In detail, N-deacetylation/N-sulfation of GlcNAc residues is catalysed by bifunctional enzymes N-deacetylase/N-sulfotransferase-1, -2, -3, -4 (NDST1-4) followed by the epimerization of a

GlcA to IdoA. During epimerization, D-GlcA adjacent to N-sulphate sugar residues are converted into L-IdoA residues by D-glucuronyl C5-epimerase (Kreuger and Kjellén, 2012). Epimerization is followed by 2-O-sulphation of IdoA and occasionally of GlcA by 2-OST using PAPS as a sulphate donor (Smeds et al., 2010). The last modification steps to occur are 6-O and 3-O-sulfation to specific chain substrates by 6- and 3-OST attributing an important role in protein binding (Jemth et al., 2003; Kreuger and Kjellén, 2012). The 2-O-sulfation can affect the degree of N-acetylglucosamine (GlcNAc) N-deacetylation/N-sulfation and 6-O sulfation and this might suggest that GlcNAc N-deacetylation/N-sulfation, epimerization, and 2-O-sulfation probably occur simultaneously (Esko and Selleck, 2002; Shriver et al., 2012). HS/heparin chain may undergo different structural modification at cell surface carried out by extracellular enzymes (i.e., endosulphatases SULF1 and 2) that are responsible for 6-O-desulphation (Annaval et al., 2020).

Often, the products of HS/heparin biosynthesis act as a template for subsequent reactions making all the reactions involved depend of one another to a certain extent. Modification steps do not often proceed to completion but the final chain variability is responsible for the structural heterogeneity that characterises these molecules. An example of this variability is disaccharide sulfation pattern in heparin (~2.7 sulphate groups) versus HS (≥ 1 sulphate group) (Esko and Selleck, 2002; Shriver et al., 2012). Table 1.4 described a list of HS/heparin chain modifications carried out by enzymes.

Table 1.3. Main modifications during HS/heparin biosynthesis and respective enzymes and function.
*Currently known molecules

Modification	Enzymes	Substrate	Function	
Epimerization	D-glucuronyl C5-epimerase (1 isozyme)	D- GlcA	Epimerization of D- GlcA changes the carboxyl group orientation adding flexibility to the molecule	(Li et al., 2001; Qin et al., 2015)
2-O-sulfation	Uronosyl-2-O-sulfotransferase (only one isozyme interacts with HS*)	L-IdoA (highly preferable) D- GlcA	Protein binding	(Smeds et al., 2010)
6-O-sulfation	Glucosaminyl 6-O-sulfotransferases (3 isozymes *)	GlcNS residues flanked by 2-O-sulfated IdoA units	Protein binding	(Jemth et al., 2003)
3-O-sulfation	Glucosaminyl 3-O-sulfotransferases (7 isozymes in mammals and 8 in zebrafish *)	Unknown	Protein binding. High affinity to antithrombin and glycoprotein D (gD) of herpes simplex virus	(Liu et al., 1999; Shukla et al., 1999)
N-sulfation	N-deacetylase/N-sulfotransferase (NDST) family (4 isozymes *)	From non-reducing to reducing end at any internal N-acetylglucosamine residue generating high sulphate domains (GlcNS) or low sulphate domains (GlcNAc-6-S)	Substitution of free amino groups with sulphate forming negatively charged groups (protein binding)	(Sheng et al., 2011)
N-deacetylation	N-deacetylase/N-sulfotransferase (NDST) family (4 isozymes *)	From non-reducing to reducing end at any internal N-acetylglucosamine	Removal of N-acetyl groups generating positively charged GlcNH ₂ residues	(Sheng et al., 2011)

1.4.5 GAG-protein Interactions

GAG-protein interactions depends on molecule conformational flexibility to spatially orient and expose its functional groups to proteins (Shriver et al., 2012). Protein binding occurs be electrostatic interactions when in the presence of a highly charged GAG molecules (Esko and Selleck, 2002). Acting as a protein scaffold HS has the ability to bring proteins to close proximity and facilitate their interaction (Xu and Esko, 2014). N-sulfation pattern determines the strength of this interaction as well as at which rate the binding occurs. Found within HS/heparin structure, binding sites are characterised as small segments containing arrangements of 3-10 disaccharides and their function depends on the arrangement of N-

acetylated and N-sulphated moieties (Esko and Selleck, 2002). Lindahl et al. was a pioneer in the identification of protein-specific GAG sequence required for antithrombin-III binding and since this discovery other protein-binding sequences were identified (Lindahl et al., 1980). In bone repair BMP-2, FGF-2 and VEGF are some of the most important proteins in study. In detail, BMP-2 and FGF-2 binding predominantly depend on HS/heparin N-sulphate regions and VEGF binding on 6-O-sulfated moieties. Other interesting factor is spacing between sulphated moieties. For VEGF/HS interaction to occur not only is required the presence of sulphated regions but also a specific minimum spacing between sulphated moieties (Robinson et al., 2006). Based on these findings, minimum chain length requirements were explored for different ligands such as FGF-1/FGF-2 (Guglieri et al., 2008), BMP-2 (Smith et al., 2018a) and VEGF (Zhao et al., 2012a). These and other binding sites characteristics are described on **Table 1.5**. Studying HS/heparin oligosaccharides allows us to understand the impact of structural differences on the bioactivity of heparin-binding proteins. As observed by Seffouh et al. oligosaccharides containing 6-O-sulfate groups were be able to fully activate FGF-2 signalling (Seffouh et al., 2013). In the same way, Smith et al., observed that heparin oligosaccharides preferably containing N-sulphated groups are able to activate BMP-2 signalling depending on oligosaccharide chain length (Smith et al., 2018a).

2.4.6 HS variants

To translate HS potential to the clinics is important to develop robust and cost effective isolation methods to obtain affinity-specific HS variants from crude heparinoid materials. Murali et al. has shown that is possible to isolate a HS variant with a high affinity to the BMP-2 heparin-binding domain using peptide affinity chromatography. This research established a robust platform to isolate target-specific HS variants (Murali et al., 2013). This platform was used to isolate a HS variants with specific affinity to VEGF (Wang et al., 2014) and FGF-2 (Wijesinghe et al., 2017). Due to the current heparin productions constrains, the by-products of heparin production are an ideal alternate source to generate HS/heparin like glycosaminoglycans (Taylor et al., 2019). Finally, HS mimicry through chemical synthesis is

also an interesting strategy which has been described for example for cytokine binding (Sarrazin et al., 2005). These approaches can be used to enhance glycomics studies and drugs development. Table 1.5 describes a list of known HS/Heparin minimum binding requirements.

Table 1.4. A partial list of minimal criteria for protein binding to HS/heparin.

Functions	Binding proteins	HS/heparin binding requirements	Reference
<u>Anticoagulation</u>	Antithrombin	Dp5; requires 3-O-sulphation	(Olson et al., 1992a)
<u>Cell proliferation and metastasis</u>	FGF-2	dp4 to dp6; 2-O-sulphation and N-sulphation	(Guerrini et al., 2002; Guglieri et al., 2008; Mach et al., 1993)
	FGF-1	dp4 to dp6; 2-O-sulphation and 6-O-sulphation	
	Selectins	≥dp4; requires highly sulphated sequences, with presence of free amine residues	(Nelson et al., 1993)
<u>Development, bone and cartilage formation</u>	BMP-2	dp10 to dp12*; requires N-sulphation (preferred), 6-O and 2-O sulphation	(Ratanavaraporn and Tabata, 2012; Smith et al., 2018a)
<u>Vasculogenesis and angiogenesis</u>	VEGF	dp8 to dp14*; N-sulfation (preferred), 6-O (preferred) and 2-O sulphated	(Robinson et al., 2006; Zhao et al., 2012a)
<u>Inflammation</u>	IL-8	dp18 to dp20; requires alternating domains of high sulphation-low	(Spillmann et al., 1998)
	SDF1α	dp12 to dp14; requires highly sulphated domains	(Sadir et al., 2001)
<u>Viral infection</u>	Herpes simplex virus gD	dp8; requires a unique 3-O-sulphated, glucosamine at the reducing end	(Copeland et al., 2008; Marks et al., 2001; Shukla et al., 1999; Vivès et al., 2005) (Marks et al., 2001)
	HIV gp120 Dengue virus envelope protein	dp10; highly sulphated sequences	
<u>Development</u>	HB-GAM	dp16 to dp18; requires highly sulphated domains	(Rauvala, 1989)

*Optimal HS/heparin length for effective ligand binding.

1.4.7 GAGs Processing

Assuming that HS sulphated domains are represented in heparin, heparin is commonly used for structural studies. Heparin can be easily digested into oligosaccharides and processed by exclusion chromatography and ion-exchange chromatography (Xu and Esko, 2014). Heparin depolymerisation is performed enzymatically (e.g. heparinases) or chemically (e.g. nitrous acid). Heparinases cleave the nonreducing end of uronic acid and there are three different heparinases with different specificities which were isolated from *Flavobacterium heparinum*: Heparinase I (digests mostly heparin N-sulphated domains), heparinase II (digests all HS and Heparin domains) and heparinase III (digests N-acetylated HS domains) (**Figure 1.10**) (Puvirajesinghe and Turnbull, 2012; Wang and Boons, 2011).

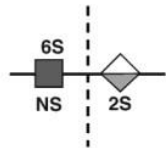
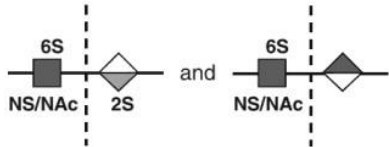
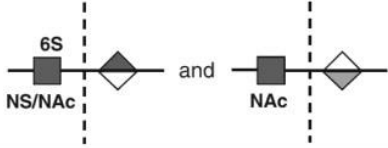
Enzyme	Specificity
Heparinase I	
Heparinase II	
Heparinase III	

Figure 1.10 Heparinases cleavage specificity. Adapted from (Wang and Boons, 2011).

Enzymes are an important tool in structural studies that can be used alone or in combination for partial or total depolymerisation. Enzymatic digestion of HS/heparin results in fragments containing unsaturated uronic residues ($\Delta 4,5$ double bond - chromophore) which strongly absorb ultraviolet (UV) light at 232 nm. Fragment separation benefits from the presence of a chromophore but the loss of the original uronic acid structure is a disadvantage. Overall, ion exchange chromatography (SAX) and size exclusion chromatography (SEC) isolation of

enzymatically digested HS/heparin is accurate, sensitive and with very sharp, symmetrical and highly reproducible elution peaks (Iozzo, 2001; Shriver et al., 2012). Heparin can also be depolymerised by nitrous acid that specifically cleaves glycosidic bonds of N-sulphated GlcN residues present on HS/heparin. During nitrous acid treatment, N-sulphoglucosamine undergoes nitrosylation forming an unstable residue leading to a subsequent ring contraction to anhydromannose bearing an aldehyde group which is normally stabilised with sodium borohydride to form a terminal 2,5-anhydro-D-mannose residue. Nitrous acid reaction is highly dependant on pH, for example, at pH lower than 2.5 direct deamination of N-sulphated residues occurs while at pH 4 N-unsubstituted residues are deaminated at a faster pace (Shively and Conrad, 1976a, 1976b). One advantage of nitrous acid depolymerisation is that uronic acids are not altered. In contrast with enzymatic digestion, chromophore absence on oligosaccharides obtained from nitrous acid digestion makes fragments separation challenging, meaning that is possible at an absorbance of 232nm but at lower sensitivity (Liang et al., 2015; Shriver et al., 2012). In glycomics studies, this sensitivity can be improved by using radiolabeling, hydrophobic tags or fluorescent tags based on the use of 2,5-anhydro-D-mannose residue produced at the reducing-end of nitrous acid digested fragments which are highly reactive.

HS/heparin structure and composition extensively vary based on the source. NMR and mass spectrometry have provided direct sequence information yet requires the combined use of specialized techniques. Quantification plus isolation of depolymerized saturated or unsaturated GAG fragments is routinely performed by high-performance liquid chromatography (HPLC)-based techniques (Wang and Boons, 2011). Oligosaccharides separation and purification can be based on their mass, charge and hydrodynamic volume.

1.4.8 High-Performance Liquid Chromatography (HPLC)

HPLC methods are used to characterise individual molecules from complex mixtures by liquid chromatography separation. Due to its high efficacy, specificity and precision HPLC methods have become progressively popular in the pharmaceutical field. Generally, a HPLC system englobes a solvent reservoir, a pump, a sample injector, columns (matrix), detector and data collection device (Akram, 2018). By monitoring different wavelengths simultaneously UV/Vis is a commonly used detector which requires a significant amount of analyte to assure detection yet fluorescence, mass and electrochemical detectors can be used (Akram, 2018; Siddiqui et al., 2017) Several pharmaceutical, environmental, forensic, food and clinical applications of HPLC are centred on quality control, purification, compound detection, quantification and separation. HPLC is divided in four groups depending on the substrate used (i.e. stationary phase) (Akram, 2018):

- **Normal phase HPLC:** separation based on polarity. The use of a polar stationary phase (i.e. silica) and a non-polar mobile phase (i.e. hexane) allows polar samples to be retained in the column.
- **Reversed phase HPLC:** separation based on polarity, reversed to normal phase. The use of a non-polar (i.e., hexane) or hydrophobic stationary phase and a polar mobile phase (i.e. methanol or acetonitrile) allows non-polar samples to be retained in the column.
- **Size exclusion HPLC:** separation based on molecular size. Column retains substrates and gradually elutes fractions according to molecular size.
- **Ion-exchange HPLC:** separation by molecular charge. The stationary phase has a surface charge inverse to sample charge while mobile phase is an aqueous buffer controlling pH and ionic strength.

Two HPLC-based techniques were used in this project: size exclusion and strong-anion exchange chromatography.

1.4.8.1 Size exclusion chromatography (SEC)

GAGs can be separated by size and charge using SEC based techniques. Using a porous stationary phase allows small molecules to permeate the column and flow along the mobile phase (**Figure 1.11**). Briefly, molecules are eluted by decreasing order of their size this means that when smaller molecules enter the porous stationary phase, move slower and present a higher elution time comparing with bigger molecules. (Moldoveanu and David, 2013; Wang et al., 2012). This can also be observed as GAG depolymerisation progresses populations of generated oligosaccharides increases from small to larger oligosaccharides until total depolarization occurs and mainly disaccharide peaks are detected. The type of heparin depolymerisation defines the presence (i.e., enzymatic) or absence (i.e., nitrous acid) of chromophores within digests affecting the sensitivity of UV detection. The chromatographic resolution of oligosaccharides is characteristic of repeating disaccharide motifs of heparin and specificity of depolymerization methods depending on the molecular weight of each obtained sized fraction that varies according with the number of disaccharide units and presence of sulphate groups. Thus, within sized populations of larger oligosaccharides, SEC peak broadening is associated with GAG chain size heterogeneity. The choice of an appropriate flow rate is an important factor since SEC is based on molecules diffusion into sized porous matrices and varies with viscosity, mobile phase, temperature and samples' molecular weight.

As previously demonstrated, optimum flow rate for GAG samples is lower than indicated by manufactures reaching values lower than 10 μ L/min for dp4 fractions. GAGs separation at high pressure decreases significantly separation time (< 3h) and sensitivity in comparison with SEC at low pressure conditions. For example, for a mixture of oligosaccharides within 0.5-13 kDa columns with bigger exclusion limits showed better resolution (Superdex 75 - globular protein exclusion 75 kDa). This is observed because GAGs behave differently from proteins by displaying high charge at neutral pH leading to repulsion within the matrix even when smaller in size (Ziegler and Zaia, 2006). The ionic strength of running buffers (i.e. ammonium bicarbonate) prevent sample-matrix electrostatic interaction tuning elution time and peak resolution Superdex 30 resin (GE Healthcare) was previously identified as a good matrix to process HS mixtures for its reproducibility, stability and durability (Powell et al., 2010). Size is not the only variable affecting elution time but also electrostatic interaction between matrix and sample. The choice of an adequate solvent, pH and matrix is vital for an effective run (Wang et al., 2012). SEC should be focused on high selectivity (peak to peak distance) than higher efficiency (narrow peaks). Assuming that column swelling/shrinkage does not occur,

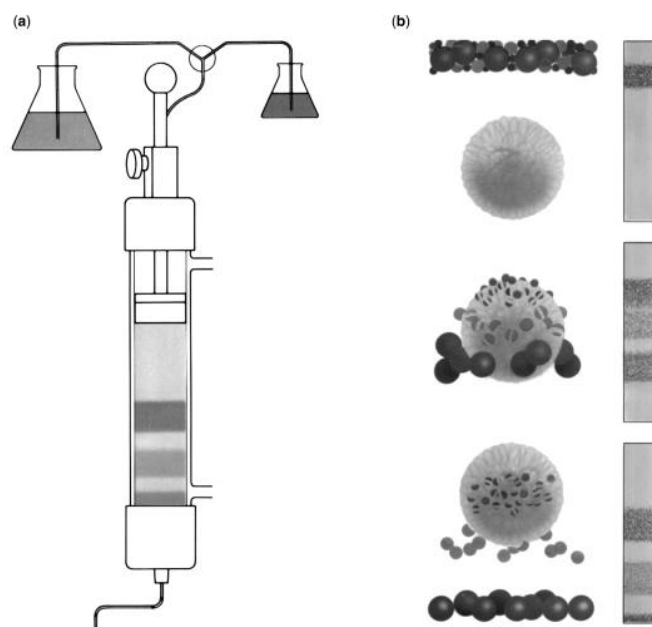


Figure 1.11. SEC fundamentals. A) Schematic of a simple experimental set up for SEC that shows a buffer and samples flasks, a supported packed column while elution occurs with the aid of gravity. b) Sample separation within a packed bed after sample injection. The sample is separated into different populations based on their molecular size (Hagel, 2011).

SEC specificity relies on the properties of the matrix and pore size distribution but it is not depended on running parameters the same way column efficiency is (Hagel, 2011). After fractionation, desalting by SEC or serial lyophilisation is necessary to remove ammonium bicarbonate. SEC does not concentrate samples and a final lyophilisation step is normally needed (Powell et al., 2010). Determining the relative molecular mass of polysaccharides can be performed by the use of electrophoresis, SEC, viscosimetry, mass spectroscopy and light scattering. Even if the combined use of mass spectroscopy and light scattering coupled to SEC would be the best combination to measure GAGs molecular weight without the need for standards, these are expensive limited techniques typically available in laboratories specialized in polymeric characterisation. Moreover, the use of mass spectrometry cannot be applied on molecules with high relative molecular weight while light scattering is only effective determining the average relative molecular weight of large molecules. One way to overcome this issue is the combined use of polyacrylamide gel electrophoresis (PAGE) and SEC versus known commercially available standards (Wang et al., 2012). Molecular weight assignment against known standard more challenging to perform on heparin fragments obtained by nitrous acid due to their lower absorbance but also due to high salt concentration present on digestion buffers (Powell et al., 2010). SEC is also known as gel permeation chromatography (GPC) in polymeric separation and polydispersity characterisation when the mobile phase is an organic solvent (Wang et al., 2012).

1.4.8.2 Strong-anion exchange (SAX)

Purity characterisation of heparinoid products has become increasingly important specially after the global crisis of adulterated heparin late 2007 when an outbreak of acute allergic reaction was reported among haemodialysis patients (Centers for Disease Control and Prevention (CDC), 2008). As a response Baxter healthcare retracted heparin batches while a investigation started to determine the cause of this crisis. Later on FDA announced that a heparin-like contaminant had been identified as chondroitin sulphate (Guerrini et al., 2008) urging United States Pharmacopeial Convention (USP) to revise heparin monographs and

implement characterisation tests to heparin contaminants. USP continues to update the heparin development process over the years. For example, analysis by $^1\text{H-NMR}$ and SAX-HPLC became a requirement by the FDA for characterisation of heparin destined for pharmaceutical use (FDA Guidance for Industry., 2013; United States Pharmacopeia., 2011). SAX-HPLC has been shown to be very sensitive at detecting and separating heparin and heparin-like components, such as oversulphated chondroitin sulphate. Disaccharide analysis by SAX-HPLC allows for the separation of oligosaccharides based on negative charge (Puvirajesinghe and Turnbull, 2012). More precisely, separation occurs at pH 3.5 when carboxylated uronic acid are protonated (uncharged) while separation will depend on charged sulphate groups (Powell et al., 2010). Silica or latex-based stationary columns are used for oligosaccharide elution that occurs by an increase of salt gradient while GAGs retention time is correlated with the number of sulphate groups. Previous studies have recommended Propac PA1 column (latex column with alkyl quaternary amine as functional groups) for HS disaccharide mixtures separation, high reproducibility, durability and stable baselines (Yang et al., 2011).

1.4.9 Modified Heparins

GAGs structure can be adjusted. Using different methods as a useful tool for structural studies, it is possible to tune N-sulfation patterns, functional groups and carbohydrate ring opening. As demonstrated by Huang et al., an alkaline peeling reaction at milder conditions (50 mM ammonium hydroxide) can remove 3-O-sulphate groups at the terminal end of monosaccharides (Huang et al., 2015). Previously, Jaseja et al. 1989 identified three novel desulphated heparin structures also obtained by alkaline treatment (0.1 N sodium hydroxide) generating heparin variants with low to absent anticoagulation activity (Jaseja et al., 1989). This data suggests that alkaline treatments might not only remove de-2-O-sulphate groups but also 3-O-sulphate groups which are critical for antithrombin binding. More, acidic treatments with methanol and hydrochloric acid (HCl) or dimethyl sulfoxide treatments can yield N-desulphated variants (Inoue and Nagasawa, 1976). Several other modification were

previously reported on heparin fragments: spacing with glycol-split (Casu et al., 2002), 6-O-desulphation (Baumann et al., 1998; Kariya et al., 2000), probe labelling and others.

1.4.10 Glycans as a therapeutic solution

Several well-known anti-viral (e.g. Relenza, Tamiflu) and anti-bacterial vaccines (e.g. Prevnar®, QuimiHib®), antibiotics (e.g. vancomycin, teicoplanin) and anticancer therapeutic agents (e.g. Herceptin, Avastin) and other drugs (Humira, Enbrel, Mabthera, Remicade, Lovenox, Lucentis) contain natural or synthetic glycans as part of their core structure (Astronomo and Burton, 2010; Lauc, 2016; Valverde et al., 2019). As previously discussed, heparin is one of the oldest and most prescribed drugs in the world, that has been used as an anticoagulant in clinics while hyaluronic acid had been used for the treatment of arthritis. Generally, glycosylation can be used to increase a proteins half-life and therefore their action. (Seeberger and Cummings, 2015). Tissue repair products containing glycans are a market in expansion where the first commercially available GAG hybrid skin scaffold was developed by Integra (**Table 1.6**).

Table 1.5 Examples of commercially available products containing glycans and/or ECM components.

Name	Company	Composition	Function	References
Matrigel®	BD biosciences	Lamin, collagen IV, enactin, growth factors, proteoglycan , matrix metalloproteinases	Cells support	(Alaribe et al., 2016)
ECM gel®	Sigma Aldrich	Lamin, collagen IV, heparan sulfate , proteoglycan , enactin	Cells support	(Alaribe et al., 2016)
Maxgel®	Sigma Aldrich	Collagen IV, lamin, fibronectin, tenascin, elastin, proteoglycan , glycosaminoglycan	Cells support	(Alaribe et al., 2016)

Stravix®	Osiris therapeutics	Cryopreserved placenta: Collagen type I, Hyaluronic acid , GFs, anti-inflammatory cytokines	Wound cover or surgical wrap	-
Amniox®	TissueTech Company	Cryopreserved Placenta: Collagen (types I, III, IV, V and VI), Fibronectin, Laminin, Hyaluronic Acid, Proteoglycans , growth factors, HC-HA/PTX3	Soft tissue repair	-
INTEGRA®	LifeSciences	Collagen-GAGs hybrid	Skin repair	(Lanza et al., 2020)
Bio Oss® and Bio-Gide®	Geitlich	Bilayer collagen membrane and bone mineral mimetic scaffolds	Dental repair	-
Evolution®	OsteoBiol	Dense collagen fiber membrane	Bone repair	-

1.5 GAG-based biomaterials

The natural ECM micro-environment can provide inspiration to design GAG-based biomaterials to increase a proteins half-life and therefore their action durability during tissue repair (Seeberger and Cummings, 2015). Heparan sulphate structure and bioactive properties are maintained after sterilisation with gamma irradiation which make GAG a good candidate for medical applications (Smith et al., 2018b)

Tissue engineering aims to restore organs and tissues functions after injury or damage. The most common approach is the use of porous bioresorbable 3D or 2D scaffolds to mimic the ECM functions to stimulate tissue formation (Alaribe et al., 2016; Choong et al., 2004). A biomaterial is defined by the European society for Biomaterials as “a material intended to interface with biological systems to evaluate, treat, augment or replace any tissue, organ or function of the body”.

Biomaterials can be from synthetic or natural source. Focusing in tissue engineering, polymers and ceramics are the most commonly used materials (Alaribe et al., 2016; O'Brien, 2011). Bio-ceramics or bioglasses are widely used for hard tissue engineering and are known for enhancing osteoblasts differentiation. For example, the incorporating of different divalent borosilicate bioactive glasses containing divalent cations (i.e., Mg^{2+}) have improved rat bone marrow MSCs osteogenesis (Fernandes et al., 2017). Bioceramics can be defined as

bioactive, resorbable or nearly inert depending on tissue response. These biomaterials have high stiffness, low elasticity and are highly compatible with the native bone mineral phase. Unfortunately, ceramics are not ideal for clinical applications due to their brittleness, difficulty to shape for implantation, slow degradation but the newly formed bone mechanical loading is not reliable (Alaribe et al., 2016; O'Brien, 2011).

Synthetic polymers are, in most cases, well defined, reproducible, cheaper and their properties can be shaped accordingly to the application. One of their disadvantages is lack of cell adhesion cues which normally requires further functionalisation process with specific biomolecules to increase cell adhesion. Natural polymers contain native cell adhesion cues, are biodegradable but their poor mechanical and physical properties as well as their high batch-to-batch variability represent a big limitation. Crosslinking or hybrid materials combining ceramic/natural polymers/ synthetic polymers are normally used as a method to improve natural and synthetic biomaterials mechanical properties (O'Brien, 2011).

1.5.1 Scaffolds manufacture

Traditional techniques for scaffold manufacture includes solvent casting, membrane lamination, phase separation, freeze drying, polymerization, gas foaming (Holmes et al., 2012), self-assembly (Lu et al., 2013), among others (**Figure 1.12**). Techniques such as electrospinning, hydrogels and microparticles are widely used to create 3D-structures as well as other two relatively new techniques, decellularization (Stratton et al., 2016) and 3D printing (Kang et al., 2016). Native decellularized ECM can be obtained from allogenic or xenogeneic tissues by using several physical, enzymatic and detergent treatments. Since the decellularization process removes all the cellular antigens but maintains the natural ECM components its major advantage, in comparison with other scaffolds, is the proximity to natural 3D tissues structure and biological properties. Nevertheless, its biggest disadvantages are the possibility of immunological response after implantation and poor cellular distribution (Alaribe et al., 2016; Chan and Leong, 2008). In cell sheet engineering, cells secrete their own ECM until confluence and subsequently are harvested by non-enzymatic methods, such as,

culturing on thermo-responsive polymers. This approach is an easy harvesting procedure with evenly distributed cells but as weakness it is the very hard to produce thick cell sheets which is needed for an effective use clinically. This approach is not recommended for ECM-rich and hypocellular tissues such as bone because as soon as cellular confluence is reached ECM secretion drastically decreases (Chan and Leong, 2008). Cell encapsulation is normally performed with water-based polymers (hydrogels) and occurs in one-step procedure combining scaffold manufacture and cell seeding. This allows a better cellular distribution and high viability for injectable application. Additionally, although hydroxyapatite containing hydrogels enhance bone regeneration plus have the advantage of being injectable (Thorpe et al., 2018), the biomaterials normally used in this approach have weak mechanical properties which is not desired for bone tissue regeneration (Choong et al., 2004).

Overall, an ideal scaffold should be (Chan and Leong, 2008):

- Porous. Pores with 200-400 μm allows cells adhesion, spreading, growth and nutrition as well as vascularization within the scaffolds;
- Mechanically strong. This characteristic should match the native tissue by supporting physiological stresses and forces;
- Biodegradable. The degradation rate should support cellular proliferation at the same time it degrades to give space for tissue growth;
- Biocompatible. The porous scaffolds should integrate within the native tissue without triggering immune response or inflammation facilitating tissue formation.
- Easily manufactured. The manufacture process should be easier, cheap and able to be produced in large scale. This will facilitate the use of the scaffolds clinically and reach a higher amount of patients. The manufacture processes should not compromise tissue properties or be cytotoxic (Chan and Leong, 2008; Choong et al., 2004).

By including specific biological cues to scaffolds stimulation of cells adhesion, proliferation and differentiation is possible. Plus, scaffolds can act as drug delivery vehicle when GFs are encapsulated (Chan and Leong, 2008).

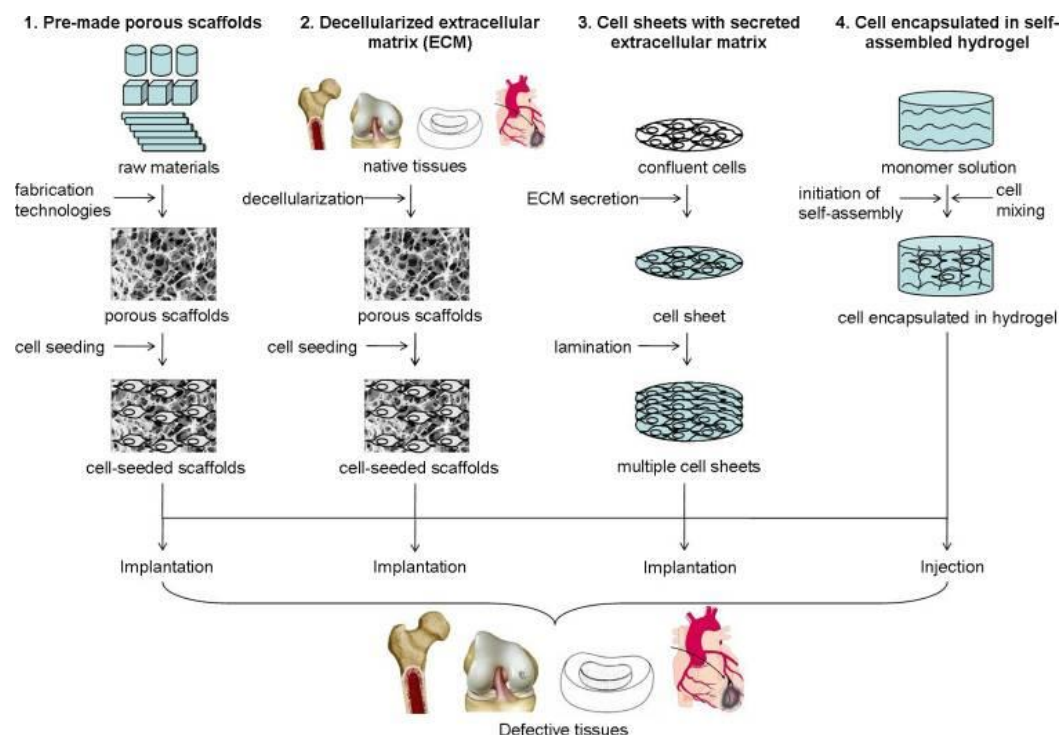


Figure 1.12 Schematic representation of scaffolding methods (Choong et al., 2004)

1.5.2 Electrospinning

Electrospinning was studied for the first time in the 1930s by Formhals but only gained researchers and industry attention in the 1990s (Rezvani et al., 2016). This versatile, easy and

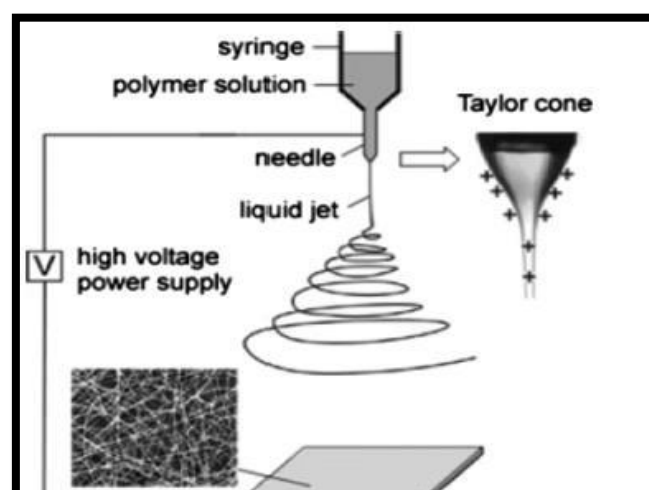


Figure 1.13 Classical electrospinning set up. The image also represents a charged “Taylor cone” and a SEM image of a nanofibrous type of scaffold as example. (Li and Xia, 2004)

flexible technique allows the production of nanofibrous scaffolds from polymers, composites, ceramics or metal (Teo and Ramakrishna, 2006). The produced fibres can mimic the natural ECM (Rezvani et al., 2016) by having diameters that range from several nanometers to several microns depending on material and electrospinning conditions (Beachley and Wen, 2010). The electrospinning setup consists on a high voltage power supply, a grounded conductive collector, a capillary and a spinneret (**Figure 1.13**) (Ke et al., 2014; Rezvani et al., 2016). During electrospinning, a high power voltage is applied to the polymer solution fed through the spinneret. When the electrostatic forces in the solution reach a critical point by surpassing the polymers solution surface tension, a conical droplet ("Taylor cone") is formed and from its tip a polymer jet is ejected. The jet process is divided into jet initiation, elongation and solidification (Garg and Bowlin, 2011). The manufactured dry polymer fibres are deposited on the metal collector while the solvent evaporates (Ke et al., 2014). The electrospinning process and fibres characteristics deeply depend on the process parameters (i.e., flow rate, distance, voltage), solution characteristics (i.e., molecular weight, viscosity, solvent) and environmental parameters (i.e., humidity and temperature) (Gong et al., 2015b; Ke et al., 2014). By using stainless steel static collectors, scaffold can be obtained with randomly oriented fibres. However, by using a rotating drum or two conductive stripes separated by a gap, aligned fibres can be obtained (Li and Xia, 2004).

1.5.2.1 Solution Concentration

Solution concentration is one of the most critical parameters during electrospinning. Electrospinning of solutions with very high concentrations and high viscosity produces fibres with higher diameters and pores size while the electrospinning of very low concentration solutions produces thinner fibres or no fibres. Moreover, by using low molecular weight polymeric solutions beads can occur more frequently while high molecular weight polymeric solutions produce fibres with huge diameters. In order to obtain uniform and smooth fibres, an appropriate solution concentration and polymer molecular weight should be carefully chosen (Rezvani et al., 2016).

1.5.2.2. Voltage, Flow rate and Distance

By applying high voltage power during electrospinning process, the probability of beads is higher, although this result is closely related with the distance between needle tip and the collector. The distance should be enough to give the polymer solution space and time to solidify before being deposited in the collector (Rezvani et al., 2016). The appropriate voltage to be applied to a polymer solution depends on many factors is debatable however it normally varies between 0-30 kV (Garg and Bowlin, 2011; Rezvani et al., 2016). Low flow rates are recommended to be used in order to give solvents enough evaporation time and obtain thinner and smoother fibres.

1.5.2.3 Humidity and Temperature

A high relative humidity during the electrospinning process can cause problems through jet solidification because the solidification process slows down. However, appropriate change to the humidity value can be useful to change nanofibers characteristics. For example, in a previous study, it was observed that poly (ethylene oxide) (PEO) decreased nanofibers diameters from 253 to 144nm by increasing humidity from 5.1 to 48.7%. Changes in temperature vary polymer solutions viscosity and therefore fibres diameters. Normally, low temperatures are related to the presence of beads on nanofibers while high temperatures are related with flat and condensed fibres (Rezvani et al., 2016).

1.5.3 Polycaprolactone

Polycaprolactone (PCL) is a bioresorbable hydrophobic synthetic polymer (Choong et al., 2004) normally synthesized by ring opening polymerization (ROP) of ϵ -caprolactone (Mondal et al., 2016). Its hydrophobicity decreases cell adhesion but it can be reversed with surface functionalization methods, such as, plasma treatment, micropatterning or surface oxidation (Choong et al., 2004). PCL degradation occurs by hydrolytic scission (Cheung et al., 2007) and not enzymatic digestion. Its slow degradation can vary between months to years depending on molecular weight, crystallinity and degradation conditions (Mondal et al., 2016). This polymer degrades into harmless by-products metabolized in the tricarboxylic acid cycle

making it a highly compatible biomaterial to be used in tissue engineering approaches (Jensen et al., 2014). In comparison with other polymers, PCL is more structurally stable, cheaper, available in large quantities (Williams et al., 2005) and FDA approved (Cheung et al., 2007). Polycaprolactone was chosen to be ideal for this research project because it is a bioresorbable, biocompatible, inexpensive polymer and easy to electrospinning high surface area fibrous scaffolds that can provide cells a similar native ECM structure (Rezvani et al., 2016). PCL nanofibers can promote osteoprogenitors differentiation as it was demonstrated by (Tutak et al., 2016). These findings may have resulted from changes in cell morphology and organelle structure once cells were exposed to a fibrous PCL topography.

1.5.4 Scaffolds Functionalisation

The surface of polymeric scaffolds can be modified with biomolecules by absorption or chemical functionalization in order to modulate cells function and adhesion. Several techniques can be used to functionalize polymeric nanofibrous surfaces, as long as the nanofibers initial structure is not damaged (Beachley and Wen, 2010).

1.5.4.1 Physical absorption

The simplest functionalisation method is scaffolds incubation with biomolecule solutions to allow the absorption of these molecules into the polymeric surface. This non-covalent bonding occurs due to interactions between biomolecules and surfaces, such as Van der Waals force, electrostatic, hydrophobic forces and hydrogen bonding. The efficiency of this method depends on materials hydrophobicity which can be decreased by air plasma treatment (Beachley and Wen, 2010; Tallawi et al., 2015).

1.5.4.2 Covalent bonding

In comparison with simple adsorption, covalent bonding produces more efficient and durable results. This chemical method is defined as the bonding of biomolecules to surfaces with relevant functional groups exposed. This technique is executed in two steps: 1) exposure of surface functional groups; 2) biomolecules covalently binding to the exposed functional groups. Normally, carboxyl groups are exposed by hydrolysis using sodium hydroxide

(NaHO), amine groups are exposed by aminolysis and to graft new functional groups in surface plasma treatment can be used. Activation of functional groups can be done by treatment with MES buffer solution containing 1-ethyl-3-(3-dimethylaminopropyl) carbodiimide (EDC). If functional groups cannot be directly grafted onto the surface, linkers molecules can be use (Beachley and Wen, 2010; Tallawi et al., 2015). Studies on GAG containing scaffolds can be found in the literature (**Table 1.7**).

Table 1.6 Examples of Heparin containing electrospinning scaffolds for drug delivery.

Scaffold	Chemistry	Reference
Electrospinning PCL/heparin scaffold for FGF-2 loading	ROMP and EDC/NHS chemistry	(Ye et al., 2011)
Electrospinning PCL/heparin scaffold	Surface modification by layer by layer	(Gao et al., 2017)
Electrospinning PCL/heparin scaffold	Three step heparinisation coupling reaction	(Jin et al., 2019)
Electrospinning PCL/heparin scaffold	Electrostatic interactions	(Luong-Van et al., 2006)
Positively charged electrospinning scaffold PLGA	Electrostatic interactions	(Bae et al., 2018)
Electrospinning PLLA/heparin scaffold	Electrostatic interactions	(Spadaccio et al., 2010)
Electrospinning poly(ethylene glycol) (PEG) functionalized with low molecular weight heparin	Thiol group functionalisation	(Casper et al., 2005)
Heparin-based hydrogels on glass substrates	UV-initiated thiolene reaction	(Shah et al., 2011)

1.5.5 Bottle-brush Polymers

To overcome functionalization limitations and in the search for more sophisticated ways to design bioactive materials, synthetic bottlebrush polymers have gained popularity in the last decades due to their potential application in drug delivery, bioengineering and molecular devices. Graft copolymers have a singular nanoscale structure containing a linear backbone with densely grafted side chains synthesized by different methods (**Figure 1.14**).

One of the advantages of brush polymer synthesis is the incorporation of therapeutic, imaging, interest molecules (Yao et al., 2013); (Johnson et al., 2011). The bio-nano interactions and properties of these materials depend on the precise control of structural and chemical aspects of brush polymers such as brush thickness, density, chemistry and architecture (Li et al.,

2021). Advances on living polymerisation techniques and development of more effective click reaction are essential for the creation of polymers with interested oriented characteristics (Uchida, 2013).

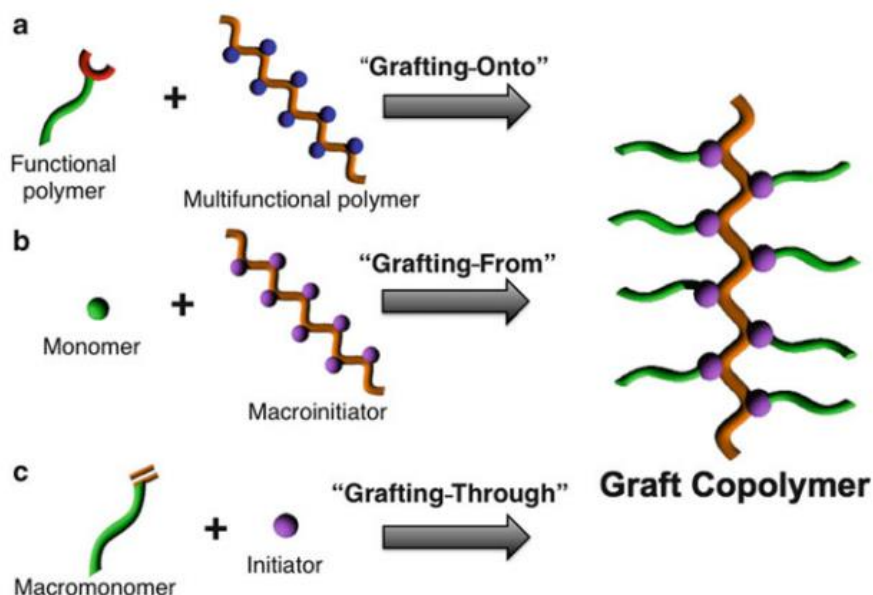


Figure 1.14 Synthetic strategies of graft copolymers. a) Graft-to, side chains are coupled to initiators side on the backbone polymer b) Graft-from: individual polymerization of backbone and side chains c) Graft-through: macromonomers copolymerization normally occurring by ROMP. Adapted from (Uchida, 2013).

1.5.6 Ring opening metathesis polymerization (ROMP)

Yves Chauvin, Robert H. Grubbs and Richard R. Schrock won the Nobel prize in 2005 for their work in the development of the metathesis of cyclic monomers in organic synthesis. (Choinopoulos, 2019). ROMP is an important polymerisation technique of strained alkene-terminated macromonomers initiated by ruthenium N-heterocyclic carbene complexes (i.e. norbornene) (Johnson et al., 2011). The synthesis of norbornene monomer occurs individually and in a controlled manner to obtain well-defined graft copolymers (precise molecular weight and low polydispersity) (Xia et al., 2009). Spacers (i.e. PEG) can be used between polynorbornene backbone and peptides to reduce steric hindrance and preserve peptide structure flexibility (Johnson et al., 2011). ROMP depends on commercially available metal

catalysts (**Figure 1.15**) with different characteristics in terms of functional groups tolerance, sensitivity to air/moisture and sensitivity to macromonomer length. Nowadays the most commonly used ROMP catalyst is the third generation Grubbs catalyst due to its activity and tolerance to functional groups and compatible with a wide range of solvents (Choinopoulos, 2019). Some examples of bioactive brush polymers were described for RGD sequences (Patel et al., 2012), GRGD sequences (Maynard et al., 2000) and sugar-based polymers (Dong et al., 2019). Noteworthy, it was previously shown that norbornene backbone polymers are not toxic even for mammalian cells lines (Patel et al., 2012). Their bioactivity depends on their

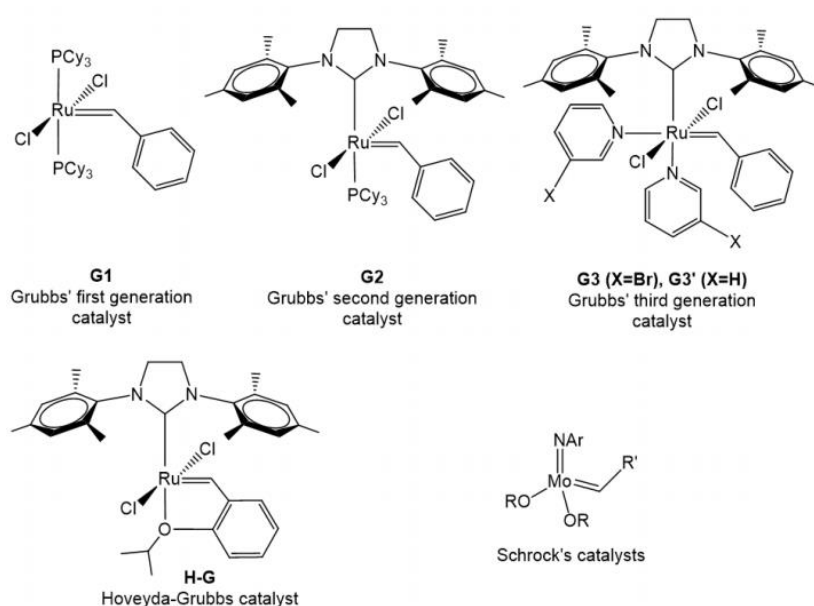


Figure 1.15 ROMP catalysts (Choinopoulos, 2019).

affinity to proteins which depends on several parameters (i.e. polymeric backbone) where, for example, glycopolymers synthesized by radical polymerisation chemistry have stronger GAG-protein interactions than the ones obtained by ROMP (Miura et al., 2016).

1.5.7 Biomaterials characterisation

Properties of bioactive polymers, such as molecular weight, polydispersity, composition and purity can be determined using a combination of techniques (i.e. NMR, GPC). These materials are used to manufacture scaffolds with properties based on their hydrophobicity (contact angle), stiffness, topography, porosity and degradation rate. The characterisation of physical

properties is important since ligand presentation and conformation within scaffolds shows that structure is as important as composition (Scott et al., 2019).

1.5.8 Commercially available bone repair substrates

GAG containing scaffolds are of interest for drug delivery and tissue repair. Different versions of GAG containing scaffolds have been developed as hydrogel, surface coatings, nano and micro particles and fibrous scaffolds (Hachim et al., 2019). Heparin containing scaffolds for growth factor loading were previously reported in the literature however there is still a need for target-specific scaffolds. This continued research for new bone tissue repair alternatives has contributed to the development of commercially available bone graft scaffolds (**Table 1.8**).

Chapter 2 summarizes the challenges and opportunities prevailing in bone tissue regeneration considering glycomics and the fabrication of synthetic 3D microenvironments as a powerful tool to be explored. Although as stated before, the bone stem cell niche is not fully characterised, the currently known structure and composition can provide us with crucial information to develop a bioinspired scaffold by emulating - to a certain degree - some aspects of the natural stem cell niche. Heparin containing scaffolds, commonly reported for vascular treatments, are not fully characterise and lack growth factor specificity. We aim to develop a highly BMP-2-specific but cost effective electrospinning scaffold for bone repair containing bioactive heparin fragments for growth release at the wound site to control stem cell behaviour, recruitment and differentiation. By choosing the appropriate FDA approved biomaterial, exploring heparin bioactive potential and ECM-like scaffold architecture we intent to develop a cost effective but innovative platform that, in the future, can be translated into clinics to improve bone regeneration and fracture healing.

Table 1.7 Example of commercially available natural and synthetic bone grafts. Adapted from (Sheikh et al., 2017)

Name	Material
Stravix®	Cryopreserved placenta
Osteopore®	Bioresorbable scaffolds
Bio oss®	Deproteinized bovine bone mineral
Biogennix®	Nanocrystalline hydroxycarbanoapatite (HCA) / calcium carbonate (CC) granules and type 1 bovine collagen in an organic binder
Actifuse baxter®	
Graftys®	Calcium phosphate cement
Biogide®	Collagen membrane
PerioGlas®	Bioactive glass
NovaBone®	Resorbable calcium phosphosilicate
Guidor easy-graft®	<i>In situ</i> hardening beta-tricalcium phosphate (β -TCP) granules coated with poly(lactic-co-glycolic acid) (PLGA)
Interpore 200®	Porous hydroxyapatite
Vitoss®	β -TCP
Synthecon	Scaffold sheets (PCL, PLLS, PGA)
Nanofibers Solutions®	PCL nanofibrous scaffolds
Interpore 200®	Porous hydroxyapatite
Biocoral®	Corraline calcium carbonate
PepGen P-15®	Anorganic Bovine Bone Mineral with a synthetic biomimetic of the 15 amino acid sequence of Type-I collagen
Osteograf/N®	Anorganic bovine bone mineral
Gen-Os®	Anorganic porcine bone mineral
MTF® - DFDBA	Demineralized freeze dried bone allograft
MTF® - FDBA Freeze Dried Bone Allograft	Mtf® - fdba freeze dried bone allograft
DBX® Putty (DBM) Demineralized Bone Matrix	Dbx® putty (dbm) demineralized bone matrix
Grafton® (DBM) Demineralized Bone Matrix	Grafton® (dbm) demineralized bone matrix
Raptos® Mineralized/ demineralized bone allograf	Raptos® Mineralized/ demineralized bone allograft
Puros® Mineralized bone allograft	Puros® Mineralized bone allograft

Chapter 2 Aims and Objectives

Aim: The overall aim of this PhD is to develop a cost-effective bioactive scaffold with the ability to bind BMP-2 and enhance bone repair.

In Chapter 1 the existing literature on bone repair focused on sugar-based scaffolds is overviewed. Chapter 3 investigates different approaches to add complexity into scaffolds (i.e. micropatterns, biomolecules coating) in order to stimulate tissue repair. These preliminary studies allowed us to set a direction to our project and develop a strategy focused on the study of heparin structure and biomaterial synthesis. Chapter 4 describes heparin oligosaccharides isolation and characterisation for the development of bioactive polymers as described in Chapter 5. The importance of glycomics is further highlighted in Chapter 6 where the bioactivity a semi-synthetic heparin sulphate (SSHS) material is explored. Results and discussion are divided in 4 chapters which individual objectives are stated below:

2.1 Chapter 1 Literature review

2.2 Chapter 3 Introducing complexity to fibrous scaffolds for enhancing bone repair

- Exploring the incorporation of micropatterns (topographical cues) into plain electrospinning membranes to study their effect on mesenchymal stem cell behaviour.
- Exploring methods of heparin incorporation on electrospinning scaffolds (Simple adsorption, encapsulation, covalent binding)
- Characterisation of functionalisation methods (stiffness, detection of heparin and respective distribution)

2.3 Chapter 4: Heparin processing and characterisation

- Optimisation of heparin depolymerisation methods (enzymatic versus nitrous acid) and processing by size exclusion chromatography (SEC).
- Characterise nitrous acid generated oligosaccharides structural properties focused on chain length size and presence of N-sulphate groups.

- Characterise the bioactivity of nitrous acid generated oligosaccharides (anti-factor Xa activity, ALP activity, expression of osteogenic markers, mineralisation, Smad 1/5/9 phosphorylation)

2.4 Chapter 5: Bioactive polymer synthesis and scaffold manufacture

- Synthesis of norbornyl linkers
- Synthesis of norbornyl macromonomers
- Synthesis and characterise GAG containing bioactive polymers (i.e., molecular weight, oligosaccharide incorporation, polydispersity)
- Manufacture of bioactive electrospinning scaffolds
- Characterise scaffolds mechanical properties and respective bioactivity

2.5 Chapter 6: Semi-synthetic heparan sulphate (SSHS)

- Establish the protocols necessary to assess the bioactivity of heparin variants

Chapter 3 Adding complexity to electrospinning scaffolds

3.1 Introduction

Through electrospinning, conductive collectors can be used to obtain randomly or aligned fibrous scaffolds. Besides fibres alignment, the ability to insert microfeatures and topographies into scaffolds has recently caught researcher's attention. For example, narrow peptide stripes micropatterned in polymer surfaces have stimulated endothelial cell organization into tubular structures inducing angiogenesis (Lei et al., 2012). Another study, presented micropatterned "niches" for skin tissue engineering. In this study, microtopographic scaffolds with different topographical geometries were produced by photolithography and co-cultured with fibroblasts and keratinocytes (Clement et al., 2013). The introduction of 3D-microstructures within electrospinning mats has been also used to improve cells penetration into PCL scaffolds (Vaquette and Cooper-White, 2011) but it could also be used to produce embed microstructures with the potential to guide cells behaviour. Micropatterned collectors designed using CAD software and manufactured through additive manufacturing techniques (for example, selective laser melting (SLM)) in combination with the electrospinning technique allows the fabrication of topographically-modified scaffolds. By electrospinning polymeric solutions into patterned collectors and controlling variables as the collectors' height, the nanofibrous mat can acquire the underlying 3D topography (Paterson et al., 2017). Based on these methods and using a variety of additive-manufactured substrates, studies of micropatterned scaffolds were previously explored for corneal repair (Ortega et al., 2013, 2014), skin (Asencio et al., 2018) and bone (Abdelmoneim et al., 2020). The following **Chapter 3** summarises the challenges and opportunities prevailing in the fabrication of synthetic 3D microenvironments for bone repair as a powerful tool to be explored.

The bone stem cell niche is not fully characterised but the currently known structure and composition can provide us with crucial information to develop a bioinspired scaffold by emulating - to a certain degree - some aspects of the natural stem cell niche. In this chapter

we have explored different ways of adding complexity to electrospinning scaffolds which includes adding microfeatures (modifying topographical cues) as well as incorporating biomolecules (i.e., heparin). As described before, heparin is an ideal candidate for scaffolds functionalisation due to their structural stability and potential to bind and protect osteogenic factors (i.e., BMP-2) increasing their bioavailability and enhance osteoinduction.

3.2 Chapter objectives

This first chapter is a “scoping chapter” in which I explored a variety of routes for incorporating complexity within an electrospinning scaffold this including topographical modifications and the incorporation of biomolecules. The aim of this chapter was to identify a promising route to focus our work on and ultimately develop a bioactive scaffold for bone repair.

This chapter was developed at The University of Sheffield and the specific objectives we established are detailed below. This preliminary research concluded that the use of heparin was a very promising approach for enhancing scaffold bioactivity and therefore heparin functionalisation was further explored in Singapore in Chapters 5.

Specific Objectives:

- Optimising the manufacture of topographically-modified electrospinning scaffolds using a combination of SLM-fabricated collectors and electrospinning (using PCL as working polymer).
- Characterising micropattern scaffolds analysing microfeature shape and distribution using SEM.
- Exploring the biocompatibility of the micropatterned electrospinning scaffolds on human mesenchymal stem cells (hMSCs) and their mechanical properties.
- Exploring methods of heparin incorporation and characterisation on electrospinning polycaprolactone scaffolds (simple adsorption, encapsulation, covalent binding)
- Explore methods of heparin detection on electrospinning scaffolds

3.3 Materials and methods

Part I

3.3.1 Polymer solutions

For micropatterned scaffolds, 10 wt.% Poly(ϵ -caprolactone) (Average $M_w=80000$; PCL; Sigma-Aldrich, UK) solutions were prepared using as solvent a mix of dichloromethane (DCM; Thermofischer, UK) and N,N-dimethylformamide (DMF; Fisher Scientific®, UK) with ratio 90:10 wt.% DCM/DMF. Before use, polymeric solutions were stirred overnight until a homogenous texture was obtained.

3.3.2 Electrospinning parameters and collectors

The custom-made electrospinning rig consists of a high power voltage supply (ALPHA IV Brandenburg model 4807, 30 kV, 3.3 mA), a syringe pump (Harvard Apparatus PHD2000 Series®, US), a stainless steel collector (grounded), a plastic syringe (1mL; Becton Dickinson, UK) and a blunt needle with an inner diameter of 0.58 mm (20-Gauge) (Intertronics, UK) (Figure 12). Electrospinning scaffolds were manufactured using a rig bottom-up setup the following parameters: a distance of 21cm between needle and collector, a voltage of 17 kV and a flow rate of 3 mL/h at room temperature.

3.3.3 Stainless-steel collectors

Non-patterned and patterned stainless steel collectors were used to collect randomly oriented fibrous scaffolds. As described by Paterson et al., patterned collectors were designed via CAD software and manufactured by selective laser melting (SLM) using Renishaw SLM 125 machine and stainless steel 316L (Paterson et al., 2017). The parameter for fabrication were the following: laser power, 200 W; speed, 480 mm/s; point distance, 50 mm and exposure time, 70ms. Each collector has 4 different sizes micropatterns (bumps) sized 2750 μm (Micropattern 1), 1000 μm (Micropattern 2), 500 μm (Micropattern 3) and 100 μm (Micropattern 4) (Figure 3.1). When a polymer solution is electrospinning into patterned collectors, the formed polymer membrane acquires its shape. In order to obtain a thick membrane, each

scaffold was manufactured by electrospinning 3 mL of polymer solution. Electrospinning membranes are cut into circles with a diameter of ~ 1.2 cm (Area = 4.4 cm^2) in order to be used in cell culture experiments.

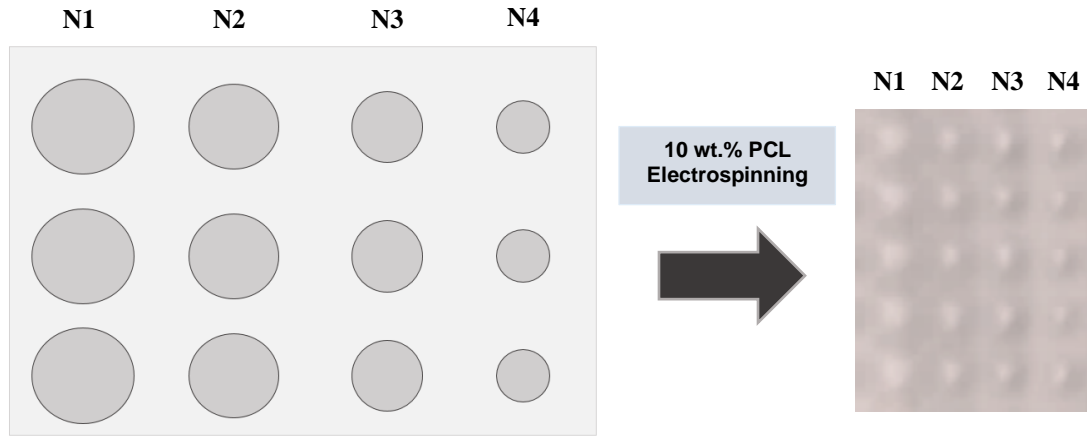


Figure 3.1 Schematic representation of micropatterns sizes on stainless steel collectors (2750 μm (N1), 1000 μm (N2), 500 μm (N3) and 100 μm (N4)). After the electrospin of 10 wt.%PCL solutions into these collectors, a PCL membrane can be created and peeled off. The produced membrane will acquire the inverse patterned from the collector and later used as an scaffold with topographical cues.

3.3.4 Scaffolds characterisation

The scaffolds fibre alignment and microfeature diameter were determined. The morphology of micropatterned scaffolds was explored using scanning electron microscope (SEM, Philips XL-20). Subsequently, measurements taken from fibres outside the micropattern structures, micropattern walls and micropattern bottoms were analysed using ImageJ software.

3.3.5 Micropattern heparin coating

The micropatterns on fibrous scaffolds were modified by simple adsorption with Fluorescein-5-isothiocyanate (FITC) heparin dissolved in PBS (1 mg/mL or 0.1 mg/mL) (Thermofisher Scientific) and heparin sodium salt (Thermofisher Scientific) dissolved in PBS (1 mg/mL or 0.1 mg/mL). Micropattern surface coating was performed with a micropipette coating each micropattern with 3-5 μL and let it dry at room temperature until evaporates. Fluorescent heparin coated surfaces were observed under fluorescent microscope (Axioplan 2, ZEISS).

3.3.6 Scaffolds sterilisation

Prior to cell culture, coated and non-coated PCL scaffolds were sterilized in ethanol 70% (v/v) solution during 1 h and soaked in phosphate buffered saline (PBS) solution overnight prior use.

3.3.7 Detecting the presence of fluorescent heparin on scaffolds

The microfeatures present in the scaffolds were coated with 0.1 mg/ml and 1 mg/ml fluorescent heparin solution. Coating detection was evaluated after 4h, 24h, 4 days, 12 days and 15 days in a humidified atmosphere at 37 °C and 5% CO₂. Heparin presence in scaffolds was assessed by detecting its fluorescence under a fluorescent microscope (Axioplan 2, ZEISS).

3.3.8 Rat Mesenchymal stem cell culture

Bone marrow mesenchymal stem cell were harvested from femora's of 5- to 6 week-old Wistar rats as described by Maniatopoulos et al., 1988 and adapted by Santocildes-Romero et al. (Maniatopoulos et al., 1988; Santocildes-Romero et al., 2015). Initially, the harvested femora were dissected under aseptic conditions, cleaned of soft tissues and immersed in 10 ml of Dulbecco's modified Eagle's medium (DMEM; Sigma Aldrich, UK) supplemented with 100 U/ml penicillin (Sigma Aldrich) and 1 mg/ml streptomycin (Sigma Aldrich). The ends of the femora were cut and the bone marrows were flushed into 5 ml DMEM supplemented with 100 U/ml penicillin, 100 µg/mL streptomycin, 20 mM L-glutamine (Sigma Aldrich) and 10% v/v foetal calf serum (FCS; Biosera, UK). The suspended cells were seeded into 75 cm² culture flasks containing 10 ml cell culture medium and incubated at 37°C and 5% CO₂ for 24 h. The non-adherent cell populations and debris were washed away twice with fresh cell culture medium. Culture media was changed every 2-3 days until cells reached near-confluence and seeded for experiments or stored for later use. For experiments, cells were expanded in T-75 flasks (Corning) with 10 mL of minimum essential media eagle (α-MEM) (Sigma Aldrich) supplemented with 100 U/mL penicillin and 100 µg/mL streptomycin (1% (v/v), Sigma Aldrich,

UK), 20 mM L- glutamine and 10% (v/v) Foetal Bovine serum (FBS) (Biosera, UK) in a humidified atmosphere at 37 °C and 5% CO₂. Cell culture medium was changed every 3 days.

3.3.9 Cells Freezing and Thaw

Rat MSCs cells were frozen or passaged when cells reach near-confluence. Prior freezing, near-confluent cells were washed twice with PBS and detached with 0.05% (v/v) trypsin/ 0.02% (v/v) ethylenediaminetetra-acetic acid solution (EDTA, Sigma) after 5 min incubation in a humidified atmosphere at 37 °C and 5% CO₂. The enzymatic reaction was stopped with 5 mL culture medium with 10% (v/v) FBS. Cells were centrifuged and resuspended in cell culture media with 10% (v/v) FBS + 10% (v/v) DMSO at a concentration 1×10^6 cell/mL and aliquoted 0.5mL per cryovial. After freezing at -80°C for 48h, vials were moved to liquid nitrogen for long term storage.

Prior experiments, cells were rapidly defrost in the water bath at 37°C, added 10mL of pre-warmed cell culture media and centrifuged at 1000 g during 5 min. The cell pellet was resuspended in 10 mL maintenance media, transferred to T75 flask and cultured for 3 days prior to use.

3.3.10 MSCs passage

MSCs were cultured up to passage 4 (P4) or P5 for cell assays. To perform cells passage, MSCs were detached with 0.05% (v/v) trypsin/0.02% (v/v) EDTA and incubated in a humidified atmosphere for 3 to 5 min at 37 °C and 5% CO₂. Once detached cells were centrifugated at 1000 rpm during 5 min in order to remove the existent trypsin in the solution. The formed cell pellet was resuspended in fresh media and the total cell number in solution was counted using a haemocytometer. After calculations, cells were seeded with fresh medium in T-75 flasks at, approximately, 10.000 cells/cm² and cultured until 80% of confluence is reached.

3.3.11 MSCs seeding onto scaffolds

Rat MSCS were seeded onto fibrous scaffolds with a cell density of 10000 cells/cm² (20000 cells/well) in 24-well plates (Corning) and cultured during 7-10days. Cells proliferation were measured every 1st, 4th and 7th day. On the last day, cell viability and morphology were

evaluated using specific staining dyes. For osteogenic assays, cells were seeded with a density of 10,000 cells/well and cultured for a minimum of 3 weeks.

3.3.12 Cell proliferation assay

Cells proliferation was assessed by PrestoBlue® assay (Thermofisher ®), according with manufacturer instructions. Each studied condition (triplicates) was incubated with culture medium plus 10% (v/v) PrestoBlue® solution and incubated for 1h. After incubation the solution was transferred to a 96-well plate (200µl solution per well), fluorescence was measured using the Infinite 200 PRO microplate reader (Tecan; excitation/emission wavelength: 560/590 nm) and Magellan data analysis software.

3.3.13 MSCs staining

Cell morphology was analysed by staining with 4',6-diamidino-2-phenylindole (DAPI) (nuclei) and conjugated fluorescein isothiocyanate (FITC) (actin fibres). After washing with Phosphate Buffered Saline (PBS), cell were fixed with 4% (v/v) paraformaldehyde or 10% (v/v) formalin solution during 20 min. Prior to labelling, a solution of 0.1% (v/v) Triton-X was added to each sample during half an hour to permeabilize cells membrane and facilitate the staining process. To each sample a PBS solution of 0.1% (v/v) DAPI and 0.3% FITC was added for 30 min at room temperature. Images were obtained using a fluorescence microscope (Axioplan 2, ZEISS).

PART II

3.3.14 Polymeric solutions and electrospinning

For heparin incorporation studies, PCL and PCL/heparin emulsion electrospinning scaffolds electrospinning were electrospinning using a 15 wt.% medical grade PCL (PURASORB PC12, Corbion, Mw 120,000 g/mol) (Bosworth et al., 2014) polymeric solutions in DCM/DMF (90:20 wt.%). Scaffolds were electrospinning at 20 kV with a flow rate of 3 mL/h and a distance of 21 cm from the collector. Electrospinning sheets were cut into circular scaffolds (4.2 cm²) with a metal punch cutter prior use.

3.3.15 Heparin incorporation into flat electrospinning scaffolds

Heparin was incorporated into PCL electrospinning scaffolds using 3 different methods as described on the **Table 3.1**. PCL/Heparin emulsion method was performed before electrospinning while simple adsorption and covalent binding methods were performed in PCL electrospinning scaffolds.

Table 3.1 Different methods of heparin incorporation into electrospinning PCL scaffolds.

Method	Protocol	Estimated heparin content per scaffold (4.2 cm ²)
Simple adsorption	1 mg/ml heparin sodium salt dissolved in water (20 µl) and spread at the surface of PCL electrospinning scaffold. Samples were moved to a petri dish, covered and kept at room temperature overnight until coating solution evaporation.	20 µg
PCL/Heparin emulsion	Heparin or heparin-FITC(Thermofisher) at a concentration of 0.5% (w/w) of total PCL was dissolved in 85 µl water + 15 µl Tween 20 was added dropwise to 15 wt.% PCL solution in DCM/DMF (90:10, v/v) (15 ml) and stirred overnight prior electrospinning. This method was adapted from (Luong-Van et al., 2006)	17 µg
Covalent binding	PCL scaffolds were incubated for 2 h in an aminolysis solution composed of 10% (v/v) 1,6-hexanediamine dissolved in isopropanol. Scaffolds were washed twice with water and let it dry overnight at room temperature. Sodium salt heparin was weighted (40 mg) and dissolve it in sodium citrate buffer (20ml) containing WSC (40 mg). Heparin/WSC solution was stored in the fridge for 5h to activate the carboxylic groups of heparin. After aminolysis, PCL scaffolds were incubated in the heparin activated solution for 48h at 4°C. After incubation scaffolds were washed 3x with PBS, 1x with 1% (v/v) Triton-X and 1x deionized water. This method was adapted from (Gümüşderelioğlu et al., 2011).	22.85 µg

The sodium citrate buffer was prepared by dissolving 2.94g of tri-sodium citrate in deionized water and mix. The pH was adjusted to 6 with 1M HCl solution and 0.5ml Tween 20 was added. The buffer was slowly missed and filtrated with a 0,22µm filter before storage for 6 months in the fridge.

3.3.16 Heparin detection

Toluidine blue

To identify and evaluate heparin distribution within electrospinning scaffolds a 0.04% toluidine blue was prepared using 0.1 M sodium acetate (pH 4.0). Samples were incubated with staining solution for 15min and wash several times. Some samples were washed previously for 30 min with PBS followed by toluidine blue staining.

Nuclear magnetic resonance (NMR)

PCL scaffolds were dissolved in 1 mL chloroform and stirred overnight. Then, 500 μ l deuterated water was added to solution and heparin was extracted to the aqueous phase (phase separation). ^1H NMR spectra were recorded with a Bruker AVIII 400MHz NMR system spectrometer. Chemical shifts are reported in ppm relative to the deuterated solvent resonances.

3.3.17 Dimethylmethylene blue dye (DMB) assay for heparin quantification

Heparin was extracted from scaffolds by phase separation (see previous section 3.3.15). Per each studied condition, extracted heparin aqueous samples were used to detect heparin by DMB assay (duplicate). A DMB aqueous stock solution (0.019 mM DMB, 1.52 g glycine, 1.18 g NaCl, 450 mL water) was prepared, mixed for 2 h and pH was adjusted to pH=3. Native heparin and samples were serially diluted in distilled water added (20 μ l) to a 96-well plate in triplicate plus 250 μ l DMB dye solution. Absorbance was measured at 525 nm and heparin quantification was extrapolated from heparin standard curve (heparin concentration range 0 – 100 μ g; 7 reading points).

3.3.18 Mechanical testing

The stiffness of electrospinning mats was determined using a unidirectional tensiometer (EnduraTEC ELF3200 BOSE). Prior mechanical testing, scaffolds were cut into strips, thickness was measured (12 mm x 5 mm) and average Young's modulus was acquired for electrospinning PCL versus PCL/heparin emulsion scaffolds by analysing 5 samples per studied condition using standard protocol for membranes characterisation established for the used tensiometer.

3.3.19 X-ray spectroscopy (XPS)

A Kratos Axis Ultra DLD system was used to collect XPS spectra using monochromatic Al $K\alpha$ X-ray source operating at 120 W (10 mA x 12 kV). Data was collected with pass energies of 160 eV for survey spectra, and 40 eV for the high-resolution scans with step sizes of 1 eV and 0.1 eV respectively. The system was operated in the Hybrid mode, using a combination of magnetic immersion and electrostatic lenses and acquired over an area approximately $300 \times 700 \mu\text{m}^2$. A magnetically confined charge compensation system was used to minimize charging of the sample surface, and all spectra were taken with a 90° take off angle. A base pressure of $\sim 1 \times 10^{-9}$ Torr was maintained during collection of the spectra. Data was analysed using CasaXPS (v2.3.19rev1.1l) after subtraction of a Shirley background and using modified Wagner sensitivity factors as supplied by the manufacturer. XPS data collection was performed at the EPSRC National Facility for XPS ('HarwellXPS'), operated by Cardiff University and UCL, under contract No. PR16195.

3.3.20 Statistics

All data is presented as the mean \pm S.D (standard deviation). For statistical analysis, unpaired t-tests of repeated measures one-way analysis of variance (ANOVA) was performed using Prism 7.02 software (GraphPad, San Diego, USA) and $P < 0.05$ was considered to indicate significance. P-values; * $p < 0.05$; ** $p < 0.01$; *** $p < 0.001$; **** $p < 0.0001$; ns – not significant ($p > 0.05$).

3.4 Results and discussion

3.4.1 Micropatterned Scaffolds

Scaffold Manufacture

Micropatterned PCL scaffolds were manufactured using an electrospinning rig and patterned collectors in order to obtain micropatterned PCL scaffolds (**Figure 3.2**) This manufacture method is easily reproducible for 10 wt. % PCL solutions and will be maintained for future experiments in this rig.

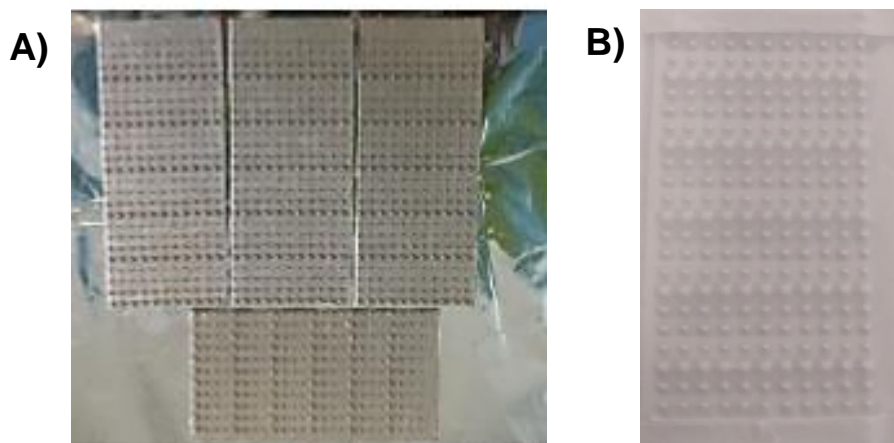


Figure 3.2 Patterned collectors and patterned PCL scaffolds. A) A patterned stainless steel collector manufactured by SLM (3cmx7cm) was used to obtain B) micropatterned electrospin 10 wt.% PCL scaffolds.

3.4.1.1 Fibres alignment and diameter

Micropatterned scaffolds were characterized based on their fibre alignment and diameter that were measured by ImageJ software using SEM images of electrospinning scaffolds. The measurements of fiber diameter and alignments were performed in different locations of the micropattern – micropattern walls, micropattern bottom and outside the micropattern – as it is represented in **Figure 3.3**. In SEM images from **Figure 3.4** it is possible to observe the differences between fibre alignments in 10 wt.% PCL electrospinning micropatterned scaffolds. SEM images only provide a qualitative analysis on fibres alignment therefore quantitative measurements on alignment and fibre diameter were analysed by ImageJ.

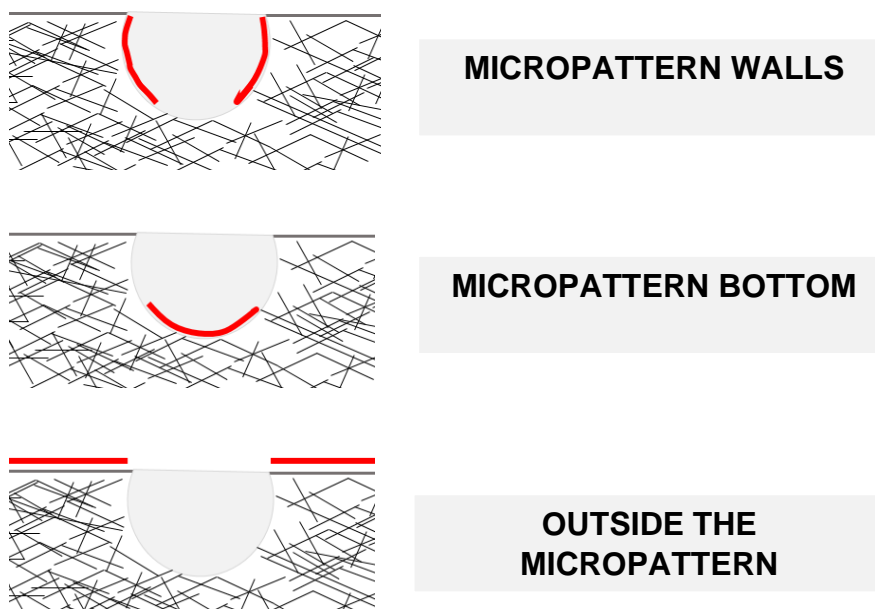


Figure 3.4 Schematic representation of an electrospinning micropattern. Scaffolds fibres were measured in different locations of the micropattern. Measurements were taken from the areas highlighted in red. SEM

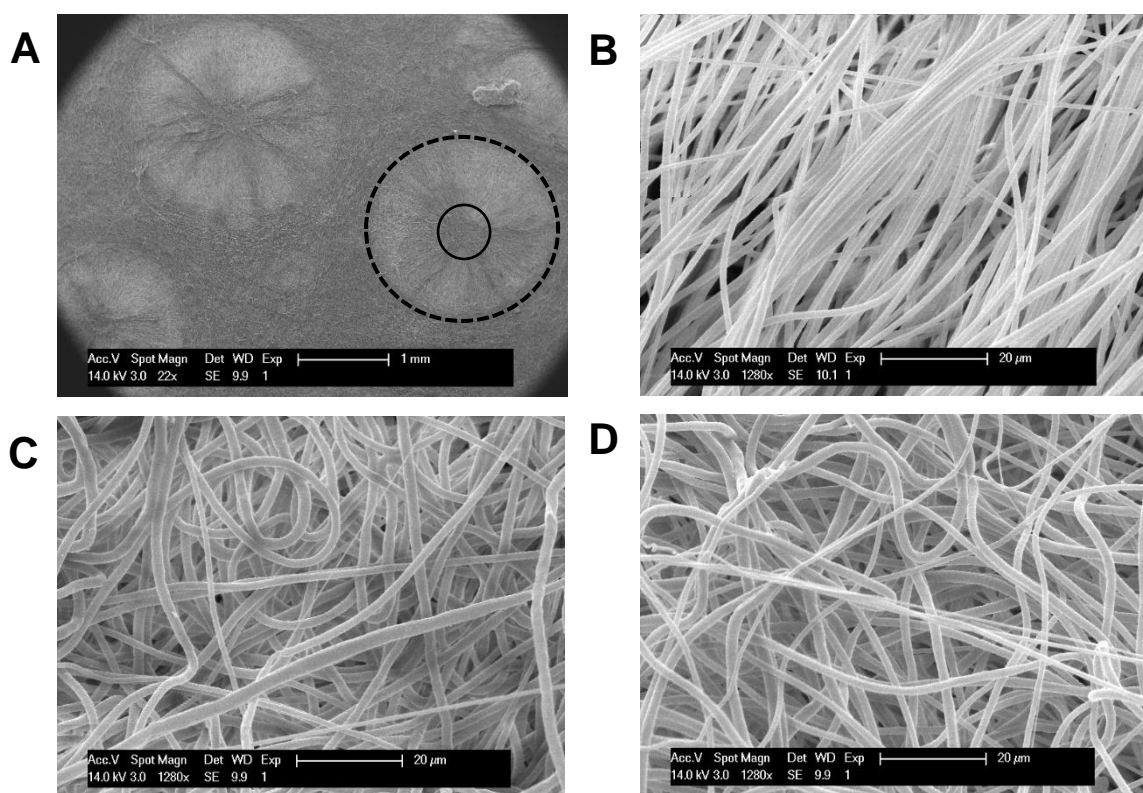


Figure 3.3 SEM images of micropatterned PCL scaffolds. A) Micropatterns B) Fibres located at bottom of the micropattern C) Fibres located at micropattern walls D) Fibres located outside the micropattern

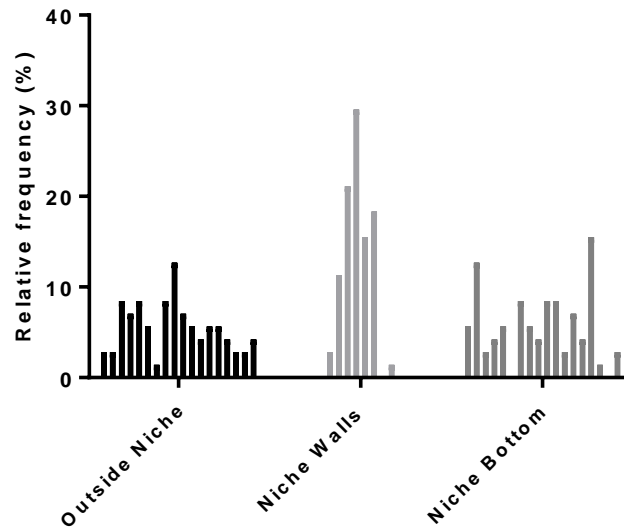


Figure 3.5 Histogram of fibres angle distribution (%) in PCL electrospinning scaffolds. Results are displayed between 80° and -80° and separated per micropattern location (n=40). Data was normalized by mean subtraction.

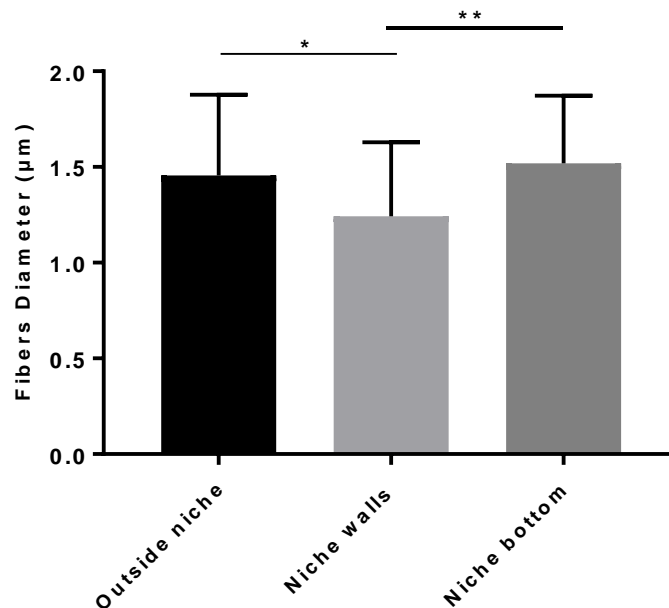


Figure 3.6 Electrospinning PCL fibres average diameters (n=10). Results are displayed as mean \pm SD, *p < 0.05; **p < 0.01; ***p < 0.001; ****p < 0.0001; ns – not significant (p > 0.05).

By analysing **Figure 3.5**, fibres located in the micropattern walls show a narrower angle distribution which can indicate a higher degree of fibres alignment in comparison with fibres outside the micropattern and in micropattern bottom. The average diameters of fibres show no significant difference between micropattern bottom (mean= $1.52 \pm 0.3 \mu\text{m}$) and outside the

micropattern (mean= $1.46 \pm 0.4 \mu\text{m}$) but are significantly different when compared with fibres located in the micropattern walls (mean= $1.24 \pm 0.4 \mu\text{m}$) (**Figure 3.6**). We hypothesize that different surface topographies present in micropatterned scaffolds, could have an impact on cell morphology by triggering specific signalling pathways that determine stem cells fate, either differentiation or stemness maintenance.

The novelty to have a microstructure that presents aligned and random topographies to cells might be promising since increasing intracellular stress can consequently stimulate osteogenesis. This result may or may not be applicable for MSCs cultures on fibrous scaffolds however more studies will be needed in order to find a specific combination between cell density, cell shape, scaffolds stiffness and biofunctionalization which stimulates MSCs osteogenic differentiation. As previously suggested, stem cells acquire round shapes on random fibrous scaffolds and elongated shapes on aligned fibrous scaffolds (McBeath et al., 2004). Elongated shapes are related with higher intracellular stress which can promote osteogenesis but also myogenesis (Newman et al., 2016). McBeath et al., showed that MSCs shape-dependent osteogenic commitment process is mediated by Rho family GTPases which have higher activity in spread cells than unspread ones. In contrast, a recent study from Newman et al., showed that adipose stem cells (ASCs) cultured on flat, random and aligned carbon nanotubes topographies do not have a significant difference when it comes to osteogenic markers upregulation.

During scaffold manufacturing, electrospinning parameters were maintained constant in order to get smooth fibre assemblies but occasionally beads were detected. Beads presence might occur due to room temperature changes, humidity changes or slight variations in solution viscosity due to solvent evaporation (Haider et al., 2018). This results shows that due to electrospinning parameters variability, some scaffolds might present beads or other differences.

3.4.1.2 Micropattern size diameters

The size of the electrospinning micropatterns was measured using SEM images and ImageJ® software. Two types of micropattern structures are presented in **Figure 3.3**. The diameter of at least 10 microstructures per type were measured and the results are presented on **Table 3.2**. These microstructures are obtained by using patterned electrospinning collectors as it was previously reported by Paterson et.al, 2017. The different micropatterned sizes were chosen based on the knowledge that a stem cell niche is a specific delimited microenvironment that might have biologically a microscale size as it was identified in cornea (Ortega et al., 2013a) and intestinal villi (Elmes et al., 1983). The biggest micropatterns (N1) were chosen for practical reasons in order to facilitate the coating process. The reproducibility of these microstructures is related with the decrease in size of the microstructure in the template. Some of the micropatterned sizes can collapse or merge after scaffold manufacture. Due to this reason, future templates should be made with 500 µm diameter micropatterns (N2) since are big enough to not collapse and small enough to not merge with surrounding patterns. In conclusion, the produced fibrous scaffolds were characterised and can mimic certain aspect of the natural ECM. Adding micropatterned is a simple technique that adds a higher degree of complexity which can be relevant to differentiation and mechanobiology studies where additional measurements should be performed (micropattern depth, fibres stiffness).

Table 3.2 Micropatterns diameters and area obtained from electrospinning patterned PCL scaffolds.

Micropattern Diameter (mm)				Circular Area (mm ²)			
Micropattern (N1)		Micropattern (N2)		Micropattern (N1)		Micropattern (N2)	
Mean	S.D.	Mean	S.D.	Mean	S.D.	Mean	S.D.
2.08	0.22	1.71	0.08	3.43	0.75	2.31	0.22

3.5.1.3 Heparin detection on coated micropatterns

The presence of fluorescent heparin on coated electrospinning micropatterns was assessed at 5 time points during 15 days at 37°C. Using a fluorescent microscope, pictures taken from coated micropattern over 14 days are displayed in Figure 3.9. Heparin presence was visually

detected after 15 days PBS incubation. Simple adsorption of biomolecules is susceptible to burst release therefore, and despite these results, heparin quantification is required to understand if the detection here observed is actually significant or residual. Although crosslinking techniques could be used, it might affect fibres morphology or cause toxicity.

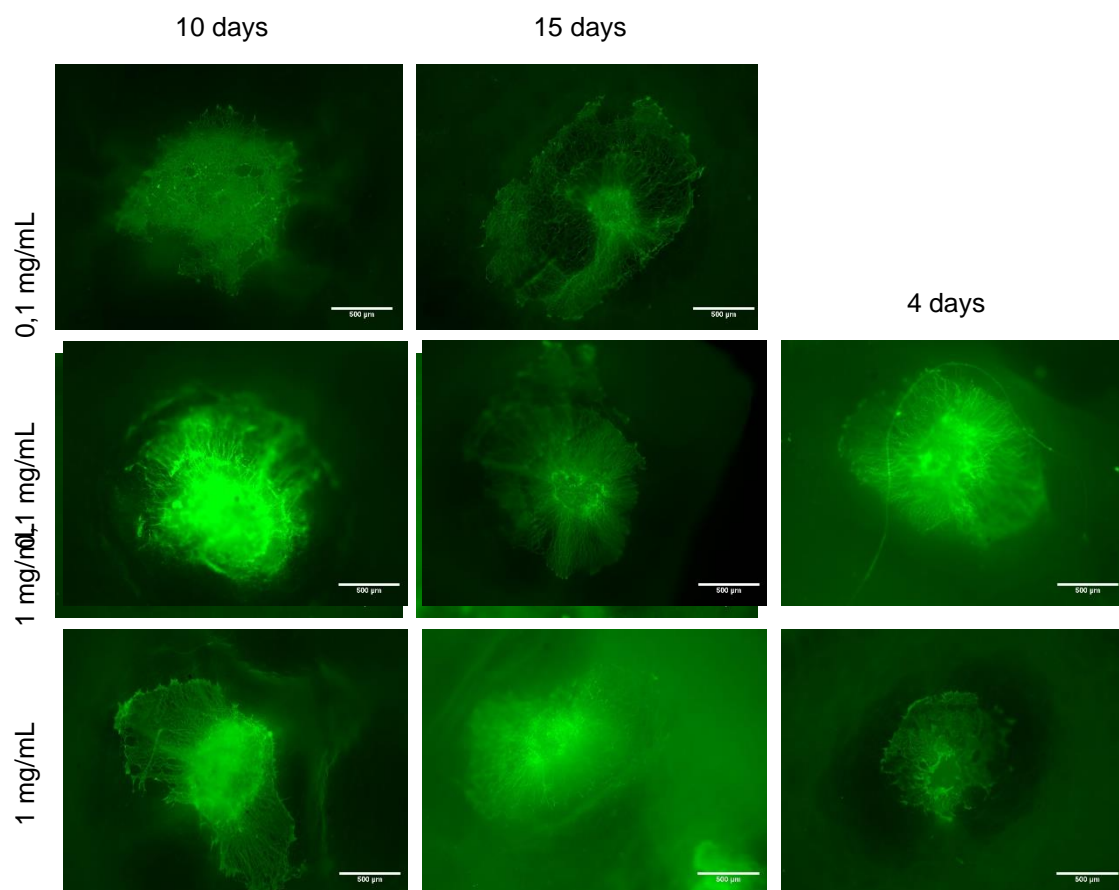


Figure 3.7 Heparin detection on micropatterned electrospinning PCL scaffolds coated with heparin-FITC. Confocal microscopy images were obtained during 15 days from samples incubated in PBS at 37°C. Scale bar = 500 µm.

3.5.2 Biocompatibility assays

To assess cells biocompatibility on electrospinning scaffolds, cells proliferation was studied on plain versus micropatterned scaffolds as well as coated versus non coated micropatterned scaffolds.

3.5.2.1 Micropatterned scaffolds vs plain scaffolds

Preliminary experiments were performed to compare rat MSCs passage 5 (P5) cultured on electrospinning PCL micropatterned scaffolds versus non-micropatterned scaffolds (plain). Cells viability was assessed by Presto Blue (Figure 3.10) assay and cells morphology was assessed by DAPI (nuclei) and FITC (actin filaments) staining after 7 days culture (Figure 3.11). Rat MSC cultured on flat polystyrene were used as control.

Cells proliferation data (**Figure 3.8**), indicates no significant differences between PCL plain scaffolds and micropatterned scaffolds. As previously stated, PCL is a biocompatible material therefore this results were expected as scaffolds are made of PCL. During manufacture organic solvent are used but are possibly totally evaporated or at such residual amount that cell proliferation is not affected. Due to the high variability of results, further replicates are needed conclusive comparison. However, presented results imply that out manufactured electrospinning PCL scaffolds are biocompatible after manufacture. On scaffolds, cells presented a good distribution on both micropattern and plain scaffolds. Moreover, on micropattern walls cells spread along the aligned fibres versus randomly aligned (plain scaffolds). This observation has been previously described in aligned electrospinning scaffolds not only for bone repair (Chen et al., 2013) therefore this indicates that cells morphology adapts differently to surface topography.

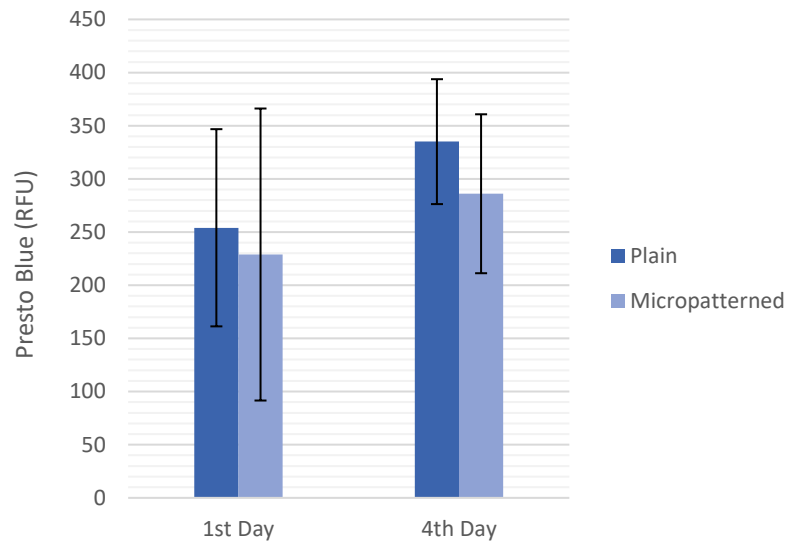


Figure 3.8 Rat MSCs proliferation on electrospun PCL scaffold with and without micropatterns during 4 days of culture. Results are displayed as mean \pm SD (standard deviation). (n=1)

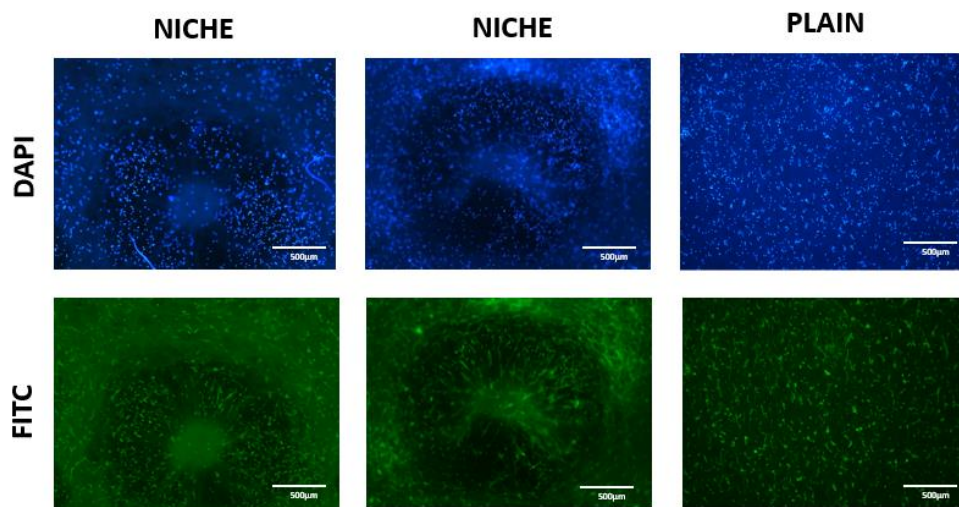


Figure 3.9 Rat MSCs (P5) nuclei (DAPI) and actin filaments (FITC) staining after 7 days of culture on scaffold with and without micropatterns. (n=1)

3.5.2.2 Heparin coated vs non-coated micropatterned scaffolds

Cells proliferation was further assessed on heparin coated micropatterned scaffolds by simple adsorption. Samples were coated with heparin or heparin-FITC at a concentration of 0.1 and 1 mg/mL during 10 days. Proliferation was measure by PrestoBlue assay on rat MSCs cultures (Figure 3.12). Comparing all studied conditions, cell proliferation did not show significant differences or significant growth during 10 days. Fluorescent heparin versus non-fluorescent have been compared in order to understand if the fluorescent label interferes in a different way to MSCs proliferation however, heparin sodium salt and fluorescent heparin have showed a similar response during cell culture viability tests. All the conditions supported cell survival however further studies are needed to understand their effect on osteogenic and MSCs markers expression.

In summary, the produced fibrous scaffolds were characterised and can mimic certain aspect of the natural ECM. Adding micropatterned is a simple technique that adds a higher degree of complexity which can be relevant to trigger cells differentiation and in future mechanobiology studies. Although cell culture experiments did not show any significant difference between studied scaffolds, all supported cells survival. To achieve an improved scaffold characterisation, additional measurements should be performed (micropattern depth, fibres stiffness). Simple adsorption proved to be a simple way to functionalise scaffolds but for lasting results heparin coating should be effectively durable and easily controllable in terms of heparin content and distribution within scaffolds. Hence, different heparin functionalisation methods will be explored in the next section.

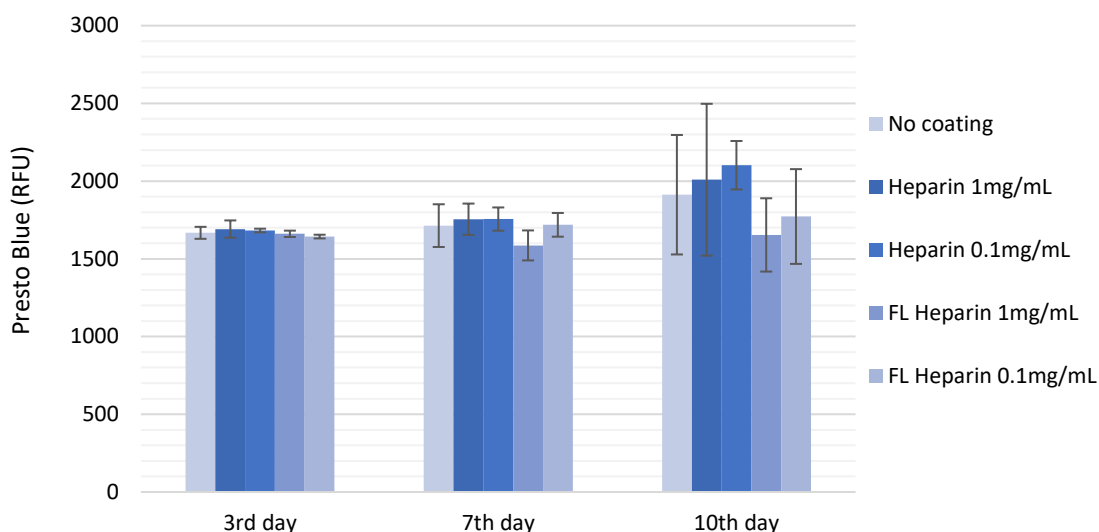


Figure 3.10 Rat MSCs (P4) cultured on micropatterned PCL electrospun scaffolds coated with heparin sodium salt (1mg/mL and 0,1mg/mL), heparin-FITC (1mg/mL and 0,1mg/mL) versus no coated scaffolds. Cells proliferation was measured every 3rd, 7th and 10th days by PrestoBlue assay. Results displayed as mean \pm SD

3.5.3 Heparin incorporation into PCL scaffolds

To incorporate heparin into the scaffolds, three different functionalisation methods were investigated:

1) Simple adsorption was explored due to its simplicity even though it has been associated with burst release in the literature instead of a controlled heparin release necessary to support tissue regeneration overtime.

2) A second approach was investigated focused on the manufacture of PCL/heparin emulsion electrospinning scaffolds. Heparin was mixed with an aqueous Tween solution into a polymeric solution prior electrospinning. Heparin has low solubility in organic solvents, therefore we hypothesise that by using an emulsion strategy allows heparin to be encapsulated within a insoluble phase of PCL + organic solvent and less susceptible to burst release than simple adsorption.

3) Heparin covalent binding was the last method to be explored. WSC coupling agent combined with heparin was applied on PCL electrospinning scaffolds after aminolysis. In theory, this method allows heparin to PCL more effectively than previous methods but did not delivered consistent results nor homogenous spread of heparin on the surface of scaffolds. Using SEM imaging, fibre characterization was performed on PCL, PCL/heparin emulsion scaffolds and heparin covalent binding showing good consistency, smoothness and similar fibres diameter despite different functionalisation methods (**Figure 3.13**). As a qualitative assessment, heparin presence and distribution on the surface of functionalised PCL electrospinning scaffolds and plain PCL films was observed by Toluidine Blue staining, GAGs = purple stain (**Figure 3.14**). In this preliminary assay, heparin was detected in all functionalised scaffolds (flat versus electrospinning) but more significantly on electrospinning scaffolds probably because of fibrous higher surface area when in comparison to flat polymeric discs. PCL films showed a more homogenous heparin binding for simple adsorption and heparin covalently bound however PCL/heparin emulsion has a lower heparin detection.

Scaffolds	PCL	PCL/Heparin Emulsion	Heparin Covalent Binding
Fibre diameter (μm)	1.58 ± 0.54	1.39 ± 0.34	1.47 ± 0.39

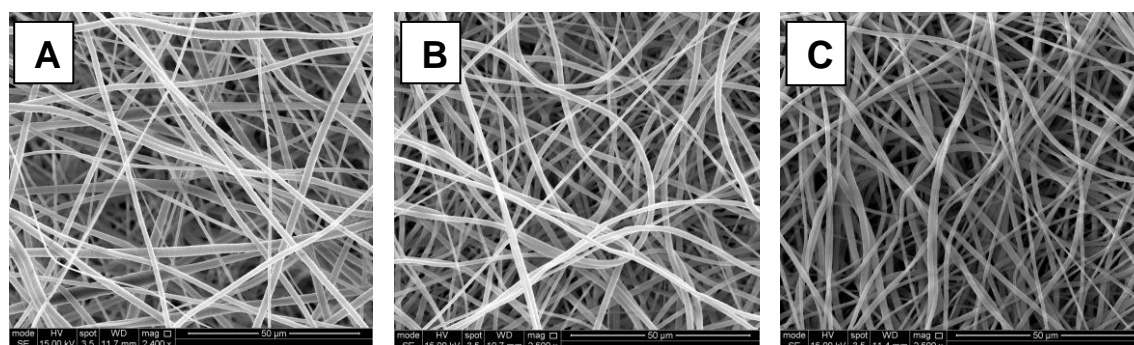


Figure 3.11 SEM images of 3 different types of electrospinning scaffolds. A) PCL only, B) PCL/heparin emulsion and C) PCL scaffold after heparin covalent binding. Scale bar represents 50 μm . The fibre diameter for PCL, PCL/heparin emulsion and PCL/Heparin covalent binding scaffolds was determined by ImageJ. Values are represented as Mean \pm SD. (n=3)

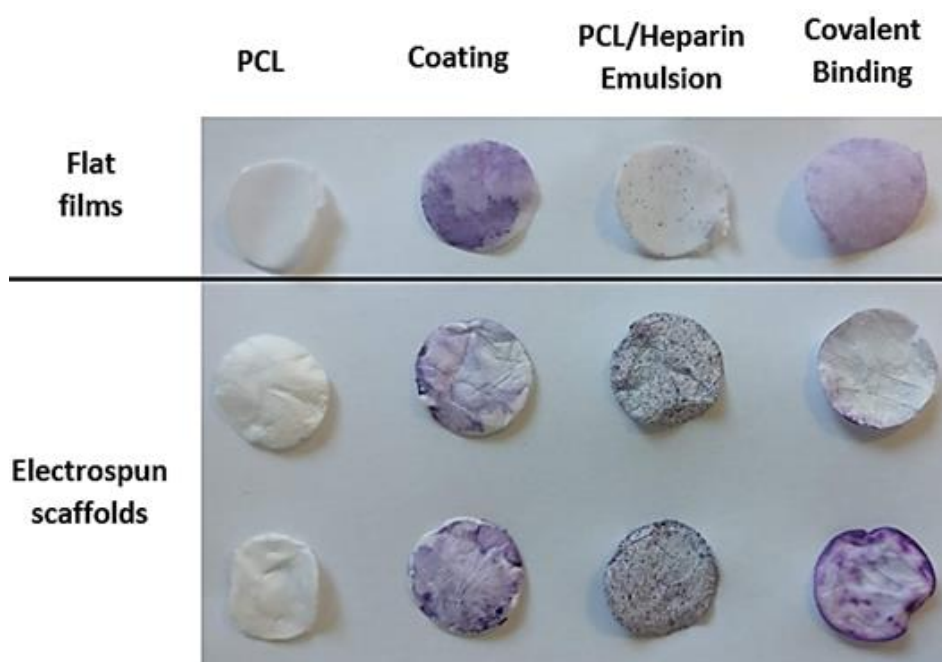


Figure 3.12 Heparin staining with toluidine blue dye solution. Heparin incorporation into PCL flat films (n=1) and electrospinning PCL scaffolds by simple adsorption, heparin emulsion and covalent binding (n=2). Purple dye identifies GAGs. PCL/heparin emulsion showed more consistency between replicate scaffolds.

Electrospinning scaffolds show a good heparin distribution for simple adsorption and heparin emulsion however covalently bound heparin did not show consistent results. According with our experience the heparin covalent binding protocol showed low reproducibility on electrospinning scaffolds and more optimisation is needed. To support these observations is important to quantify heparin content per scaffold and respective elution profile over time. For example a PCL scaffold was previously described for the control release of fluorescently labelled heparin (Luong-Van et al., 2006). A similar quantification strategy could be applied to determine heparin release over time for each functionalisation in study. We briefly explored two quantification methods based on Toluidine Blue or DMB staining using previous established protocols within our research group. The studied quantification methods proved to be quite variable on electrospinning scaffolds because of scaffolds structural variability (i.e., weight, surface area). Quantification based on toluidine blue dye did not deliver reliable results for heparin detection. DMB quantitative assay was able to detect heparin on electrospinning scaffolds however it still requires further protocol optimisation to be considered a robust and reliable protocol (data not showed).

PCL/heparin emulsion electrospinning scaffolds was selected for further analysis due to manufacture simplicity, novelty and functionalisation consistency observed from toluidine blue staining. First, PCL/heparin-FITC emulsion electrospinning scaffolds were analysed using confocal microscopy to confirm heparin presence and distribution. To support this observation, heparin detection on PCL/heparin emulsion scaffolds was also analysed by NMR and XPS (Figure 3.15 – 3.17). NMR results clearly show the presence of heparin within the PCL/heparin emulsion scaffold (Figure 3.15) in comparison to PCL scaffold. XPS mapping provided preliminary data not only about heparin presence but also distribution (Figure 3.16 and 3.17).

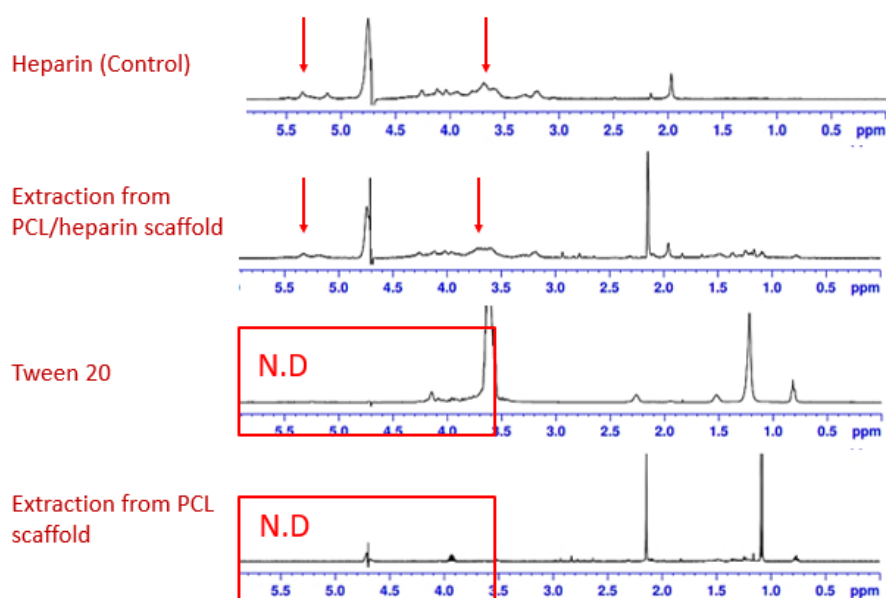


Figure 3.13 ¹H-NMR spectra of heparin, PCL/heparin emulsion electrospinning scaffolds extract and PCL electrospinning scaffolds extract (water peak suppression at 4.7 ppm). NMR, nuclear magnetic resonance.

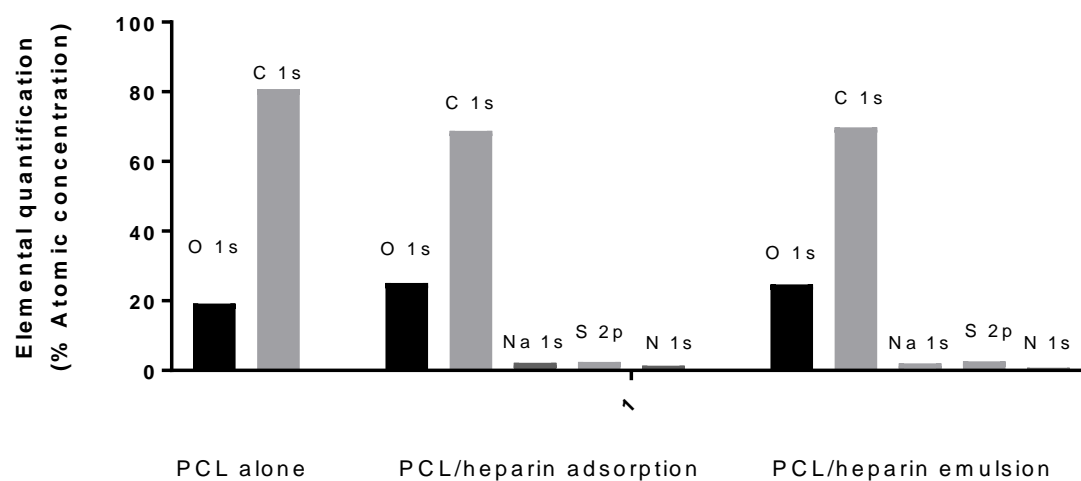
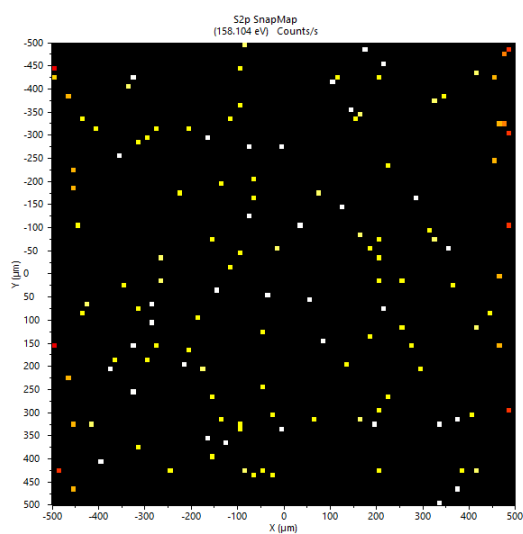
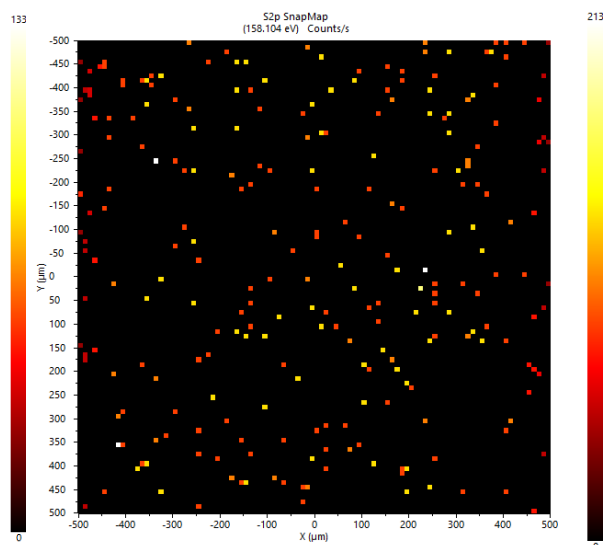


Figure 3.14 XPS elemental quantification of C (carbon 1s), O (oxygen 1s), N (nitrogen 1s) and Sulphur (S 2p) on heparin functionalised scaffolds. C and O are the main elements from PCL scaffolds with residual detection of N and S present on heparin. (n=1)

1. PCL (control)



2. PCL/heparin simple adsorption



3. PCL/heparin emulsion

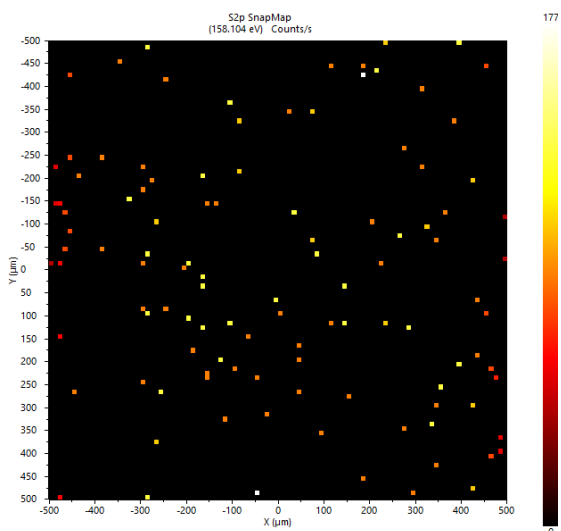


Figure 3.15 XPS surface mapping (sulphur) of heparin functionalised electrospinning scaffolds versus non-functionalised PCL electrospinning scaffold. Sample 2 (simple coating) contains the most N and S followed by sample 3 (PCL/heparin emulsion). PCL control only contains C and O.

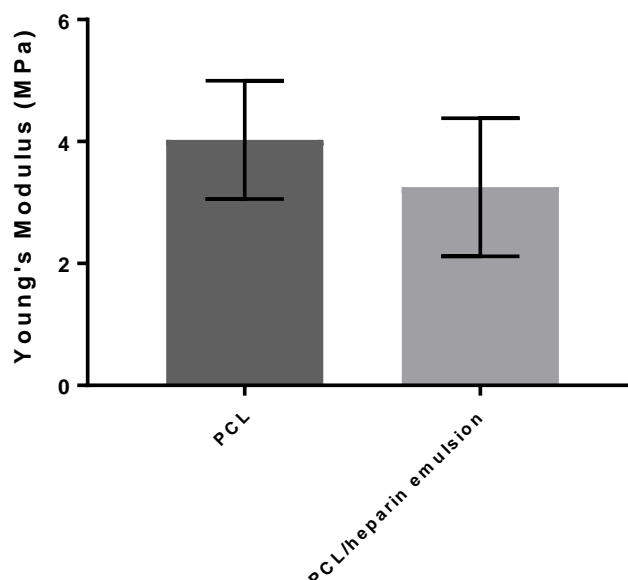


Figure 3.16 Shown data compares stiffness of polycaprolactone (PCL) versus PCL/Heparin emulsion electrospinning scaffolds, obtained using a unidirectional tensiometer (EnduraTEC elf3200 BOSE) Results are shown as mean±SD. Data from 2 independent experiments including five technical repeats per condition. Statistical analysis shows no significant differences between groups ($p > 0.05$).

XPS data shows heparin mapping and heparin content (N and S tracing) on electrospinning functionalised scaffold (simple adsorption and PCL/heparin emulsion) at atomic concentrations. XPS mapping indicates a higher heparin content on PCL/heparin simple adsorption and a lower content and heparin dispersion for PCL/heparin emulsion scaffolds (**Figure 3.16 and 3.17**). This preliminary data can be used to further optimise manufacture protocols and should also be compared with PCL/heparin covalent binding scaffolds for a better comparison overview of functionalisation methods. Stiffness was also explored evaluated between PCL alone and PCL/heparin emulsion but no significant differences were found (**Figure 3.18**).

From these preliminary experiments, we were able to investigate different ways to introduce complexity into electrospinning scaffolds. Due to the initial promising results using heparin and the expertise in the area from our collaborators at A*STAR therefore, we have decided to develop a method for the generation of heparin oligosaccharides (i.e., dp12) that enhance BMP-2-mediated bone regeneration. Moreover, when functionalized to electrospinning

scaffolds by ROMP-based chemistry, heparin oligosaccharides will possibly sustain BMP-2 signals over a prolonged period. ECM chemical and structural stimuli are essential for cell differentiation and tissue repair however is still difficult to recreate synthetically all the features that contribute for bone tissue repair. Instead we will explore mimicking certain aspects of the natural ECM structure by selecting small osteogenic factor binding heparin oligosaccharides to functionalise fibrous polymeric scaffolds. In contrast with the use of complex molecules such as heparin, the use of immobilised oligosaccharides may lead to easier tunability of biomaterial formulations (Benoit et al., 2008; Maia et al., 2013).

7.5 Final conclusion

This study suggests that nitrous acid depolymerisation is a simple and affordable method to obtain bioactive heparin oligosaccharides in comparison to enzymatic depolymerisation. Chain length homogenous populations of nitrous acid generated oligosaccharides enhanced BMP-2 activity and can be successfully incorporated into ROMP-based polymers. These findings can be used to develop affordable and factor-specified glycotherapies and to develop novel ROMP-based oligosaccharide containing copolymers for bone tissue engineering. Although the characterisation of bioactive copolymer scaffolds needs to be further explored in terms of heparin distribution, content and BMP-2 binding ability, the development of such advanced materials could be combined with a wide range of scaffolds manufacturing routes to control cells behaviour using chemical and mechanical cues.

Covid-19 Impact on the PhD project

As early as January 2020, Singapore started being mildly affected by the spread of the virus. Gradually supply chains were affected and additional on/off working shifts were implemented. This disruption affected all the final PhD year and ongoing experiments were lost. After, 2 months' lockdown we continued to work in rotational shifts until September 2020. Aside how this pandemic has affected us personally, this entire situation has contributed to the lack of replicates in some experiments, lack of time to optimise immunostaining protocols as well as proper biomaterials and scaffolds characterisation. Nevertheless, I am thankful for A*STAR

(Singapore) support as well as my supervisors support letters who granted me extra 6 months of funding that allowed me to present a more composed thesis.

References

- Abdelmoneim, D., Alhamdani, G.M., Paterson, T.E., Santocildes Romero, M.E., Monteiro, B.J.C., Hatton, P.V., and Ortega Asencio, I. (2020). Bioactive and Topographically-Modified Electrospinning Membranes for the Creation of New Bone Regeneration Models. *Processes* 8, 1341.
- Abou Neel, E.A., Aljabo, A., Strange, A., Ibrahim, S., Coathup, M., Young, A.M., Bozec, L., and Mudera, V. (2016). Demineralization–remineralization dynamics in teeth and bone. *Int. J. Nanomedicine* 11, 4743–4763.
- Akram, N. (2018). A Review on High Performance Liquid Chromatography (HPLC). *Int. J. Res. Appl. Sci. Eng. Technol.* 6, 488–492.
- Alaribe, F.N., Manoto, S.L., and Motaung, S.C.K.M. (2016). Scaffolds from biomaterials: advantages and limitations in bone and tissue engineering. *Biologia (Bratisl.)* 71, 353–366.
- Amini, A.R., Laurencin, C.T., and Nukavarapu, S.P. (2012). Bone Tissue Engineering: Recent Advances and Challenges. *Crit. Rev. Biomed. Eng.* 40, 363–408.
- Annaval, T., Wild, R., Créton, Y., Sadir, R., Vivès, R.R., and Lortat-Jacob, H. (2020). Heparan Sulfate Proteoglycans Biosynthesis and Post Synthesis Mechanisms Combine Few Enzymes and Few Core Proteins to Generate Extensive Structural and Functional Diversity. *Molecules* 25, 4215.
- Asencio, I.O., Mittar, S., Sherborne, C., Raza, A., Claeysens, F., and MacNeil, S. (2018). A methodology for the production of microfabricated electrospinning membranes for the creation of new skin regeneration models. *J. Tissue Eng.* 9, 2041731418799851.
- Aspray, T.J., and Hill, T.R. (2019). Osteoporosis and the Ageing Skeleton. *Subcell. Biochem.* 91, 453–476.
- Astronomo, R.D., and Burton, D.R. (2010). Carbohydrate vaccines: developing sweet solutions to sticky situations? *Nat. Rev. Drug Discov.* 9, 308–324.
- Atkins, G.J., Kostakis, P., Vincent, C., Farrugia, A.N., Houchins, J.P., Findlay, D.M., Evdokiou, A., and Zannettino, A.C. (2006). RANK Expression as a Cell Surface Marker of Human Osteoclast Precursors in Peripheral Blood, Bone Marrow, and Giant Cell Tumors of Bone. *J. Bone Miner. Res.* 21, 1339–1349.
- Bae, S., DiBalsi, M.J., Meilinger, N., Zhang, C., Beal, E., Korneva, G., Brown, R.O., Kornev, K.G., and Lee, J.S. (2018). Heparin-Eluting Electrospinning Nanofiber Yarns for Antithrombotic Vascular Sutures. *ACS Appl. Mater. Interfaces* 10, 8426–8435.
- Baik, J.Y., Wang, C., Yang, B., Linhardt, R., and Sharfstein, S. (2012). Toward a bioengineered heparin. *Bioengineered* 3, 227–231.
- Bara, L., Billaud, E., Gramond, G., Kher, A., and Samama, M. (1985). Comparative pharmacokinetics of a low molecular weight heparin (PK 10 169) and unfractionated heparin after intravenous and subcutaneous administration. *Thromb. Res.* 39, 631–636.
- Baumann, H., Scheen, H., Huppertz, B., and Keller, R. (1998). Novel regio- and stereoselective O-6-desulfation of the glucosamine moiety of heparin with N-

methylpyrrolidinone-water or N,N-dimethylformamide-water mixtures. *Carbohydr. Res.* 308, 381–388.

Beachley, V., and Wen, X. (2010). Polymer nanofibrous structures: Fabrication, biofunctionalization, and cell interactions. *Prog. Polym. Sci.* 35, 868–892.

Ben-Ami, E., Berrih-Aknin, S., and Miller, A. (2011). Mesenchymal stem cells as an immunomodulatory therapeutic strategy for autoimmune diseases. *Autoimmun. Rev.* 10, 410–415.

Benoit, D.S.W., Schwartz, M.P., Durney, A.R., and Anseth, K.S. (2008). Small functional groups for controlled differentiation of hydrogel-encapsulated human mesenchymal stem cells. *Nat. Mater.* 7, 816–823.

Bertozzi, C.R., and Sasisekharan, R. (2009). Glycomics. In *Essentials of Glycobiology*, A. Varki, R.D. Cummings, J.D. Esko, H.H. Freeze, P. Stanley, C.R. Bertozzi, G.W. Hart, and M.E. Etzler, eds. (Cold Spring Harbor (NY): Cold Spring Harbor Laboratory Press), p.

Bhakta, G., Rai, B., Lim, Z.X.H., Hui, J.H., Stein, G.S., van Wijnen, A.J., Nurcombe, V., Prestwich, G.D., and Cool, S.M. (2012). Hyaluronic acid-based hydrogels functionalized with heparin that support controlled release of bioactive BMP-2. *Biomaterials* 33, 6113–6122.

Bianco, P. (2015). Stem cells and bone: A historical perspective. *Bone* 70, 2–9.

Bosworth, L.A., Rathbone, S.R., Bradley, R.S., and Cartmell, S.H. (2014). Dynamic loading of electrospinning yarns guides mesenchymal stem cells towards a tendon lineage. *J. Mech. Behav. Biomed. Mater.* 39, 175–183.

Brignier, A.C., and Gewirtz, A.M. (2010). Embryonic and adult stem cell therapy. *J. Allergy Clin. Immunol.* 125, S336–S344.

Calvi, L.M., Adams, G.B., Weibrecht, K.W., Weber, J.M., Olson, D.P., Knight, M.C., Martin, R.P., Schipani, E., Divieti, P., Bringham, F.R., et al. (2003). Osteoblastic cells regulate the haematopoietic stem cell niche. *Nature* 425, 841–846.

Candela, M.E., Yasuhara, R., Iwamoto, M., and Enomoto-Iwamoto, M. (2014). Resident mesenchymal progenitors of articular cartilage. *Matrix Biol.* 39, 44–49.

Casper, C.L., Yamaguchi, N., Kiick, K.L., and Rabolt, J.F. (2005). Functionalizing Electrospinning Fibers with Biologically Relevant Macromolecules. *Biomacromolecules* 6, 1998–2007.

Casu, B., Guerrini, M., Naggi, A., Perez, M., Torri, G., Ribatti, D., Carminati, P., Giannini, G., Penco, S., Pisano, C., et al. (2002). Short Heparin Sequences Spaced by Glycol-Split Uronate Residues Are Antagonists of Fibroblast Growth Factor 2 and Angiogenesis Inhibitors [†]. *Biochemistry* 41, 10519–10528.

Centers for Disease Control and Prevention (CDC) (2008). Acute allergic-type reactions among patients undergoing hemodialysis--multiple states, 2007-2008. *MMWR Morb. Mortal. Wkly. Rep.* 57, 124–125.

Chan, B.P., and Leong, K.W. (2008). Scaffolding in tissue engineering: general approaches and tissue-specific considerations. *Eur. Spine J.* 17, 467–479.

Chen, G., Deng, C., and Li, Y.-P. (2012). TGF- β and BMP Signaling in Osteoblast Differentiation and Bone Formation. *Int. J. Biol. Sci.* 8, 272–288.

Chen, X., Fu, X., Shi, J., and Wang, H. (2013). Regulation of the osteogenesis of pre-osteoblasts by spatial arrangement of electrospinning nanofibers in two- and three-dimensional environments. *Nanomedicine Nanotechnol. Biol. Med.* 9, 1283–1292.

Chen, Y., Shao, J.-Z., Xiang, L.-X., Dong, X.-J., and Zhang, G.-R. (2008). Mesenchymal stem cells: A promising candidate in regenerative medicine. *Int. J. Biochem. Cell Biol.* 40, 815–820.

Cheng, C.W., Solorio, L.D., and Alsberg, E. (2014). Decellularized Tissue and Cell-Derived Extracellular Matrices as Scaffolds for Orthopaedic Tissue Engineering. *Biotechnol. Adv.* 32, 462–484.

Cheung, H.-Y., Lau, K.-T., Lu, T.-P., and Hui, D. (2007). A critical review on polymer-based bio-engineered materials for scaffold development. *Compos. Part B Eng.* 38, 291–300.

Choinopoulos, I. (2019). Grubbs' and Schrock's Catalysts, Ring Opening Metathesis Polymerization and Molecular Brushes—Synthesis, Characterization, Properties and Applications. *Polymers* 11, 298.

Choong, C., Triffitt, J.T., and Cui, Z.F. (2004). Polycaprolactone Scaffolds for Bone Tissue Engineering. *Food Bioprod. Process.* 82, 117–125.

Chuang, W.-L., Christ, M.D., and Rabenstein, D.L. (2001). Determination of the Primary Structures of Heparin- and Heparan Sulfate-Derived Oligosaccharides Using Band-Selective Homonuclear-Decoupled Two-Dimensional ^1H NMR Experiments. *Anal. Chem.* 73, 2310–2316.

Clarke, B. (2008). Normal Bone Anatomy and Physiology. *Clin. J. Am. Soc. Nephrol. CJASN* 3, S131–S139.

Clement, A.L., Moutinho, T.J., and Pins, G.D. (2013). Micropatterned dermal-epidermal regeneration matrices create functional niches that enhance epidermal morphogenesis. *Acta Biomater.* 9, 9474–9484.

Copeland, R., Balasubramaniam, A., Tiwari, V., Zhang, F., Bridges, A., Linhardt, R.J., Shukla, D., and Liu, J. (2008). Using A 3-O-Sulfated Heparin Octasaccharide To Inhibit The Entry Of Herpes Simplex Virus-1. *Biochemistry* 47, 5774–5783.

Coulson-Thomas, Y.M., Coulson-Thomas, V.J., Norton, A.L., Gesteira, T.F., Cavaleiro, R.P., Meneghetti, M.C.Z., Martins, J.R., Dixon, R.A., and Nader, H.B. (2015). The Identification of Proteoglycans and Glycosaminoglycans in Archaeological Human Bones and Teeth. *PLOS ONE* 10, e0131105.

Crockett, J.C., Rogers, M.J., Coxon, F.P., Hocking, L.J., and Helfrich, M.H. (2011). Bone remodelling at a glance. *J Cell Sci* 124, 991–998.

Croisier, F., Duwez, A.-S., Jérôme, C., Léonard, A.F., van der Werf, K.O., Dijkstra, P.J., and Bennink, M.L. (2012). Mechanical testing of electrospinning PCL fibers. *Acta Biomater.* 8, 218–224.

Discher, D.E., Mooney, D.J., and Zandstra, P.W. (2009). Growth factors, matrices, and forces combine and control stem cells. *Science* 324, 1673–1677.

Dominici, M., Le Blanc, K., Mueller, I., Slaper-Cortenbach, I., Marini, F., Krause, D., Deans, R., Keating, A., Prockop, D., and Horwitz, E. (2006). Minimal criteria for defining multipotent mesenchymal stromal cells. The International Society for Cellular Therapy position statement. *Cytotherapy* 8, 315–317.

Dong, M., Wessels, M.G., Lee, J.Y., Su, L., Wang, H., Letteri, R.A., Song, Y., Lin, Y.-N., Chen, Y., Li, R., et al. (2019). Experiments and Simulations of Complex Sugar-Based Coil–Brush Block Polymer Nanoassemblies in Aqueous Solution. *ACS Nano* 13, 5147–5162.

Duan, J., and Amster, I.J. (2018). An Automated, High-Throughput Method for Interpreting the Tandem Mass Spectra of Glycosaminoglycans. *J. Am. Soc. Mass Spectrom.* 29, 1802–1811.

Einhorn, T.A., and Gerstenfeld, L.C. (2015). Fracture healing: mechanisms and interventions. *Nat. Rev. Rheumatol.* 11, 45–54.

Elmes, M.E., Jones, J.G., and Stanton, M.R. (1983). Changes in the Paneth cell population of human small intestine assessed by image analysis of the secretory granule area. *J. Clin. Pathol.* 36, 867–872.

Engler, A.J., Sen, S., Sweeney, H.L., and Discher, D.E. (2006). Matrix Elasticity Directs Stem Cell Lineage Specification. *Cell* 126, 677–689.

Esko, J.D., and Lindahl, U. (2001). Molecular diversity of heparan sulfate. *J. Clin. Invest.* 108, 169–173.

Esko, J.D., and Selleck, S.B. (2002). Order out of chaos: assembly of ligand binding sites in heparan sulfate. *Annu. Rev. Biochem.* 71, 435–471.

Esko, J.D., Kimata, K., and Lindahl, U. (2009). Proteoglycans and Sulfated Glycosaminoglycans. In *Essentials of Glycobiology*, A. Varki, R.D. Cummings, J.D. Esko, H.H. Freeze, P. Stanley, C.R. Bertozzi, G.W. Hart, and M.E. Etzler, eds. (Cold Spring Harbor (NY): Cold Spring Harbor Laboratory Press), p.

Farini, A., Sitzia, C., Erratico, S., Meregalli, M., and Torrente, Y. (2014). Clinical Applications of Mesenchymal Stem Cells in Chronic Diseases. *Stem Cells Int.* 2014.

FDA Guidance for Industry. (2013). Heparin for Drug and Medical Device Use: Monitoring Crude Heparin for Quality (FDA).

Fernandes, J., Gentile, P., Crawford, A., Pires, R., Hatton, P., and Reis, R.L. (2017). Substituted Borosilicate Glasses with Improved Osteogenic Capacity for Bone Tissue Engineering. *Tissue Eng. - Part A* 23.

Fernández, C., Hattan, C.M., and Kerns, R.J. (2006). Semi-synthetic heparin derivatives: chemical modifications of heparin beyond chain length, sulfate substitution pattern and N-sulfo/N-acetyl groups. *Carbohydr. Res.* 341, 1253–1265.

Florencio-Silva, R., Sasso, G.R. da S., Sasso-Cerri, E., Simões, M.J., and Cerri, P.S. (2015). Biology of Bone Tissue: Structure, Function, and Factors That Influence Bone Cells. *BioMed Res. Int.* 2015.

Foster, J.C., Grocott, M.C., Arkinstall, L.A., Varlas, S., Redding, M.J., Grayson, S.M., and O'Reilly, R.K. (2020). It is Better with Salt: Aqueous Ring-Opening Metathesis Polymerization at Neutral pH. *J. Am. Chem. Soc.* 142, 13878–13885.

Frantz, C., Stewart, K.M., and Weaver, V.M. (2010). The extracellular matrix at a glance. *J Cell Sci* 123, 4195–4200.

Fraser, C., and Grubbs, R.H. (1995). Synthesis of Glycopolymers of Controlled Molecular Weight by Ring-Opening Metathesis Polymerization Using Well-Defined Functional Group Tolerant Ruthenium Carbene Catalysts. *Macromolecules* 28, 7248–7255.

Gao, J., Wang, Y., Chen, S., Tang, D., Jiang, L., Kong, D., and Wang, S. (2017). Electrospinning poly- ϵ -caprolactone scaffold modified with catalytic nitric oxide generation and heparin for small-diameter vascular graft. *RSC Adv.* 7, 18775–18784.

Garg, K., and Bowlin, G.L. (2011). Electrospinning jets and nanofibrous structures. *Biomicrofluidics* 5.

Gauthier, M.A., and Klok, H.-A. (2008). Peptide/protein–polymer conjugates: synthetic strategies and design concepts. *Chem. Commun.* 2591–2611.

GBD 2017 Disease and Injury Incidence and Prevalence Collaborators (2018). Global, regional, and national incidence, prevalence, and years lived with disability for 354 diseases and injuries for 195 countries and territories, 1990–2017: a systematic analysis for the Global Burden of Disease Study 2017. *Lancet Lond. Engl.* 392, 1789–1858.

Ghali, O., Broux, O., Falgayrac, G., Haren, N., van Leeuwen, J.P.T.M., Penel, G., Hardouin, P., and Chauveau, C. (2015). Dexamethasone in osteogenic medium strongly induces adipocyte differentiation of mouse bone marrow stromal cells and increases osteoblast differentiation. *BMC Cell Biol.* 16, 9.

Gibon, E., Lu, L., and Goodman, S.B. (2016). Aging, inflammation, stem cells, and bone healing. *Stem Cell Res. Ther.* 7.

Gong, T., Xie, J., Liao, J., Zhang, T., Lin, S., and Lin, Y. (2015a). Nanomaterials and bone regeneration. *Bone Res.* 329.

Gong, T., Xie, J., Liao, J., Zhang, T., Lin, S., and Lin, Y. (2015b). Nanomaterials and bone regeneration. *Bone Res.* 3, 15029.

Gordon, E.J., Sanders, W.J., and Kiessling, L.L. (1998). Synthetic ligands point to cell surface strategies. *Nature* 392, 30–31.

Guerrini, M., Agulles, T., Bisio, A., Hricovini, M., Lay, L., Naggi, A., Poletti, L., Sturiale, L., Torri, G., and Casu, B. (2002). Minimal Heparin/Heparan Sulfate Sequences for Binding to Fibroblast Growth Factor-1. *Biochem. Biophys. Res. Commun.* 292, 222–230.

Guerrini, M., Beccati, D., Shriver, Z., Naggi, A.M., Bisio, A., Capila, I., Lansing, J., Guglieri, S., Fraser, B., Al-Hakim, A., et al. (2008). Oversulfated Chondroitin Sulfate is a major contaminant in Heparin associated with Adverse Clinical Events. *Nat. Biotechnol.* 26, 669–675.

Guerrouahen, B.S., Al-Hijji, I., and Tabrizi, A.R. (2011). Osteoblastic and Vascular Endothelial Niches, Their Control on Normal Hematopoietic Stem Cells, and Their Consequences on the Development of Leukemia. *Stem Cells Int.* 2011, e375857.

Guglieri, S., Hricovini, M., Raman, R., Polito, L., Torri, G., Casu, B., Sasisekharan, R., and Guerrini, M. (2008). Minimum FGF2 Binding Structural Requirements of Heparin and Heparan Sulfate Oligosaccharides As Determined by NMR Spectroscopy. *Biochemistry* 47, 13862–13869.

Gümüşderelioğlu, M., Karakeçili, A., and Demirtaş, T.T. (2011). Osteogenic activities of MC3T3-E1 cells on heparin-immobilized poly(caprolactone) membranes. *J. Bioact. Compat. Polym.* 26, 257–269.

Hachim, D., Whittaker, T.E., Kim, H., and Stevens, M.M. (2019). Glycosaminoglycan-based biomaterials for growth factor and cytokine delivery: Making the right choices. *J. Controlled Release* 313, 131–147.

Hadjidakis, D.J., and Androulakis, I.I. (2006). Bone Remodeling. *Ann. N. Y. Acad. Sci.* 1092, 385–396.

Hagel, L. (2011). Gel filtration: size exclusion chromatography. *Methods Biochem. Anal.* 54, 51–91.

Haider, A., Haider, S., and Kang, I.-K. (2018). A comprehensive review summarizing the effect of electrospinning parameters and potential applications of nanofibers in biomedical and biotechnology. *Arab. J. Chem.* 11, 1165–1188.

Hart, G.W., and Copeland, R.J. (2010). Glycomics Hits the Big Time. *Cell* 143, 672–676.

Harting, M., Jimenez, F., Pati, S., Baumgartner, J., and Cox, C. (2008). Immunophenotype characterization of rat mesenchymal stromal cells. *Cytotherapy* 10, 243–253.

Hettiaratchi, M.H., Krishnan, L., Rouse, T., Chou, C., McDevitt, T.C., and Guldberg, R.E. (2020). Heparin-mediated delivery of bone morphogenetic protein-2 improves spatial localization of bone regeneration. *Sci. Adv.* 6, 24.

Holmes, B., Castro, N.J., Zhang, L.G., and Zussman, E. (2012). Electrospinning Fibrous Scaffolds for Bone and Cartilage Tissue Generation: Recent Progress and Future Developments. *Tissue Eng. Part B Rev.* 18, 478–486.

Houschyar, K.S., Tapking, C., Borrelli, M.R., Popp, D., Duscher, D., Maan, Z.N., Chelliah, M.P., Li, J., Harati, K., Wallner, C., et al. (2019). Wnt Pathway in Bone Repair and Regeneration – What Do We Know So Far. *Front. Cell Dev. Biol.* 6, 170.

Hu, D.P., Ferro, F., Yang, F., Taylor, A.J., Chang, W., Miclau, T., Marcucio, R.S., and Bahney, C.S. (2017). Cartilage to bone transformation during fracture healing is coordinated by the invading vasculature and induction of the core pluripotency genes. *Development* 144, 221–234.

Huang, Y., Mao, Y., Zong, C., Lin, C., Boons, G.-J., and Zaia, J. (2015). Discovery of a Heparan Sulfate 3-O-Sulfation Specific Peeling Reaction. *Anal. Chem.* 87, 592–600.

Hwang, N.S., Zhang, C., Hwang, Y.-S., and Varghese, S. (2009). Mesenchymal stem cell differentiation and roles in regenerative medicine. *Wiley Interdiscip. Rev. Syst. Biol. Med.* 1, 97–106.

Inoue, Y., and Nagasawa, K. (1976). Selective N-desulfation of heparin with dimethyl sulfoxide containing water or methanol. *Carbohydr. Res.* 46, 87–95.

Iozzo, R.V. (2001). *Proteoglycan Protocols* (Humana Press).

James, A.W., LaChaud, G., Shen, J., Asatrian, G., Nguyen, V., Zhang, X., Ting, K., and Soo, C. (2016). A Review of the Clinical Side Effects of Bone Morphogenetic Protein-2. *Tissue Eng. Part B Rev.* 22, 284–297.

Jaseja, M., Rej, R.N., Sauriol, F., and Perlin, A.S. (1989). Novel regio- and stereoselective modifications of heparin in alkaline solution. Nuclear magnetic resonance spectroscopic evidence. *Can. J. Chem.* 67, 1449–1456.

Jemth, P., Smeds, E., Do, A.-T., Habuchi, H., Kimata, K., Lindahl, U., and Kusche-Gullberg, M. (2003). Oligosaccharide Library-based Assessment of Heparan Sulfate 6-O-Sulfotransferase Substrate Specificity*. *J. Biol. Chem.* 278, 24371–24376.

Jensen, J., Rölfing, J.H.D., Svend Le, D.Q., Kristiansen, A.A., Nygaard, J.V., Hokland, L.B., Bendtsen, M., Kassem, M., Lysdahl, H., and Bünger, C.E. (2014). Surface-modified functionalized polycaprolactone scaffolds for bone repair: In vitro and in vivo experiments. *J. Biomed. Mater. Res. A* 102, 2993–3003.

Jeon, O., Song, S.J., Kang, S.-W., Putnam, A.J., and Kim, B.-S. (2007). Enhancement of ectopic bone formation by bone morphogenetic protein-2 released from a heparin-conjugated poly(L-lactic-co-glycolic acid) scaffold. *Biomaterials* 28, 2763–2771.

Jeong, J.-O., Jeong, S.I., Park, J.-S., Gwon, H.-J., Ahn, S.-J., Shin, H., Lee, J.Y., and Lim, Y.-M. (2017). Development and characterization of heparin-immobilized polycaprolactone nanofibrous scaffolds for tissue engineering using gamma-irradiation. *RSC Adv.* 7, 8963–8972.

J Hill, M., Qi, B., Bayaniahangar, R., Araban, V., Bakhtiary, Z., Doschak, M.R., Goh, B.C., Shokouhimehr, M., Vali, H., Presley, J.F., et al. (2019). Nanomaterials for bone tissue regeneration: updates and future perspectives. *Nanomed.* 14, 2987–3006.

Jin, X., Geng, X., Jia, L., Xu, Z., Ye, L., Gu, Y., Zhang, A.-Y., and Feng, Z.-G. (2019). Preparation of Small-Diameter Tissue-Engineered Vascular Grafts Electrospinning from Heparin End-Capped PCL and Evaluation in a Rabbit Carotid Artery Replacement Model. *Macromol. Biosci.* 19, e1900114.

Johnson, J.A., Lu, Y.Y., Burts, A.O., Lim, Y.-H., Finn, M.G., Koberstein, J.T., Turro, N.J., Tirrell, D.A., and Grubbs, R.H. (2011). Core-Clickable PEG-Branch-Azide Bivalent-Bottle-Brush Polymers by ROMP: Grafting-Through and Clicking-To. *J. Am. Chem. Soc.* 133, 559–566.

Kanai, M., Mortell, K.H., and Kiessling, L.L. (1997). Varying the Size of Multivalent Ligands: The Dependence of Concanavalin A Binding on Neoglycopolymer Length. *J. Am. Chem. Soc.* 119, 9931–9932.

Kang, H.-W., Lee, S.J., Ko, I.K., Kengla, C., Yoo, J.J., and Atala, A. (2016). A 3D bioprinting system to produce human-scale tissue constructs with structural integrity. *Nat. Biotechnol.* 34, 312–319.

Kariya, Y., Kyogashima, M., Suzuki, K., Isomura, T., Sakamoto, T., Horie, K., Ishihara, M., Takano, R., Kamei, K., and Hara, S. (2000). Preparation of completely 6-O-desulfated heparin and its ability to enhance activity of basic fibroblast growth factor. *J. Biol. Chem.* 275, 25949–25958.

Katagiri, T., Yamaguchi, A., Komaki, M., Abe, E., Takahashi, N., Ikeda, T., Rosen, V., Wozney, J.M., Fujisawa-Sehara, A., and Suda, T. (1994). Bone morphogenetic protein-2 converts the differentiation pathway of C2C12 myoblasts into the osteoblast lineage. *J. Cell Biol.* 127, 1755–1766.

Ke, P., Jiao, X.-N., Ge, X.-H., Xiao, W.-M., and Yu, B. (2014). From macro to micro: structural biomimetic materials by electrospinning. *RSC Adv.* 4, 39704–39724.

Kiessling, L., and Mangold, S. (2012). Current and Forthcoming Applications of ROMP Polymers - Biorelated Polymers. *Polym. Sci. Compr. Ref.* 10 Vol. Set 4, 695–717.

Kim, J., Bae, W.-G., Choung, H.-W., Lim, K.T., Seonwoo, H., Jeong, H.E., Suh, K.-Y., Jeon, N.L., Choung, P.-H., and Chung, J.H. (2014). Multiscale patterned transplantable stem cell patches for bone tissue regeneration. *Biomaterials* 35, 9058–9067.

Kini, U., and Nandeesh, B.N. (2012). Physiology of Bone Formation, Remodeling, and Metabolism. In *Radionuclide and Hybrid Bone Imaging*, I. Fogelman, G. Gnanasegaran, and H. van der Wall, eds. (Springer Berlin Heidelberg), pp. 29–57.

Kjaer, M. (2004). Role of extracellular matrix in adaptation of tendon and skeletal muscle to mechanical loading. *Physiol. Rev.* 84, 649–698.

Kolf, C.M., Cho, E., and Tuan, R.S. (2007). Mesenchymal stromal cells. Biology of adult mesenchymal stem cells: regulation of niche, self-renewal and differentiation. *Arthritis Res. Ther.* 9, 204.

Kreuger, J., and Kjellén, L. (2012). Heparan Sulfate Biosynthesis. *J. Histochem. Cytochem.* 60, 898–907.

van Kuppevelt, T.H., Oosterhof, A., Versteeg, E.M.M., Podhumljak, E., van de Westerlo, E.M.A., and Daamen, W.F. (2017). Sequencing of glycosaminoglycans with potential to interrogate sequence-specific interactions. *Sci. Rep.* 7, 14785.

Lancot, P.M. (2007). The glycans of stem cells. *Curr. Opin. Chem. Biol.* 11, 373–380.

Lane, D.A., Denton, J., Flynn, A.M., Thunberg, L., and Lindahl, U. (1984). Anticoagulant activities of heparin oligosaccharides and their neutralization by platelet factor 4. *Biochem. J.* 218, 725–732.

Langenbach, F., and Handschel, J. (2013). Effects of dexamethasone, ascorbic acid and β -glycerophosphate on the osteogenic differentiation of stem cells in vitro. *Stem Cell Res. Ther.* 4, 117.

Lanza, R., Langer, R., Vacanti, J.P., and Atala, A. (2020). *Principles of Tissue Engineering* (Academic Press).

Lauc, G. (2016). Mechanisms of disease: The human N-glycome. *Biochim. Biophys. Acta BBA - Gen. Subj.* 1860, 1574–1582.

Lee, J., Wee, S., Gunaratne, J., Chua, R.J.E., Smith, R.A.A., Ling, L., Fernig, D.G., Swaminathan, K., Nurcombe, V., and Cool, S.M. (2015). Structural determinants of heparin–transforming growth factor- β 1 interactions and their effects on signaling. *Glycobiology* 25, 1491–1504.

Lei, Y., Zouani, O.F., Rémy, M., Ayela, C., and Durrieu, M.-C. (2012). Geometrical Microfeature Cues for Directing Tubulogenesis of Endothelial Cells. *PLoS ONE* 7, e41163.

Levental, I., Georges, P.C., and Janmey, P.A. (2007). Soft biological materials and their impact on cell function. *Soft Matter* 3, 299–306.

- Li, D., and Xia, Y. (2004). Electrospinning of Nanofibers: Reinventing the Wheel? *Adv. Mater.* **16**, 1151–1170.
- Li, D., Xu, L., Wang, J., and Gautrot, J.E. (2021). Responsive Polymer Brush Design and Emerging Applications for Nanotheranostics. *Adv. Healthc. Mater.* **10**, 2000953.
- Li, J.P., Gong, F., El Darwish, K., Jalkanen, M., and Lindahl, U. (2001). Characterization of the D-glucuronyl C5-epimerase involved in the biosynthesis of heparin and heparan sulfate. *J. Biol. Chem.* **276**, 20069–20077.
- Liang, Q.T., Xiao, X.M., Lin, J.H., and Wei, Z. (2015). A new sequencing approach for N-unsubstituted heparin/heparan sulfate oligosaccharides. *Glycobiology* **25**, 714–725.
- Lin, W., Xu, L., Zwingenberger, S., Gibon, E., Goodman, S.B., and Li, G. (2017). Mesenchymal stem cells homing to improve bone healing. *J. Orthop. Transl.* **9**, 19–27.
- Lindahl, U., Bäckström, G., Thunberg, L., and Leder, I.G. (1980). Evidence for a 3-O-sulfated D-glucosamine residue in the antithrombin-binding sequence of heparin. *Proc. Natl. Acad. Sci. U. S. A.* **77**, 6551–6555.
- Ling, L., Murali, S., Stein, G.S., van Wijnen, A.J., and Cool, S.M. (2010a). Glycosaminoglycans modulate RANKL induced osteoclastogenesis. *J. Cell. Biochem.* **109**, 1222–1231.
- Ling, L., Dombrowski, C., Foong, K.M., Haupt, L.M., Stein, G.S., Nurcombe, V., van Wijnen, A.J., and Cool, S.M. (2010b). Synergism between Wnt3a and heparin enhances osteogenesis via a phosphoinositide 3-kinase/Akt/RUNX2 pathway. *J. Biol. Chem.* **285**, 26233–26244.
- Ling, L., Camilleri, E.T., Helledie, T., Samsonraj, R.M., Titmarsh, D.M., Chua, R.J., Dreesen, O., Dombrowski, C., Rider, D.A., Galindo, M., et al. (2016). Effect of heparin on the biological properties and molecular signature of human mesenchymal stem cells. *Gene* **576**, 292–303.
- Liu, J., Pervin, A., Gallo, C.M., Desai, U.R., Van Gorp, C.L., and Linhardt, R.J. (1994). New Approaches for the Preparation of Hydrophobic Heparin Derivatives. *J. Pharm. Sci.* **83**, 1034–1039.
- Liu, J., Shriver, Z., Blaiklock, P., Yoshida, K., Sasisekharan, R., and Rosenberg, R.D. (1999). Heparan Sulfate d-Glucosaminyl 3-O-Sulfotransferase-3A SulfatesN-Unsubstituted Glucosamine Residues*. *J. Biol. Chem.* **274**, 38155–38162.
- Liu, Q., Chen, G., and Chen, H. (2018). Chemical synthesis of glycosaminoglycan-mimetic polymers. *Polym. Chem.* **10**, 164–171.
- Lu, T., Li, Y., and Chen, T. (2013). Techniques for fabrication and construction of three-dimensional scaffolds for tissue engineering. *Int. J. Nanomedicine* **8**, 337–350.
- Luong-Van, E., Grøndahl, L., Chua, K.N., Leong, K.W., Nurcombe, V., and Cool, S.M. (2006). Controlled release of heparin from poly(ϵ -caprolactone) electrospinning fibers. *Biomaterials* **27**, 2042–2050.
- Mach, H., Volkin, D.B., Burke, C.J., Middaugh, C.R., Linhardt, R.J., Fromm, J.R., Loganathan, D., and Mattsson, L. (1993). Nature of the interaction of heparin with acidic fibroblast growth factor. *Biochemistry* **32**, 5480–5489.
- Maia, F.R., Bidarra, S.J., Granja, P.L., and Barrias, C.C. (2013). Functionalization of biomaterials with small osteoinductive moieties. *Acta Biomater.* **9**, 8773–8789.

- Majidinia, M., Sadeghpour, A., and Yousefi, B. (2018). The roles of signaling pathways in bone repair and regeneration. *J. Cell. Physiol.* 233, 2937–2948.
- Mali, S.M., Kumar, M.G., Katariya, M.M., and Gopi, H.N. (2014). HBTU mediated 1-hydroxybenzotriazole (HOBt) conjugate addition: synthesis and stereochemical analysis of β -benzotriazole N-oxide substituted γ -amino acids and hybrid peptides. *Org. Biomol. Chem.* 12, 8462–8472.
- Maniatopoulos, C., Sodek, J., and Melcher, A.H. (1988). Bone formation in vitro by stromal cells obtained from bone marrow of young adult rats. *Cell Tissue Res.* 254, 317–330.
- Manning, D.D., Bertozzi, C.R., Pohl, N.L., Rosen, S.D., and Kiessling, L.L. (1995). Selectin-Saccharide Interactions: Revealing Structure-Function Relationships with Chemical Synthesis. *J. Org. Chem.* 60, 6254–6255.
- Marks, R.M., Lu, H., Sundaresan, R., Toida, T., Suzuki, A., Imanari, T., Hernáiz, M.J., and Linhardt, R.J. (2001). Probing the interaction of dengue virus envelope protein with heparin: assessment of glycosaminoglycan-derived inhibitors. *J. Med. Chem.* 44, 2178–2187.
- Marot, D., Knezevic, M., and Novakovic, G.V. (2010). Bone tissue engineering with human stem cells. *Stem Cell Res. Ther.* 1, 10.
- Marsell, R., and Einhorn, T.A. (2011). The Biology Of Fracture Healing. *Injury* 42, 551–555.
- Martin, E., Dubois, P., and Jérôme, R. (2000). Controlled Ring-Opening Polymerization of ϵ -Caprolactone Promoted by “in Situ” Formed Yttrium Alkoxides. *Macromolecules* 33, 1530–1535.
- Mathews, S., Mathew, S.A., Gupta, P.K., Bhonde, R., and Totey, S. (2014). Glycosaminoglycans enhance osteoblast differentiation of bone marrow derived human mesenchymal stem cells. *J. Tissue Eng. Regen. Med.* 8, 143–152.
- Matson, J.B., and Grubbs, R.H. (2008). Synthesis of Fluorine-18 Functionalized Nanoparticles for use as in vivo Molecular Imaging Agents. *J. Am. Chem. Soc.* 130, 6731–6733.
- Maynard, H.D., Okada, S.Y., and Grubbs, R.H. (2000). Synthesis of Norbornenyl Polymers with Bioactive Oligopeptides by Ring-Opening Metathesis Polymerization. *Macromolecules* 33, 6239–6248.
- McBeath, R., Pirone, D.M., Nelson, C.M., Bhadriraju, K., and Chen, C.S. (2004). Cell Shape, Cytoskeletal Tension, and RhoA Regulate Stem Cell Lineage Commitment. *Dev. Cell* 6, 483–495.
- Meneghetti, M.C.Z., Hughes, A.J., Rudd, T.R., Nader, H.B., Powell, A.K., Yates, E.A., and Lima, M.A. (2015). Heparan sulfate and heparin interactions with proteins. *J. R. Soc. Interface* 12.
- Moldoveanu, S.C., and David, V. (2013). Chapter 3 - Equilibrium Types in HPLC. In *Essentials in Modern HPLC Separations*, S.C. Moldoveanu, and V. David, eds. (Elsevier), pp. 85–114.
- Mondal, D., Griffith, M., and Venkatraman, S.S. (2016). Polycaprolactone-based biomaterials for tissue engineering and drug delivery: Current scenario and challenges. *Int. J. Polym. Mater. Polym. Biomater.* 65, 255–265.

Montano M. (2014). Model systems. Translational Biology in Medicine (Woodhead Publishing).

Muir, J.M., Hirsh, J., Weitz, J.I., Andrew, M., Young, E., and Shaughnessy, S.G. (1997). A Histomorphometric Comparison of the Effects of Heparin and Low-Molecular-Weight Heparin on Cancellous Bone in Rats. *Blood* 89, 3236–3242.

Mulloy, B., and Forster, M.J. (2000). Conformation and dynamics of heparin and heparan sulfate. *Glycobiology* 10, 1147–1156.

Murali, S., Rai, B., Dombrowski, C., Lee, J.L.J., Lim, Z.X.H., Bramono, D.S., Ling, L., Bell, T., Hinkley, S., Nathan, S.S., et al. (2013). Affinity-selected heparan sulfate for bone repair. *Biomaterials* 34, 5594–5605.

Murugesan, S., Xie, J., and Linhardt, R.J. (2008). Immobilization of Heparin: Approaches and Applications. *Curr. Top. Med. Chem.* 8, 80–100.

Nelson, R.M., Cecconi, O., Roberts, W.G., Aruffo, A., Linhardt, R.J., and Bevilacqua, M.P. (1993). Heparin oligosaccharides bind L- and P-selectin and inhibit acute inflammation. *Blood* 82, 3253–3258.

Newman, P., Galenano-Niño, J.L., Graney, P., Razal, J.M., Minett, A.I., Ribas, J., Ovalle-Robles, R., Biro, M., and Zreiqat, H. (2016). Relationship between nanotopographical alignment and stem cell fate with live imaging and shape analysis. *Sci. Rep.* 6, 37909.

Nezarati, R.M., Eifert, M.B., and Cosgriff-Hernandez, E. (2013). Effects of Humidity and Solution Viscosity on Electrospinning Fiber Morphology. *Tissue Eng. Part C Methods* 19, 810–819.

Nomura, K., and Schrock, R.R. (1996). Preparation of “Sugar-Coated” Homopolymers and Multiblock ROMP Copolymers. *Macromolecules* 29, 540–545.

O’Brien, F.J. (2011). Biomaterials & scaffolds for tissue engineering. *Mater. Today* 14, 88–95.

Odén, A., McCloskey, E.V., Kanis, J.A., Harvey, N.C., and Johansson, H. (2015). Burden of high fracture probability worldwide: secular increases 2010-2040. *Osteoporos. Int. J. Establ. Result Coop. Eur. Found. Osteoporos. Natl. Osteoporos. Found. USA* 26, 2243–2248.

Olson, S.T., Björk, I., Sheffer, R., Craig, P.A., Shore, J.D., and Choay, J. (1992a). Role of the antithrombin-binding pentasaccharide in heparin acceleration of antithrombin-proteinase reactions. Resolution of the antithrombin conformational change contribution to heparin rate enhancement. *J. Biol. Chem.* 267, 12528–12538.

Olson, S.T., Björk, I., Sheffer, R., Craig, P.A., Shore, J.D., and Choay, J. (1992b). Role of the antithrombin-binding pentasaccharide in heparin acceleration of antithrombin-proteinase reactions. Resolution of the antithrombin conformational change contribution to heparin rate enhancement. *J. Biol. Chem.* 267, 12528–12538.

Ortega, Í., Deshpande, P., Gill, A.A., MacNeil, S., and Claeysens, F. (2013a). Development of a microfabricated artificial limbus with micropockets for cell delivery to the cornea. *Biofabrication* 5, 025008.

Ortega, I., Ryan, A.J., Deshpande, P., MacNeil, S., and Claeysens, F. (2013b). Combined microfabrication and electrospinning to produce 3-D architectures for corneal repair. *Acta Biomater.* 9, 5511–5520.

Ortega, Í., Sefat, F., Deshpande, P., Paterson, T., Ramachandran, C., Ryan, A.J., MacNeil, S., and Claeysens, F. (2014). Combination of Microstereolithography and Electrospinning to Produce Membranes Equipped with Niches for Corneal Regeneration. *J. Vis. Exp. JoVE*.

Patel, J.J., Flanagan, C.L., and Hollister, S.J. (2015). Bone Morphogenetic Protein-2 Adsorption onto Poly-ε-caprolactone Better Preserves Bioactivity In Vitro and Produces More Bone In Vivo than Conjugation Under Clinically Relevant Loading Scenarios. *Tissue Eng. Part C Methods* 21, 489–498.

Patel, P.R., Kiser, R.C., Lu, Y.Y., Fong, E., Ho, W.C., Tirrell, D.A., and Grubbs, R.H. (2012). Synthesis and Cell Adhesive Properties of Linear and Cyclic RGD Functionalized Polynorbornene Thin Films. *Biomacromolecules* 13, 2546–2553.

Paterson, T.E., Beal, S.N., Santocildes-Romero, M.E., Sidambe, A.T., Hatton, P.V., and Asencio, I.O. (2017). Selective laser melting-enabled electrospinning: Introducing complexity within electrospinning membranes. *Proc. Inst. Mech. Eng. [H]* 231, 565–574.

Percival, C.J., and Richtsmeier, J.T. (2013). Angiogenesis and Intramembranous Osteogenesis. *Dev. Dyn. Off. Publ. Am. Assoc. Anat.* 242, 909–922.

Pohl, N.L., and Kiessling, L.L. (1999). Scope of Multivalent Ligand Function: Lactose-Bearing Neoglycopolymers By Ring-Opening Metathesis Polymerization. *Synthesis* 1999, 1515–1519.

Powell, A.K., Ahmed, Y.A., Yates, E.A., and Turnbull, J.E. (2010). Generating heparan sulfate saccharide libraries for glycomics applications. *Nat. Protoc.* 5, 821–833.

Poynton, A.R., and Lane, J.M. (2002). Safety profile for the clinical use of bone morphogenetic proteins in the spine. *Spine* 27, S40–48.

Prodinger, P.M., Burgkart, R., Kreutzer, K., Liska, F., Pilge, H., Schmitt, A., Knödler, M., Holzapfel, B.M., Hapfelmeier, A., Tischer, T., et al. (2016). Does Anticoagulant Medication Alter Fracture-Healing? A Morphological and Biomechanical Evaluation of the Possible Effects of Rivaroxaban and Enoxaparin Using a Rat Closed Fracture Model. *PLoS ONE* 11, e0159669.

Puvirajesinghe, T.M., and Turnbull, J.E. (2012). Glycomics Approaches for the Bioassay and Structural Analysis of Heparin/Heparan Sulphates. *Metabolites* 2, 1060–1089.

Qin, Y., Ke, J., Gu, X., Fang, J., Wang, W., Cong, Q., Li, J., Tan, J., Brunzelle, J.S., Zhang, C., et al. (2015). Structural and Functional Study of d-Glucuronyl C5-epimerase. *J. Biol. Chem.* 290, 4620–4630.

Ratanavaraporn, J., and Tabata, Y. (2012). Enhanced osteogenic activity of bone morphogenetic protein-2 by 2-O-desulfated heparin. *Acta Biomater.* 8, 173–182.

Rauvala, H. (1989). An 18-kd heparin-binding protein of developing brain that is distinct from fibroblast growth factors. *EMBO J.* 8, 2933–2941.

Rezvani, Z., Venugopal, J.R., Urbanska, A.M., Mills, D.K., Ramakrishna, S., and Mozafari, M. (2016). A bird's eye view on the use of electrospinning nanofibrous scaffolds for bone tissue engineering: Current state-of-the-art, emerging directions and future trends. *Nanomedicine Nanotechnol. Biol. Med.* 12, 2181–2200.

Robinson, C.J., Mulloy, B., Gallagher, J.T., and Stringer, S.E. (2006). VEGF165-binding Sites within Heparan Sulfate Encompass Two Highly Sulfated Domains and Can Be Liberated by K5 Lyase. *J. Biol. Chem.* 281, 1731–1740.

Rodan, G.A. (1992). Introduction to bone biology. *Bone* 13 Suppl 1, S3-6.

Rompolas, P., and Greco, V. (2014). Stem cell dynamics in the hair follicle niche. *Semin. Cell Dev. Biol.* 25–26, 34–42.

Rosa, D.S., Guedes, C.G.F., Casarin, F., and Bragança, F.C. (2005). The effect of the Mw of PEG in PCL/CA blends. *Polym. Test.* 24, 542–548.

Ruppert, R., Hoffmann, E., and Sebald, W. (1996). Human Bone Morphogenetic Protein 2 Contains a Heparin-Binding Site which Modifies Its Biological Activity. *Eur. J. Biochem.* 237, 295–302.

Sadir, R., Baleux, F., Grosdidier, A., Imbert, A., and Lortat-Jacob, H. (2001). Characterization of the Stromal Cell-derived Factor-1 α -Heparin Complex*. *J. Biol. Chem.* 276, 8288–8296.

Santocildes-Romero, M.E., Crawford, A., Hatton, P.V., Goodchild, R.L., Reaney, I.M., and Miller, C.A. (2015). The osteogenic response of mesenchymal stromal cells to strontium-substituted bioactive glasses. *J. Tissue Eng. Regen. Med.* 9, 619–631.

Sarrazin, S., Bonnaffé, D., Lubineau, A., and Lortat-Jacob, H. (2005). Heparan sulfate mimicry: a synthetic glycoconjugate that recognizes the heparin binding domain of interferon-gamma inhibits the cytokine activity. *J. Biol. Chem.* 280, 37558–37564.

Schermer, A., Galvin, S., and Sun, T.T. (1986). Differentiation-related expression of a major 64K corneal keratin in vivo and in culture suggests limbal location of corneal epithelial stem cells. *J. Cell Biol.* 103, 49–62.

Schindler, A., Hibionada, Y.M., and Pitt, C.G. (1982). Aliphatic polyesters. III. Molecular weight and molecular weight distribution in alcohol-initiated polymerizations of ϵ -caprolactone. *J. Polym. Sci. Polym. Chem. Ed.* 20, 319–326.

Schofield, R. (1978). The relationship between the spleen colony-forming cell and the haemopoietic stem cell. *Blood Cells* 4, 7–25.

Scott, K.E., Rychel, K., Ranamukhaarachchi, S., Rangamani, P., and Fraley, S.I. (2019). Emerging themes and unifying concepts underlying cell behavior regulation by the pericellular space. *Acta Biomater.* 96, 81–98.

Seeberger, P.H., and Cummings, R.D. (2015). Glycans in Biotechnology and the Pharmaceutical Industry. In *Essentials of Glycobiology*, A. Varki, R.D. Cummings, J.D. Esko, P. Stanley, G.W. Hart, M. Aebi, A.G. Darvill, T. Kinoshita, N.H. Packer, J.H. Prestegard, et al., eds. (Cold Spring Harbor (NY): Cold Spring Harbor Laboratory Press), p.

Seffouh, A., Milz, F., Przybylski, C., Laguri, C., Oosterhof, A., Bourcier, S., Sadir, R., Dutkowski, E., Daniel, R., van Kuppevelt, T.H., et al. (2013). HSulf sulfatases catalyze processive and oriented 6-O-desulfation of heparan sulfate that differentially regulates fibroblast growth factor activity. *FASEB J. Off. Publ. Fed. Am. Soc. Exp. Biol.* 27, 2431–2439.

Shadish, J.A., Benuska, G.M., and DeForest, C.A. (2019). Bioactive Site-Specifically Modified Proteins for 4D Patterning of Gel Biomaterials. *Nat. Mater.* 18, 1005–1014.

Shah, S.S., Kim, M., Cahill-Thompson, K., Tae, G., and Revzin, A. (2011). Micropatterning of bioactive heparin-based hydrogels. *Soft Matter* 7, 3133–3140.

Sheikh, Z., Hamdan, N., Ikeda, Y., Grynpas, M., Ganss, B., and Glogauer, M. (2017). Natural graft tissues and synthetic biomaterials for periodontal and alveolar bone reconstructive applications: a review. *Biomater. Res.* 21, 9.

Sheng, J., Liu, R., Xu, Y., and Liu, J. (2011). The Dominating Role of N-Deacetylase/N-Sulfotransferase 1 in Forming Domain Structures in Heparan Sulfate*. *J. Biol. Chem.* 286, 19768–19776.

Shively, J.E., and Conrad, H.E. (1976a). Formation of anhydrosugars in the chemical depolymerization of heparin. *Biochemistry* 15, 3932–3942.

Shively, J.E., and Conrad, H.E. (1976b). Nearest neighbor analysis of heparin: identification and quantitation of the products formed by selective depolymerization procedures. *Biochemistry* 15, 3943–3950.

Shriver, Z., Capila, I., Venkataraman, G., and Sasisekharan, R. (2012). Heparin and Heparan Sulfate: Analyzing Structure and Microheterogeneity. *Handb. Exp. Pharmacol.* 159–176.

Shukla, D., Liu, J., Blaiklock, P., Shworak, N.W., Bai, X., Esko, J.D., Cohen, G.H., Eisenberg, R.J., Rosenberg, R.D., and Spear, P.G. (1999). A novel role for 3-O-sulfated heparan sulfate in herpes simplex virus 1 entry. *Cell* 99, 13–22.

Siddiqui, M.R., AlOthman, Z.A., and Rahman, N. (2017). Analytical techniques in pharmaceutical analysis: A review. *Arab. J. Chem.* 10, S1409–S1421.

Silverstein, R.M., and Bassler, G.C. (1962). Spectrometric identification of organic compounds. *J. Chem. Educ.* 39, 546.

Singh, S., Wu, B.M., and Dunn, J.C.Y. (2011). Accelerating Vascularization in Polycaprolactone Scaffolds by Endothelial Progenitor Cells. *Tissue Eng. Part A* 17, 1819–1830.

Smeds, E., Feta, A., and Kusche-Gullberg, M. (2010). Target selection of heparan sulfate hexuronic acid 2-O-sulfotransferase. *Glycobiology* 20, 1274–1282.

Smeltzer, S.C.O., Bare, B.G., Hinkle, J.L., and Cheever, K.H. (2010a). *Brunner & Suddarth's Textbook of Medical-surgical Nursing* (Lippincott Williams & Wilkins).

Smeltzer, S.C.O., Bare, B.G., Hinkle, J.L., and Cheever, K.H. (2010b). *Brunner & Suddarth's Textbook of Medical-surgical Nursing* (Lippincott Williams & Wilkins).

Smith, R.A.A., Murali, S., Rai, B., Lu, X., Lim, Z.X.H., Lee, J.J.L., Nurcombe, V., and Cool, S.M. (2018a). Minimum structural requirements for BMP-2-binding of heparin oligosaccharides. *Biomaterials* 184, 41–55.

Smith, R.A.A., Chua, R.J.E., Carnachan, S.M., Tan, C.L.L., Sims, I.M., Hinkley, S.F.R., Nurcombe, V., and Cool, S.M. (2018b). Retention of the Structure and Function of Heparan Sulfate Biomaterials After Gamma Irradiation. *Tissue Eng. Part A* 24, 729–739.

Smith, R.A.A., Murali, S., Rai, B., Lu, X., Lim, Z.X.H., Lee, J.J.L., Nurcombe, V., and Cool, S.M. (2018c). Minimum structural requirements for BMP-2-binding of heparin oligosaccharides. *Biomaterials* 184, 41–55.

Soares da Costa, D., Reis, R.L., and Pashkuleva, I. (2017). Sulfation of Glycosaminoglycans and Its Implications in Human Health and Disorders. *Annu. Rev. Biomed. Eng.* 19, 1–26.

Sophia Fox, A.J., Bedi, A., and Rodeo, S.A. (2009). The Basic Science of Articular Cartilage. *Sports Health* 1, 461–468.

Spadaccio, C., Rainer, A., Centola, M., Trombetta, M., Chello, M., Lusini, M., Covino, E., Toyoda, Y., and Genovese, J.A. (2010). Heparin-releasing scaffold for stem cells: a differentiating device for vascular aims. *Regen. Med.* 5, 645–657.

Spillmann, D., Witt, D., and Lindahl, U. (1998). Defining the Interleukin-8-binding Domain of Heparan Sulfate *. *J. Biol. Chem.* 273, 15487–15493.

Stiers, P.-J., van Gastel, N., and Carmeliet, G. (2016). Targeting the hypoxic response in bone tissue engineering: A balance between supply and consumption to improve bone regeneration. *Mol. Cell. Endocrinol.* 432, 96–105.

Stratton, S., Shelke, N.B., Hoshino, K., Rudraiah, S., and Kumbar, S.G. (2016). Bioactive polymeric scaffolds for tissue engineering. *Bioact. Mater.* 1, 93–108.

Sun, L., Pereira, D., Wang, Q., Barata, D.B., Truckenmüller, R., Li, Z., Xu, X., and Habibovic, P. (2016). Controlling Growth and Osteogenic Differentiation of Osteoblasts on Microgrooved Polystyrene Surfaces. *PLoS ONE* 11, e0161466.

Sun, Z., Morishita, K., and Nomura, K. (2018). Synthesis of Soluble Star-Shaped Polymers via In and Out Approach by Ring-Opening Metathesis Polymerization (ROMP) of Norbornene: Factors Affecting the Synthesis. *Catalysts* 8, 670.

Takahashi, K., and Yamanaka, S. (2006). Induction of pluripotent stem cells from mouse embryonic and adult fibroblast cultures by defined factors. *Cell* 126, 663–676.

Tallawi, M., Rosellini, E., Barbani, N., Cascone, M.G., Rai, R., Saint-Pierre, G., and Boccaccini, A.R. (2015). Strategies for the chemical and biological functionalization of scaffolds for cardiac tissue engineering: a review. *J. R. Soc. Interface* 12.

Taylor, S.L., Hogwood, J., Guo, W., Yates, E.A., and Turnbull, J.E. (2019). By-Products of Heparin Production Provide a Diverse Source of Heparin-like and Heparan Sulfate Glycosaminoglycans. *Sci. Rep.* 9, 2679.

Tellier, L.E., Miller, T., McDevitt, T.C., and Temenoff, J.S. (2015). Hydrolysis and sulfation pattern effects on release of bioactive bone morphogenetic protein-2 from heparin-based microparticles. *J. Mater. Chem. B* 3, 8001–8009.

Teo, W.E., and Ramakrishna, S. (2006). A review on electrospinning design and nanofibre assemblies. *Nanotechnology* 17, R89–R106.

Thorpe, A., Freeman, C., Farthing, P., Callaghan, J., Hatton, P.V., Brook, I.M., Sammon, C., and Le Maitre, C. (2018). In vivo safety and efficacy testing of a thermally triggered injectable hydrogel scaffold for bone regeneration and augmentation in a rat model. *Oncotarget* 9, 18277–18295.

Thunberg, L., Bäckström, G., and Lindahl, U. (1982). Further characterization of the antithrombin-binding sequence in heparin. *Carbohydr. Res.* 100, 393–410.

Tsai, C.-C., Chen, Y.-J., Yew, T.-L., Chen, L.-L., Wang, J.-Y., Chiu, C.-H., and Hung, S.-C. (2011). Hypoxia inhibits senescence and maintains mesenchymal stem cell properties through down-regulation of E2A-p21 by HIF-TWIST. *Blood* 117, 459–469.

Tsao, Y.-T., Huang, Y.-J., Wu, H.-H., Liu, Y.-A., Liu, Y.-S., and Lee, O.K. (2017). Osteocalcin Mediates Biomineralization during Osteogenic Maturation in Human Mesenchymal Stromal Cells. *Int. J. Mol. Sci.* 18, 159.

Turner, L.-A., and Dalby, M.J. (2014). Nanotopography – potential relevance in the stem cell niche. *Biomater. Sci.* 2, 1574–1594.

Tutak, W., Jyotsnendu, G., Bajcsy, P., and Simon, C.G. (2016). Nanofiber scaffolds influence organelle structure and function in bone marrow stromal cells. *J. Biomed. Mater. Res. B Appl. Biomater.* 989–1001.

Uchida, S. (2013). Graft Copolymer Synthesis. In *Encyclopedia of Polymeric Nanomaterials*, S. Kobayashi, and K. Müllen, eds. (Berlin, Heidelberg: Springer), pp. 1–4.

United States Pharmacopeia. (2011). Official monographs: Heparin Sodium.

Valverde, P., Ardá, A., Reichardt, N.-C., Jiménez-Barbero, J., and Gimeno, A. (2019). Glycans in drug discovery. *MedChemComm* 10, 1678–1691.

Vaquette, C., and Cooper-White, J.J. (2011). Increasing electrospinning scaffold pore size with tailored collectors for improved cell penetration. *Acta Biomater.* 7, 2544–2557.

Viganò, M., Sansone, V., d'Agostino, M.C., Romeo, P., Perucca Orfei, C., and de Girolamo, L. (2016). Mesenchymal stem cells as therapeutic target of biophysical stimulation for the treatment of musculoskeletal disorders. *J. Orthop. Surg.* 11, 163.

Vivès, R.R., Imberty, A., Sattentau, Q.J., and Lortat-Jacob, H. (2005). Heparan Sulfate Targets the HIV-1 Envelope Glycoprotein gp120 Coreceptor Binding Site*. *J. Biol. Chem.* 280, 21353–21357.

Vukicevic, S., Oppermann, H., Verbanac, D., Jankolija, M., Popek, I., Curak, J., Brkljacic, J., Pauk, M., Erjavec, I., Francetic, I., et al. (2014). The clinical use of bone morphogenetic proteins revisited: a novel biocompatible carrier device OSTEOGROW for bone healing. *Int. Orthop.* 38, 635–647.

Walmsley, G.G., Ransom, R.C., Zielins, E.R., Leavitt, T., Flacco, J.S., Hu, M.S., Lee, A.S., Longaker, M.T., and Wan, D.C. (2016). Stem Cells in Bone Regeneration. *Stem Cell Rev. Rep.* 12, 524–529.

Wang, B., and Boons, G.-J. (2011). *Carbohydrate Recognition: Biological Problems, Methods, and Applications* (John Wiley & Sons).

Wang, A.B., Jain, P., and Tumber, T. (2015). The Hair Follicle Stem Cell Niche: The Bulge and Its Environment. In *Tissue-Specific Stem Cell Niche*, K. Turksen, ed. (Springer International Publishing), pp. 1–26.

Wang, C., Poon, S., Murali, S., Koo, C.-Y., Bell, T.J., Hinkley, S.F., Yeong, H., Bhakoo, K., Nurcombe, V., and Cool, S.M. (2014). Engineering a vascular endothelial growth factor 165-binding heparan sulfate for vascular therapy. *Biomaterials* 35, 6776–6786.

Wang, Z., Zhang, F., Dordick, J.S., and Linhardt, R.J. (2012). Molecular Mass Characterization of Glycosaminoglycans with Different Degrees of Sulfation in Bioengineered Heparin Process by Size Exclusion Chromatography. *Curr. Anal. Chem.* 8, 506–511.

Wei, Q., Holle, A., Li, J., Posa, F., Biagioni, F., Croci, O., Benk, A.S., Young, J., Nouredine, F., Deng, J., et al. (2020). BMP-2 Signaling and Mechanotransduction Synergize to Drive Osteogenic Differentiation via YAP/TAZ. *Adv. Sci.* 7, 1902931.

Weiss, R.J., Esko, J.D., and Tor, Y. (2017). Targeting Heparin– and Heparan Sulfate–Protein Interactions. *Org. Biomol. Chem.* 15, 5656–5668.

Wells, R.G. (2008). The role of matrix stiffness in regulating cell behavior. *Hepatology* 47, 1394–1400.

Wijesinghe, S.J., Ling, L., Murali, S., Qing, Y.H., Hinkley, S.F.R., Carnachan, S.M., Bell, T.J., Swaminathan, K., Hui, J.H., Wijnen, A.J. van, et al. (2017). Affinity Selection of FGF2-Binding Heparan Sulfates for Ex Vivo Expansion of Human Mesenchymal Stem Cells. *J. Cell. Physiol.* 232, 566–575.

Williams, J.M., Adewunmi, A., Schek, R.M., Flanagan, C.L., Krebsbach, P.H., Feinberg, S.E., Hollister, S.J., and Das, S. (2005). Bone tissue engineering using polycaprolactone scaffolds fabricated via selective laser sintering. *Biomaterials* 26, 4817–4827.

Wu, J., Zhao, C., Lin, W., Hu, R., Wang, Q., Chen, H., Li, L., Chen, S., and Zheng, J. (2014). Binding characteristics between polyethylene glycol (PEG) and proteins in aqueous solution. *J. Mater. Chem. B* 2, 2983–2992.

Wu, M., Chen, G., and Li, Y.-P. (2016). TGF- β and BMP signaling in osteoblast, skeletal development, and bone formation, homeostasis and disease. *Bone Res.* 4, 1–21.

Xia, Y., Kornfield, J.A., and Grubbs, R.H. (2009). Efficient Synthesis of Narrowly Dispersed Brush Polymers via Living Ring-Opening Metathesis Polymerization of Macromonomers. *Macromolecules* 42, 3761–3766.

Xu, D., and Esko, J.D. (2014). Demystifying heparan sulfate-protein interactions. *Annu. Rev. Biochem.* 83, 129–157.

Yang, B., Solakyildirim, K., Chang, Y., and Linhardt, R.J. (2011). Hyphenated techniques for the analysis of heparin and heparan sulfate. *Anal. Bioanal. Chem.* 399, 541–557.

Yao, K., Chen, Y., Zhang, J., Bunyard, C., and Tang, C. (2013). Cationic salt-responsive bottle-brush polymers. *Macromol. Rapid Commun.* 34, 645–651.

Ye, B., Luo, X., Li, Z., Zhuang, C., Li, L., Lu, L., Ding, S., Tian, J., and Zhou, C. (2016). Rapid biomimetic mineralization of collagen fibrils and combining with human umbilical cord mesenchymal stem cells for bone defects healing. *Mater. Sci. Eng. C* 68, 43–51.

Ye, L., Wu, X., Mu, Q., Chen, B., Duan, Y., Geng, X., Gu, Y., Zhang, A., Zhang, J., and Feng, Z. (2011). Heparin-Conjugated PCL Scaffolds Fabricated by Electrospinning and Loaded with Fibroblast Growth Factor 2. *J. Biomater. Sci. Polym. Ed.* 22, 389–406.

Yin, T., and Li, L. (2006). The stem cell niches in bone. *J. Clin. Invest.* 116, 1195–1201.

Yin, H., Price, F., and Rudnicki, M.A. (2013). Satellite Cells and the Muscle Stem Cell Niche. *Physiol. Rev.* 93, 23–67.

Zhang, L., Hu, J., and Athanasiou, K.A. (2009). The Role of Tissue Engineering in Articular Cartilage Repair and Regeneration. *Crit. Rev. Biomed. Eng.* 37, 1–57.

Zhao, B., Katagiri, T., Toyoda, H., Takada, T., Yanai, T., Fukuda, T., Chung, U., Koike, T., Takaoka, K., and Kamijo, R. (2006). Heparin potentiates the in vivo ectopic bone formation induced by bone morphogenetic protein-2. *J. Biol. Chem.* 281, 23246–23253.

Zhao, W., McCallum, S.A., Xiao, Z., Zhang, F., and Linhardt, R.J. (2012a). Binding affinities of vascular endothelial growth factor (VEGF) for heparin-derived oligosaccharides. *Biosci. Rep.* 32, 71–81.

Zhao, W., McCallum, S.A., Xiao, Z., Zhang, F., and Linhardt, R.J. (2012b). Binding affinities of vascular endothelial growth factor (VEGF) for heparin-derived oligosaccharides. *Biosci. Rep.* 32, 71–81.

Ziegler, A., and Zaia, J. (2006). Size-exclusion chromatography of heparin oligosaccharides at high and low pressure. *J. Chromatogr. B Analyt. Technol. Biomed. Life. Sci.* 837, 76–86.

